Pontifícia Universidade Católica
do Rio de Janeiro

Diana Marcela Viveros Melo

Advanced Precoding Techniques With Zero-Crossing Modulation for Channels With 1-bit ADCs and Temporal Oversampling

Tese de Doutorado

Thesis presented to the Programa de Pós–graduação em Engenharia Elétrica of PUC-Rio in partial fulfillment of the requirements for the degree of Doutor em Engenharia Elétrica.

Advisor: Prof. Lukas Tobias Nepomuk Landau

Rio de Janeiro
April 2024

Pontifícia Universidade Católica
do Rio de Janeiro

Diana Marcela Viveros Melo

Advanced Precoding Techniques With Zero-Crossing Modulation for Channels With 1-bit ADCs and Temporal Oversampling

Thesis presented to the Programa de Pós–graduação em Engenharia Elétrica of PUC-Rio in partial fulfillment of the requirements for the degree of Doutor em Engenharia Elétrica. Approved by the Examination Committee.

Prof. Lukas Tobias Nepomuk Landau
Advisor
Departamento de Engenharia Elétrica – PUC-Rio

Prof. Rodrigo Caiado de Lamare
Departamento de Engenharia Elétrica – PUC-Rio

Prof. Marco Antonio Grivet Mattoso Maia
Departamento de Engenharia Elétrica – PUC-Rio

Prof. Luciano Leonel Mendes
Instituto Nacional de Telecomunicações – Inatel

Dr. André Robert Flores Manrique
Departamento de Engenharia Elétrica – PUC-Rio

Dr.-Ing. Peter Friedrich Neuhaus
Rohde & Schwarz – GmbH & Company KG

Rio de Janeiro, April the 26th, 2024

Diana Marcela Viveros Melo

The author received the B.Sc. degree in Electronic Engineering in Universidad de Nariño, Colombia and M.Sc. degree in Electrical Engineering from Pontifícia Universidade Católica do Rio de Janeiro, Brazil in 2020.

Bibliographic data

Melo, Diana Marcela Viveros

Advanced Precoding Techniques With Zero-Crossing Modulation for Channels With 1-bit ADCs and Temporal Oversampling / Diana Marcela Viveros Melo; advisor: Lukas Tobias Nepomuk Landau. – 2024.

104 f: il. color. ; 30 cm

Tese (doutorado) - Pontifícia Universidade Católica do Rio de Janeiro, Departamento de Engenharia Elétrica, 2024.

Inclui bibliografia

1. Engenharia Elétrica – Teses. 2. Quantização de 1 bit. 3. Sobreamostragem. 4. MSE pré-codificação. 5. Máquina de Moore. 6. mmWave. I. Landau, Lukas Tobias Nepomuk. II. Pontifícia Universidade Católica do Rio de Janeiro. Departamento de Engenharia Elétrica. III. Título.

CDD: 621.3

This thesis is dedicated to Arya, Nikita, and Cielo
for waking me up early every day.

Acknowledgments

I would first like to thank my advisor Professor Lukas Landau for trusting me and allowing me to work with him. I am grateful to him for his support, guidance and always being willing to solve my doubts and show me the best way to carry out my research. I am also grateful to have Professor Rodrigo de Lamare guidance and support.

I would like to thank the members of my defense committee, Professor Rodrigo de Lamare, Professor Marco Antonio Grivet Mattoso Maia, Professor Luciano Leonel Mendes, Dr. André Flores and Dr.-Ing. Peter Friedrich Neuhaus, generously took their time and effort to evaluate my thesis.

I would also like to thank Professor Rodrigo de Lamare, Dr. Peter Friedrich Neuhaus, Dr. Lucas Ribeiro, Professor Martin Haardt, and Professor Gerhard Fettweis with whom I participated in joint work and who contributed ideas, reviews, comments, and feedback.

Moreover, I would like to thank my colleagues and friends Erico, Alireza, and Tonny who helped and supported me during the development of my research.

I want to thank God for giving me strength and never abandoning me, to my mother Sandra, my brother Andres, and my sister Viviana for their support. I also would like to thank John for his company and support.

Finally, I want to thank the government of Brazil for financial support to complete my PhD. This study was financed in part by the Coordenação de Aperfeiçoamento de Pessoal de Nivel Superior - Brasil (CAPES) - Finance Code 001, and in part by the Fundação Carlos Chagas Filho de Amparo à Pesquisa do Estado do Rio de Janeiro - Brasil (FAPERJ) - process 276492.

Abstract

Melo, Diana Marcela Viveros; Landau, Lukas Tobias Nepomuk (Advisor). **Advanced Precoding Techniques With Zero-Crossing Modulation for Channels With 1-bit ADCs and Temporal Oversampling**. Rio de Janeiro, 2024. 104p. PhD Dissertation – Departament of , Pontifícia Universidade Católica do Rio de Janeiro.

A promising approach to reduce energy consumption is to consider coarse quantization at the receiver. In this study, we investigate novel precoding techniques in space and time for bandlimited multiuser MIMO downlink channels with 1-bit quantization and oversampling at the receiver, considering zero-crossing modulation. The proposed time-instance zero-crossing modulation conveys the information into the time-instances of zero-crossings. Two design criteria for time-instance zero-crossing modulation are investigated, namely, the minimum distance to the decision threshold and the mean-square error between the received and the desired signal. The maximization of the minimum distance to the decision threshold can be formulated as a quadratically constraint quadratic program. As an alternative, an equivalent problem is formulated based on power minimization, which reduces computational complexity. Moreover, another method is implemented where the information is conveyed into the time-instances of zero-crossings using waveform segments. Departing from the conventional mean-square error based technique, a more sophisticated algorithm is developed, which implies active constellation extension to improve the performance at high SNR. The extended problem is solved with two approaches: by formulating the problem as a second-order cone program and by considering an alternating optimization algorithm. Another method based on the gradient descent algorithm is implemented with the mean-square error technique to reduce computational complexity further. Besides, a lower bound on the spectral efficiency is obtained. Numerical results show that the proposed time-instance zero-crossing precoding methods significantly improve the bit error rate compared to the state-of-the-art methods. Finally, the maximization of the minimum distance to the decision threshold and the mean-square error based precoding techniques are evaluated considering a frequency-selective millimeter wave channel. Numerical results show that both precoding techniques respond well to the frequency selectivity of the channel.

Keywords

1-bit Quantization Oversampling MSE precoding Moore machine mmWave

Resumo

Melo, Diana Marcela Viveros; Landau, Lukas Tobias Nepomuk. **Técnicas avançadas de pré-codificação com modulação de cruzamento zero para canais com ADCs de 1 bit e sobreamostragem temporal**. Rio de Janeiro, 2024. 104p. Tese de Doutorado – Departamento de Engenharia Elétrica, Pontifícia Universidade Católica do Rio de Janeiro.

Uma abordagem promissora para reduzir o consumo de energia é considerar a quantização grosseira no receptor. Neste estudo, investigamos novas técnicas de pré-codificação no espaço e no tempo para canais de downlink MIMO multiusuário limitados em banda com quantização de 1 bit e sobreamostragem no receptor, considerando a modulação de cruzamento zero. A modulação de instância de tempo de zero cruzamento proposta transmite a informação nas instâncias de tempo de cruzamento zero. Dois critérios de projeto para a instância de tempo de cruzamento zero são investigados, a saber, a distância mínima até o limiar de decisão e o erro quadrático médio entre o sinal recebido e o desejado. A maximização da distância mínima para o limiar de decisão pode ser formulada como um programa quadrático restrito quadraticamente. Como alternativa, um problema equivalente pode ser formulado com base na minimização de potência, o que reduz a complexidade computacional. Além disso, outro método é implementado onde a informação é transmitida nas instâncias de tempo de cruzamento zero em segmentos de forma de onda. Partindo da técnica convencional baseada no erro quadrático médio, um algoritmo mais sofisticado é desenvolvido, o que implica a extensão ativa da constelação para melhorar o desempenho em alta SNR. O problema estendido é resolvido com duas abordagens: formulando o problema como um programa de cone de segunda ordem e considerando um algoritmo de otimização alternada. Outro método baseado no algoritmo de descida de gradiente é implementado com a técnica do erro quadrático médio para reduzir ainda mais a complexidade computacional. Além disso, um limite inferior para a eficiência espectral é obtido. Os resultados numéricos mostram que os métodos de pré-codificação de cruzamento zero de instância de tempo propostos melhoram significativamente a taxa de erro de bit em comparação com os métodos de última geração. Finalmente, a maximização da distância mínima ao limiar de decisão e as técnicas de pré-codificação baseadas no erro quadrático médio são avaliadas considerando um canal de onda milimétrica seletivo em frequência. Os resultados numéricos mostram que ambas as técnicas de pré-codificação respondem bem à seletividade de frequência do canal.

Palavras-chave

Quantização de 1 bit   Sobreamostragem   MSE pré-codificação   Máquina de Moore   mmWave

Table of contents

1 Introduction **15**
1.1 Motivation and Context 15
1.2 State-of-the-art 16
1.3 Contributions 17
1.4 Structure of the Work 20
1.5 Notation 20

2 System Model **21**

3 Proposed Time Instance Zero-Crossing Modulation **25**
3.1 Construction of the TI ZX Sequence 26
3.2 Gray Coding for Time-Instance Zero-Crossing Modulation 27
3.3 Detection 29

4 Optimization Based Precoding Methods **31**
4.1 MMDDT Criterion 31
4.1.1 MMDDT Criterion in Space and Time 32
4.1.1.1 Joint MMDDT 32
4.1.1.2 Joint MMDDT ZF 34
4.1.2 Numerical Results 35
4.2 MMSE Criterion in Space and Time 38
4.2.1 MMSE With Active Constellation Extension 39
4.2.1.1 Optimal MMSE ACE 40
4.2.1.2 Iterative MMSE ACE Algorithm 42
4.2.2 Iterative MMSE Gradient Descent Method 42
4.2.3 Numerical Results 47
4.3 Performance Comparison Between the Optimization Based Precoding Methods 51
4.3.1 BER Performance and PSD Evaluation 51
4.3.2 Time Offset Analysis 54
4.3.3 Computational Complexity Evaluation 55
4.4 Zero-Crossing Waveform Comparison 57
4.4.1 Spectral Efficiency 58
4.4.2 Numerical Results 59

5 Proposed State Machine-based Waveform Design With TI ZX Modulation **62**
5.1 Waveform Design Optimization 63
5.1.1 Autocorrelation for TI ZX Modulation 64
5.1.2 Waveform Design 66
5.2 A Practical Waveform Design Optimization Strategy 68
5.3 Numerical Results 70

6 TI ZX for mmWave Channels **76**
6.1 Precoding Framework 76

6.2 Numerical Results 78

7 Conclusions **83**

8 Future Work **85**

A Appendix **94**
A.1 Derivation of The Space-Time MMSE Precoding 94
A.2 MMSE Precoding Performance Bound 95
A.3 MMDDT Precoding Performance Bound 98
A.4 Runlength-Limited Zero-Crossing Precoding 100
A.4.1 Runlength-Limited Sequence Detection 101
A.5 Published Papers 103

List of figures

Figure 2.1 Multiuser MIMO system model. 22

Figure 3.1 Example of the construction of $\boldsymbol{c}_{\text{out}}$ for $M_{\text{Rx}} = 3$. 29
Figure 3.2 Representation of the $\boldsymbol{z}_{b,i}$ subsequences. 30

Figure 4.1 BER comparison of the considered modulations. In (a) for $M_{\text{Rx}} = 2$ and in (b) for $M_{\text{Rx}} = 3$. 36
Figure 4.2 BER vs. SNR for Joint MMDDT and total MMDDT ZF with $M_{\text{Rx}} = M_{\text{Tx}} = 2$, considering the proposed TI ZX modulation. 38
Figure 4.3 Active constellation extension example for a given $\boldsymbol{c}_{\text{out}}$. 39
Figure 4.4 Multiuser MIMO system model for the Iterative Gradient Descent method. 43
Figure 4.5 Comparison between the optimal MMSE ACE and the iterative MMSE ACE for different number of iterations for $M_{\text{Rx}} = M_{\text{Tx}} = 2$. 48
Figure 4.6 MSE comparison for different configurations. In (a) $M_{\text{Rx}} = 2$, $M_{\text{Tx}} = 1$. In (b) $M_{\text{Rx}} = M_{\text{Tx}} = 3$. In (c) $M_{\text{Rx}} = 3$, $M_{\text{Tx}} = 1$. 49
Figure 4.7 MSE cost function for different precoding strategies. 50
Figure 4.8 BER performance comparison. 51
Figure 4.9 BER vs. SNR for $M_{\text{Rx}} = M_{\text{Tx}} = 2$. 52
Figure 4.10 BER vs. SNR for different configurations. In (a) $M_{\text{Rx}} = 2$, $M_{\text{Tx}} = 1$. In (b) $M_{\text{Rx}} = M_{\text{Tx}} = 3$. In (c) $M_{\text{Rx}} = 3$, $M_{\text{Tx}} = 1$. 53
Figure 4.11 Power spectral density for $M_{\text{Rx}} = M_{\text{Tx}} = 2$. 54
Figure 4.12 BER vs. time delay for $M_{\text{Rx}} = M_{\text{Tx}} = 2$ considering different values of SNR. In (a) for SNR [dB] = 10 and in (b) for SNR [dB] = 30. 55
Figure 4.13 Computational complexity. (a) vs. the number of transmit antennas. (b) comparison between the optimal and iterative MMSE ACE. 57
Figure 4.14 Uncoded BER. 60
Figure 4.15 Lower bound on the SE for a bandlimited channel. All ZX mappings achieve a substantially higher SE as compared to standard QPSK signaling with 1-bit quantization [1]. 61
Figure 4.16 Comparison SE lower bound of the considered ZX mappings to QP modulation [2] 61

Figure 5.1 Considered multi-user MIMO downlink system model. 63
Figure 5.2 Mapping process for construction of $\boldsymbol{s}_g$ with the set of optimal coefficients $\boldsymbol{G}$ for $M_{\text{Rx}} = 3$. 72
Figure 5.3 γ vs η with $N_{\text{u}} = 1$. 73
Figure 5.4 BER vs SNR for γ_M with $N_u = 2$. 73
Figure 5.5 BER vs SNR for the proposed waveform with $\delta = 0.95$. 74
Figure 5.6 BER vs SNR for $M_{\text{Rx}} = 3$ for all the considered methods. 74

Figure 5.7 PSD for $M_{\mathrm{Rx}} = 3$. 75

Figure 6.1 BER vs. β for $M_{\mathrm{Rx}} = M_{\mathrm{Tx}} = 2$, $L_k = 5$ and SNR = 20dB. 78
Figure 6.2 BER vs. SNR. for different sets of signaling and sampling rates with $L_k = 5$ and $\beta = 1.5$. 79
Figure 6.3 BER vs. SNR. for different sets of signaling and sampling rates with $L_k = 5$ and $\beta = 0$. 79
Figure 6.4 BER vs. SNR with $M_{\mathrm{Rx}} = M_{\mathrm{Tx}} = 2$ and $L_k = 5$ for different values of β for joint MMDDT. 80
Figure 6.5 BER vs. SNR with $M_{\mathrm{Rx}} = M_{\mathrm{Tx}} = 2$ and $L_k = 5$ for different values of β for MMSE. 80
Figure 6.6 BER vs. SNR with $M_{\mathrm{Rx}} = M_{\mathrm{Tx}} = 2$ and $\beta = 1.5$ for different values of L_k for joint MMDDT. 81
Figure 6.7 BER vs. SNR with $M_{\mathrm{Rx}} = M_{\mathrm{Tx}} = 2$ and $\beta = 1.5$ for different values of L_k for MMSE. 81
Figure 6.8 Power spectral density for $M_{\mathrm{Rx}} = M_{\mathrm{Tx}} = 2$, $L_k = 5$ and $\beta = 1.5$. 82

Figure A.1 Equivalent Moore machine for $M_{\mathrm{Rx}} = 3$. 95
Figure A.2 Analytical and numerical MSE comparison for $M_{\mathrm{Rx}} = 2$ and $M_{\mathrm{Rx}} = 3$. 97
Figure A.3 Semi-analytical and numerical SER comparison for the MMDDT precoding method with $M_{\mathrm{Rx}} = M_{\mathrm{Tx}} = 3$, $N = 1$ and $\sigma^2 = 1$. 99

List of tables

Table 3.1 Zero-crossing assignment $\boldsymbol{c}_{\text{map}}$ 27
Table 3.2 Sequence patterns $\boldsymbol{c}_{\text{s}}$ 27
Table 3.3 *Gray code* for $M_{\text{Rx}} = 3$ 28
Table 3.4 Proposed *Gray code* for $M_{\text{Rx}} = 2$ 28
Table 3.5 $\mathcal{C}_{\text{det}}$ for $M_{\text{Rx}} = 3$ 30

Table 4.1 Computational Complexity analysis 56
Table 4.2 Considered zero-crossing mapping configurations. 59
Table 5.1 Set of optimal coefficients $\mathcal{G}$ for $M_{\text{Rx}} = 3$. 64
Table 5.2 Equivalent Moore machine for TI ZX mapping for $M_{\text{Rx}} = 3$. 66
Table 5.3 Equivalent Moore machine for TI ZX mapping for $M_{\text{Rx}} = 2$. 66
Table 5.4 Parameters values 74
Table 5.5 Simulation parameters 75
Table 5.6 Optimal set $\boldsymbol{G}$ for $M_{\text{Rx}} = 2$ with $N_{\text{u}} = 1$ and $\delta = 0.95$ 75
Table 5.7 Optimal set $\boldsymbol{G}$ for $M_{\text{Rx}} = 3$ with $N_{\text{u}} = 1$ and $\delta = 0.95$ 75

Table A.1 Equivalent Moore machine for $M_{\text{Rx}} = 3$. 96
Table A.2 Integration regions $\mathcal{R}$ for each symbol b_j. 99
Table A.3 Finite-state machine encoder for $(1, \infty)$ RLL constraint with code rate $R_{\text{RLL}} = 2/3$. 101
Table A.4 Finite-state machine encoder for $(2, \infty)$ RLL constraint with code rate $R_{\text{RLL}} = 1/2$. 101

List of Abreviations

ADC – Analog-to-Digital Converter
IoT – Internet of Things
mmWave – Millimeter-Wave
AGC – Automatic Gain Control
RLL – Runlength-limited
QP – Quantization Precoding
TI ZX – Time-Instance Zero-Crossing
ACE – Active Constellation Extension
SOCP – Second Order Cone Program
GD – Gradient Descent
AWGN – Additive White Gaussian Noise
BER – Bit Error Rate
BS – Base station
MIMO – Multiple-Input Multiple-Output
MMDDT – Maximization of the Minimum Distance to the Decision Threshold
MSE – Mean Square Error
MMSE – Minimum Mean Square Error
PDF – Probability Density Function
QPSK – Quadrature Phase Shift Keying
SE – Spectral Efficiency
ZX – Zero-crossing
FSM – Finite-State Machine
SNR – Signal-to-noise ratio
DAC – Digital to-Analog Converter
ZF – Zero Forcing
QCQP – Quadratically Constrained Quadratic Program

1
Introduction

1.1
Motivation and Context

Future wireless communication systems will have to support a massive number of devices for promising technologies such as the internet of things (IoT), which has a wide variety of applications in industrial automation systems, intelligent transportation, and health care, among others [3,4]. Moreover, these systems will be required to transmit higher data rates, and for this, the spectrum in the millimeter-wave (mmWave) is promising [5,6]. In this sense, the design of systems in this frequency band can also represent a challenge regarding the analog-to-digital converter (ADC) power consumption. Therefore, these scenarios have important restrictions, since low-complexity and low-power consumption devices are required. Considering the use case of IoT networks with more than 1 million devices, the energy consumption of the receiving devices is extremely constrained and in some cases, the devices are supposed to run for several years on the same battery. For this reason, when IoT systems are targeted, it is necessary to simplify all the other hardware components as well. That is why it is necessary to propose approaches in terms of spatial-temporal waveform design and also consider practical detectors since 1-bit quantization is a non-linear operation and complexity at the receiver needs to be reduced [2].

In this sense, it is of great interest to study and develop communication systems with low-resolution ADCs. Employing 1-bit quantization is promising because the energy consumption of the ADCs grows exponentially with their resolution in bits [7]. Moreover, systems with 1-bit quantization do not require linear amplifiers, and the automatic gain control (AGC) can potentially be omitted. In addition, for 1-bit quantization systems, it is not necessary to provide a number of reference voltages as required for flash ADCs.

By increasing the sampling rate, it is possible to partially compensate for the loss of information due to the coarse quantization. In this context, the achievable rate for bandlimited 1-bit quantized processes improves considerably with oversampling. In a noise free environment, rates of $\log_2(M_{\mathrm{Rx}} + 1)$ bits per Nyquist interval are achievable with M_{Rx}-fold oversampling [8].

1.2 State-of-the-art

Different studies have been conducted concerning communication systems with 1-bit quantization and oversampling at the receiver. New processing techniques such as zero-crossing modulation have been studied in [8] where a Zakai bandlimited process sampled with n times the Nyquist rate is considered. The Zakai bandlimited process is constructed with one zero-crossing per Nyquist interval and alternatively with L zero-crossings per each L-Nyquist interval. Moreover, for systems with oversampling, the study in [9] investigates the benefits of capacity per unit cost, and [10] studies the numerical computation and maximization of the achievable rate for noisy bandlimited channels. Furthermore, practical implementations of systems with 1-bit quantization and temporal oversampling consider ASK transmit sequences [11–14] and runlength-limited (RLL) transmit sequences [14], [15–19] and other methods based on zero-crossing [20]. The study in [21] exploits the approach of faster than-Nyquist (FTN) signaling [22] for sequence design optimization using 1-bit quantization and oversampling at the receiver and [23] considers the case of 1-bit quantization oversampling considering matched pulse shaping filters and faster than Nyquist signaling.

Other modern methods that consider the reduction of energy consumption in the ADCs are based on sub-Nyquist sampling methods such as the one presented in [24].

The authors of [25] consider the maximization of the minimum distance to the decision threshold (MMDDT) for 16-QAM modulation with a linear transmit filter for a channel with 1-bit quantization and oversampling at the receiver. The study in [26] devises a practical waveform design where a waveform set is constructed which conveys the information into the zero-crossings as suggested in [8]. Other related studies, such as [27–29], also have shown the benefit of oversampling.

Related approaches for multiple-input multiple-output (MIMO) uplink systems with 1-bit quantization and oversampling at the base station (BS) have been investigated in [30–34]. An achievable rate analysis that relies on the zero-forcing (ZF) receiver and linear channel estimation is presented in [30]. In [31], a related study with orthogonal frequency division multiplexing is investigated. The work in [32] proposes a dynamic oversampling technique, whereas [33] investigates oversampling for channel estimation and corresponding performance bounds. On the other hand, different methods for downlink systems with 1-bit quantization and oversampling at the receivers exist. For the multiple-input single-output case, [35] proposed a similar waveform design as in [25]. Moreover, for the multiuser MIMO downlink channel, the work in [2] devises the so called quantization precoding (QP) technique based on an optimal codebook search which allows high spectral efficiency and symbol-by-symbol detection. The approach in [2] relies on the MMDDT criterion, which is a well-established design criterion in literature [25, 36–39], that is mathematically tractable and suitable for low-resolution techniques. The study in [40] constructs an upper and a lower bound on the spectral efficiency for a MIMO system considering zero-crossing modulation.

Furthermore, given the increasing demand for higher data rates, future wireless communication systems will be required to utilize a broad spectrum in the mmWave and sub terahertz bands [41]. In this context, high-resolution ADCs are not energy-efficient for the design of systems with such large bandwidths. Therefore, related approaches with low-resolution ADCs have been proposed in the literature, such as [42–44] considering mmWave MIMO systems. In [45], a practical transceiver design is proposed for a zero-crossing modulation waveform, which combines faster-than-Nyquist signaling and RLL transmit sequences while considering a mmWave channel.

1.3 Contributions

In the present study, a bandlimited downlink channel with 1-bit quantization and oversampling at the receivers is considered with variable signaling rate including faster-than-Nyquist signaling. For this channel, two different precoding strategies are proposed, which are constructed for 1-bit quantization with the novel time-instance zero-crossing (TI ZX) modulation. The proposed TI ZX modulation is a sophisticated method for 1-bit quantization and M_{Rx}-fold oversampling, where each Nyquist interval is associated with M_{Rx} binary samples. With the proposed modulation, at the receiver, there is at most one zero-crossing per Nyquist interval in one of the M_{Rx} sub-intervals. Unlike the closely related approach from [8], the proposed method also considers the absence of zero-crossings during the Nyquist interval as a valid symbol, resulting in $M_{\mathrm{Rx}}+1$ unique patterns. Note that TI ZX modulation results in a smaller average number of zero-crossings compared to the scheme in [8], which facilitates the waveform design in practice.

The first proposed precoding strategy is based on the MMDDT criterion [25], [2] and on the existing techniques introduced in [46] [47]. Unlike previous works, the novel joint MMDDT is solved in space and time together for all the transmit sequences and for the in-phase and quadrature components of the signal. An equivalent problem with lower computational complexity can be formulated by considering the minimization of the transmit power for a given minimum distance criterion constraint and a subsequent power scaling of the solution vector. Moreover, a similar strategy is proposed in conjunction with a spatial ZF precoding which further reduces the computational complexity.

The second proposed precoding strategy is based on the minimum mean square error (MMSE) criterion with TI ZX modulation, which was previously introduced in [46] and [48] where the problem is formulated jointly in space and time for the whole transmit sequence and for the in-phase and quadrature components in a stacked vector approach. A more sophisticated technique is developed by considering the active constellation extension (ACE) method [49], which implies a relaxation for the desired output signal. For solving the latter problem, two different approaches are proposed. The first approach to solve the MMSE ACE design problem optimally is given by considering the symbol sequences as optimization variables, which can then be expressed as a second-order cone program (SOCP). Alternatively, the MMSE ACE can be solved by considering an iterative optimization algorithm where the symbol sequences and the precoding vector are optimized by an alternating optimization strategy. Besides, for the generic MMSE problem, an alternating approach involving two separate precoding matrices for space and time is proposed to further reduce the computational complexity. In this sense, a joint optimization problem is formulated and solved iteratively with gradient descent (GD) projection method [50]. Then, considering the MMSE problem formulation, a lower bound on the spectral efficiency is presented, and a waveform comparison is done for the TI ZX modulation and RLL sequences [51].

Additionally, in this work it is also developed a modulation based on the TI ZX waveform design where a predefined level of out-of-band radiation is tolerated. The proposed waveform design considers the TI ZX modulation and follows a similar idea as presented in [26]. The proposed method conveys the information into the time-instances of zero-crossings but instead of considering sequences of samples, input bits are mapped into waveform segments according to the TI ZX mapping rules. The temporal precoding vector is then used in conjunction with a simple pulse shaping filter. The optimal set of coefficients is computed with an optimization problem which is formulated to maximize the minimum distance to the decision threshold, constrained with some tolerated out-of-band radiation.

Finally, a precoding framework with the established TI ZX modulation for the established mmWave channel model is developed. For this channel, the generic MMSE precoding and the joint MMDDT precoding are considered.

The presented precoding techniques are evaluated in terms of their bit error rate (BER) and computational complexity. The results show that in general the MMDDT based precoding techniques achieve better performance at high signal-to-noise ratio (SNR), whereas the MMSE techniques are good at low SNR. The MMSE approach with the ACE strategy shows a considerable improvement at high SNR in terms of the BER and has the best performance at low SNR. In general TI ZX precoding yields a significantly lower BER than QP modulation [2].

When the lower bound spectral efficiency is compared for ZX modulations as RLL and TI ZX, it is observed that in general, both considered ZX mappings achieve similar performance in the SE at low SNR. Especially the TI ZX modulation also offers a low complexity detection scheme.

In terms of the mmWave channel, different parameters are evaluated for a comprehensive numerical analysis of the performance of precoding techniques with TI ZX in more realistic environments. The results show that both bandlimited precoding techniques respond well to the frequency selectivity of the mmWave channel.

The contributions in this work can be summarized as follows:

- A novel TI ZX modulation approach is presented which conveys the information in the time-instances of zero-crossings.
- A low complexity detection scheme for time-instance zero-crossing precoding is presented.
- A joint MMDDT precoding technique is developed with an alternative approach with lower computational complexity.
- The derivation of a TI ZX MMSE precoding approach and a more advanced approach that relies on ACE, which further improves the performance.
- The development of an iterative algorithm to find the ACE vector and the optimal precoding vector with low computational complexity.
- The development of an iterative algorithm with a gradient projection method to further reduce the computational complexity of the generic MMSE.
- A waveform design based on the TI ZX modulation is developed where waveform segments are considered instead of samples.
- The development of a precoding framework with the TI ZX modulation for a mmWave channel model.
- A lower bound on the spectral efficiency is developed.
- A simulation study of the BER, spectral efficiency, power spectral density, and computational complexity is presented.

1.4 Structure of the Work

The document is organized as follows. Chapter 2 presents the system model. In Chapter 3, the TI ZX modulation is explained in detail, including the detection process. The proposed precoding design is discussed in Chapter 4, where the techniques based on the MMDDT and MMSE criteria are presented with their respective simulation results. The performance evaluation, where the precoding techniques are compared under BER, power spectral density, and computational complexity are also presented in Chapter 4. The zero-crossing waveform comparison and the lower bound on the spectral efficiency are presented in Chapter 4. In Chapter 5, the state machine-based waveform design with TI ZX modulation is presented including the numerical evaluation. The TI ZX framework for mmWave channels is presented in Chapter 6. Finally, the conclusion is given in Chapter 7. The appendices contain the derivation of the MMSE, the RLL mapping, the MMSE performance bound, and the list of published papers.

1.5 Notation

Scalar values are represented by lowercase and regular fonts, e.g., a. Complex vectors and matrices are represented by bold lowercase and bold uppercase fonts, e.g., $\boldsymbol{x}$ and $\boldsymbol{X}$, respectively. The subscript R represents a real-valued notation. The $\mathrm{vec}(\cdot)$ operator applies a matrix vectorization by stacking the matrix columns. The $\mathrm{sgn}(\cdot)$ operator denotes the sign of the argument, where $\mathrm{sgn}\,(x) = +1$ if $x \geq 0$, and $\mathrm{sgn}\,(x) = -1$ if $x < 0$. The semicolon denotes a vertical concatenation in terms of vectors and matrices. The Kronecker product is denoted by $\otimes$. The subscript $\mathcal{R}/\mathcal{J}$ implies that the process is done separately and in the same way for the in-phase and quadrature components.

2
System Model

The downlink of a multiuser MIMO system shown in Fig. 2.1 is considered with N_t transmit antennas at the BS and N_u single antenna users. The vector $\boldsymbol{x}_k$ is the transmit symbol sequence of the k-th user with N complex symbols, each denoted as $x_i = x_i^I + jx_i^Q$ with symbol duration T. The sequence $\boldsymbol{x}_k$ is fed into the TI ZX modulator to be mapped on the desired output pattern $\boldsymbol{c}_{\mathrm{out}_k}$ with dimensions $N_\mathrm{tot} = NM_\mathrm{Rx} + 1$. Employing $M_\mathrm{Tx} > 1$ corresponds to faster-than-Nyquist signaling and is related to the oversampling factor M_Rx by $MM_\mathrm{Tx} = M_\mathrm{Rx}$, where M is the factor that relates the different sampling rate domains. $M = M_\mathrm{Rx}/M_\mathrm{Tx}$ corresponds to the relative oversampling factor with respect to the signaling rate M_Tx/T. Each symbol $x_i^{I/Q}$ is drawn from the set $\mathcal{X}_\mathrm{in} := \{b_1, b_2, \cdots, b_{R_\mathrm{in}}\}$ where $R_\mathrm{in} = M_\mathrm{Rx} + 1$. At the BS ideal digital-to-analog converters (DACs) and pulse shaping filters $g_\mathrm{Tx}(t)$ with bandwidth W_Tx are considered. The transmit filter is normalized to unit energy in terms of $\int_{-\infty}^{\infty} |g_\mathrm{Tx}(t)|^2 \, dt = 1$. In discrete time, the filter $g_\mathrm{Tx}(t)$ is represented by the Toeplitz matrix $\boldsymbol{G}_\mathrm{Tx}$ given by

$$\boldsymbol{G}_\mathrm{Tx} = a_\mathrm{Tx} \begin{bmatrix} \left[\ \boldsymbol{g}_\mathrm{Tx}^T \ \right] & 0 \cdots & & 0 \\ 0 & \left[\ \boldsymbol{g}_\mathrm{Tx}^T \ \right] & 0 \cdots & 0 \\ & \ddots & \ddots & \ddots \\ 0 \cdots & & 0 & \left[\ \boldsymbol{g}_\mathrm{Tx}^T \ \right] \end{bmatrix}_{N_\mathrm{tot} \times 3N_\mathrm{tot}} , \tag{2-1}$$

with $\boldsymbol{g}_\mathrm{Tx} = [g_\mathrm{Tx}(-T(N + \frac{1}{M_\mathrm{Rx}})), g_\mathrm{Tx}(-T(N + \frac{1}{M_\mathrm{Rx}}) + \frac{T}{M_\mathrm{Rx}}), \ldots, \; g_\mathrm{Tx}(T(N + \frac{1}{M_\mathrm{Rx}}))]^T$ and normalization factor $a_\mathrm{Tx} = (T/M_\mathrm{Rx})^{1/2}$. The factor a_Tx corresponds to the normalization to unit energy in discrete time which relies on unit energy normalization in continuous time for g_Tx. The matrix $\boldsymbol{H}$ with dimensions $N_\mathrm{u} \times N_\mathrm{t}$ describes a frequency flat fading channel. The receivers consist of the receive filter $g_\mathrm{Rx}(t)$ with bandwidth W_Rx and the 1-bit ADC.

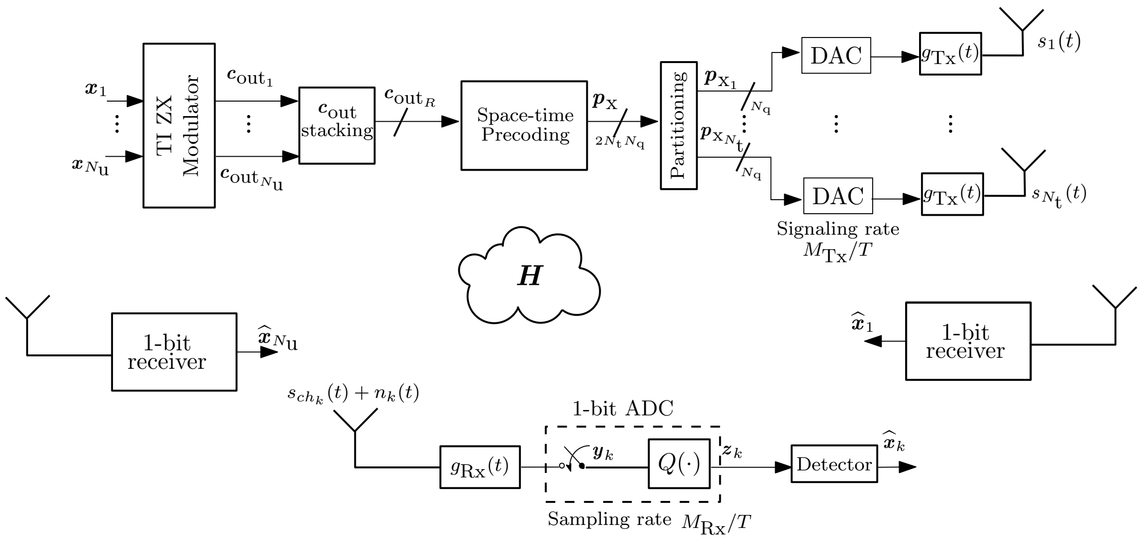

Figure 2.1: Multiuser MIMO system model.

The receive filter is represented by the following Toeplitz matrix:

$$\boldsymbol{G}_{\text{Rx}} = a_{\text{Rx}} \begin{bmatrix} \left[\ \boldsymbol{g}_{\text{Rx}}^T\ \right] & 0 \cdots & 0 \\ 0 & \left[\ \boldsymbol{g}_{\text{Rx}}^T\ \right] & 0 \cdots 0 \\ & \ddots \ddots \ddots & \\ 0 \cdots & 0 & \left[\ \boldsymbol{g}_{\text{Rx}}^T\ \right] \end{bmatrix}_{N_{\text{tot}} \times 3N_{\text{tot}}}, \tag{2-2}$$

with $\boldsymbol{g}_{\text{Rx}} = [g_{\text{Rx}}(-T(N+\frac{1}{M_{\text{Rx}}})), g_{\text{Rx}}(-T(N+\frac{1}{M_{\text{Rx}}}) + \frac{T}{M_{\text{Rx}}}), \ldots, g_{\text{Rx}}(T(N+\frac{1}{M_{\text{Rx}}}))]^T$ as the coefficients of the $g_{\text{Rx}}(t)$ filter and $a_{\text{Rx}} = (T/M_{\text{Rx}})^{1/2}$ that corresponds to unit energy normalization. The combined waveform determined by the transmit and receive filters can be described by $v(t) = g_{\text{Tx}}(t) * g_{\text{Rx}}(t)$. The combined waveform is represented by the Toeplitz matrix $\mathbf{V}$, denoted as

$$\mathbf{V} = \begin{bmatrix} v\left(0\right) & v\left(\frac{T}{M_{\text{Rx}}}\right) & \cdots & v\left(TN\right) \\ v\left(-\frac{T}{M_{\text{Rx}}}\right) & v\left(0\right) & \cdots & v\left(T\left(N - \frac{1}{M_{\text{Rx}}}\right)\right) \\ \vdots & \vdots & \ddots & \vdots \\ v\left(-TN\right) & v\left(T\left(-N + \frac{1}{M_{\text{Rx}}}\right)\right) & \cdots & v\left(0\right) \end{bmatrix}_{N_{\text{tot}} \times N_{\text{tot}}}. \tag{2-3}$$

At the ADC, the signal $y(t)$ is oversampled at rate $\frac{M_{\text{Rx}}}{T} = \frac{MM_{\text{Tx}}}{T}$. The matrix $\boldsymbol{U}$ with dimensions $N_{\text{tot}} \times N_{\text{q}}$, describes the M-fold upsampling operation and is defined by

$$\boldsymbol{U}_{m,n} = \begin{cases} 1, & \text{for} \quad m = M \cdot (n-1) + 1 \\ 0, & \text{else,} \end{cases} \tag{2-4}$$

where $m, n \geq 1$ and $N_{\mathrm{q}} = M_{\mathrm{Tx}}N + 1$. The upsampling operation is used to describe systems with different signaling and sampling rates. At the receiver, the signal is processed by a matched filter and quantized. The quantized vector at user k of length N_{tot} is given by

$$\begin{aligned} \boldsymbol{z}_k &= Q_1\left(\sum_{i=1}^{N_{\mathrm{t}}} h_{k_i}\boldsymbol{V}\boldsymbol{U}\boldsymbol{p}_{\mathrm{x}_i} + \boldsymbol{G}_{\mathrm{Rx}}\boldsymbol{n}_k\right), \\ &= Q_1\left(\left(\boldsymbol{h}_k \otimes \boldsymbol{I}_{N_{\mathrm{tot}}}\right)\left(\boldsymbol{I}_{N_{\mathrm{t}}} \otimes \boldsymbol{V}\boldsymbol{U}\right)\boldsymbol{p}_{\mathrm{x}} + \boldsymbol{G}_{\mathrm{Rx}}\boldsymbol{n}_k\right), \end{aligned} \tag{2-5}$$

where the stacked vector $\boldsymbol{p}_{\mathrm{x}} = \left[\boldsymbol{p}_{\mathrm{x}_1}^T, \boldsymbol{p}_{\mathrm{x}_2}^T, \cdots, \boldsymbol{p}_{\mathrm{x}_i}^T, \cdots, \boldsymbol{p}_{\mathrm{x}_{N_{\mathrm{t}}}}^T\right]^T$ and $\boldsymbol{p}_{\mathrm{x}_i}$ corresponds to the spatial and temporal precoding vector of the i-th transmit antenna. Note that, the vector $\boldsymbol{p}_{\mathrm{x}}$ depends on the channel $\boldsymbol{H}$ and the sequences $\boldsymbol{c}_{\mathrm{out}_k}$, which will be detailed in Section 4. The vector $\boldsymbol{h}_k$ is the k-th row vector of the matrix $\boldsymbol{H}$ and h_{k_i} corresponds to the ith entry of $\boldsymbol{h}_k$. The vector $\boldsymbol{n}_k$ with length $3N_{\mathrm{tot}}$ contains i.i.d. complex Gaussian noise samples with zero mean and variance σ_n^2.

Stacking the received sequences of the N_{u} users in the vector $\boldsymbol{z} = \left[\boldsymbol{z}_1^T, \boldsymbol{z}_2^T, \cdots, \boldsymbol{z}_k^T, \cdots, \boldsymbol{z}_{N_{\mathrm{u}}}^T\right]^T$ yields the vector $\boldsymbol{z} = Q_1(\boldsymbol{y})$ with length $N_{\mathrm{u}}N_{\mathrm{tot}}$ given by

$$\boldsymbol{z} = Q_1\left(\left(\boldsymbol{H} \otimes \boldsymbol{I}_{N_{\mathrm{tot}}}\right)\left(\boldsymbol{I}_{N_{\mathrm{t}}} \otimes \boldsymbol{V}\boldsymbol{U}\right)\boldsymbol{p}_{\mathrm{x}} + \left(\boldsymbol{I}_{N_{\mathrm{u}}} \otimes \boldsymbol{G}_{\mathrm{Rx}}\right)\boldsymbol{n}\right). \tag{2-6}$$

Defining the effective channel matrix as:

$$\boldsymbol{H}_{\mathrm{eff}} = \left(\boldsymbol{H} \otimes \boldsymbol{I}_{N_{\mathrm{tot}}}\right)\left(\boldsymbol{I}_{N_{\mathrm{t}}} \otimes \boldsymbol{V}\boldsymbol{U}\right), \tag{2-7}$$

the received signal $\boldsymbol{z}$ is rewritten as:

$$\boldsymbol{z} = Q_1\left(\boldsymbol{H}_{\mathrm{eff}}\boldsymbol{p}_{\mathrm{x}} + \boldsymbol{G}_{\mathrm{Rx,eff}}\boldsymbol{n}\right), \tag{2-8}$$

where the vector $\boldsymbol{n}$ with length $3N_{\mathrm{tot}}N_{\mathrm{u}}$ represents the complex Gaussian noise vector with zero mean and variance σ_n^2. The quantization operator is denoted by $Q_1(\cdot)$ which is defined by $Q_1(\boldsymbol{y}) = \mathrm{sgn}\left(\mathcal{R}\{\boldsymbol{y}\}\right) + j\mathrm{sgn}\left(\mathcal{J}\{\boldsymbol{y}\}\right)$, where $\mathcal{R}\{\cdot\}$ and $\mathcal{J}\{\cdot\}$ correspond to the real and imaginary parts, respectively such that $\boldsymbol{z} \in \{1+j, 1-j, -1+j, -1-j\}$. The stacked received sequence of the N_{u}

users from (2-8) can be reformulated in real-valued notation, which yields

$$\begin{aligned}\boldsymbol{z}_R &= \begin{bmatrix}\mathcal{R}\{\boldsymbol{z}\}\\ \mathcal{J}\{\boldsymbol{z}\}\end{bmatrix} = Q_1\left(\begin{bmatrix}\mathcal{R}\{\boldsymbol{y}\}\\ \mathcal{J}\{\boldsymbol{y}\}\end{bmatrix}\right)\\ &= Q_1\left(\begin{bmatrix}\mathcal{R}\{\boldsymbol{H}_{\text{eff}}\} & -\mathcal{J}\{\boldsymbol{H}_{\text{eff}}\}\\ \mathcal{J}\{\boldsymbol{H}_{\text{eff}}\} & \mathcal{R}\{\boldsymbol{H}_{\text{eff}}\}\end{bmatrix}\begin{bmatrix}\mathcal{R}\{\boldsymbol{p}_{\boldsymbol{x}}\}\\ \mathcal{J}\{\boldsymbol{p}_{\boldsymbol{x}}\}\end{bmatrix} + \begin{bmatrix}\mathcal{R}\{\boldsymbol{G}_{\text{Rx,eff}}\} & -\mathcal{J}\{\boldsymbol{G}_{\text{Rx,eff}}\}\\ \mathcal{J}\{\boldsymbol{G}_{\text{Rx,eff}}\} & \mathcal{R}\{\boldsymbol{G}_{\text{Rx,eff}}\}\end{bmatrix}\begin{bmatrix}\mathcal{R}\{\boldsymbol{n}\}\\ \mathcal{J}\{\boldsymbol{n}\}\end{bmatrix}\right).\end{aligned} \tag{2-9}$$

With this, the real-valued notation of $\boldsymbol{z}$ is given by $\boldsymbol{z}_R$ of length $2N_{\text{u}}N_{\text{tot}}$ described by $\boldsymbol{z}_R = Q_1(\boldsymbol{y}_R) = Q_1\left(\boldsymbol{H}_{\text{eff}_R}\boldsymbol{p}_{\text{x}_R} + \boldsymbol{G}_{\text{Rx,eff}_R}\boldsymbol{n}_R\right)$. The vector $\boldsymbol{p}_{\text{x}_R}$ with length $2N_{\text{t}}N_{\text{q}}$ corresponds to the space-time precoding vector in real-valued notation of all the transmitted segments.

3
Proposed Time Instance Zero-Crossing Modulation

In [8], a Zakai bandlimited process [52] was constructed considering the sign information within L Nyquist intervals. The study in [8] shows the benefits of oversampling to compensate for the loss of information due to 1-bit quantization. The results of [8] prove that the achievable rate increases with the oversampling factor.

In this work, the TI ZX modulation is proposed for systems with oversampling. This modulation conveys the information in the time-instances of zero-crossings and also includes the absence of zero-crossings per time interval as a valid transmit symbol. Note that the consideration of the absence of zero-crossings is different from the methods in [8] and [2], which implies a lower average number of zero-crossings per Nyquist interval. The reduced number of zero-crossings can be understood as a relaxation of the waveform design with bandlimitation. The essential idea of TI ZX modulation is to allocate at most one zero-crossing per symbol interval. When more than one zero-crossing per symbol interval is allowed, a significant performance degradation with respect to the optimization criteria MSE and γ, which is defined as the minimum distance to the decision threshold, can be observed [47], [48]. Moreover, mapping methods such as QP modulation [2] with more than one zero-crossings per Nyquist interval present a large number of "peaks" which correspond to high frequencies in the transmit signal. The realization of such a signal is difficult due to the bandwidth constraint which then finally leads to a waveform with a small distance to the decision threshold γ, as shown in [47]. In this sense, considering the input cardinality given by $R_{\text{in}} = M_{\text{Rx}} + 1$, all the symbols x taken from the input set $\mathcal{X}_{\text{in}} = \{b_1, b_2 \cdots, b_{R_{\text{in}}}\}$, are mapped onto a codeword defined by the time instant within the symbol interval, in which the zero-crossing occurs or not.

Mapping each symbol of the transmit sequence into the respective codeword given by the TI ZX modulation, generates the binary sequence $\boldsymbol{c}_{\text{out}}$, which corresponds to the desired output pattern at the receiver after quantization in a noise free case. In the following, it is described how to construct the sequence $\boldsymbol{c}_{\text{out}}$. As the process is done in the same way for each user and separately for the in-phase and quadrature-phase components of the sequence, the focus is on the construction of $\boldsymbol{c}_{\text{out}}$, considering only the in-phase component.

3.1 Construction of the TI ZX Sequence

Given the oversampling factor M_{Rx}, each Nyquist interval is divided into M_{Rx} segments, so each symbol b_j from the input alphabet corresponds to a specific binary codeword, which conveys the information about the time instant in which the zero-crossing occurs or not within the Nyquist interval. The mapping table $\boldsymbol{c}_{\text{map}}$ relates each symbol b_j to its respective time instance in which the zero-crossing occurs. As mentioned above, the proposed TI ZX modulation also considers the absence of a zero-crossing for one of the symbols of the input alphabet.

In Table 3.1, the zero-crossing assignment is presented for an arbitrary value of M_{Rx}. Note that the assignment can be arbitrarily permuted.

The considered mapping is assumed to be fixed and known by the receivers. Therefore, it is not required to send additional information. The latter corresponds to a benefit in comparison to the approach in [2], where the dynamic codebook mapping requires additional bandwidth for informing the receivers. Once the table mapping $\boldsymbol{c}_{\text{map}}$ is established, each component in terms of the real and imaginary parts of the symbol x_i taken from the input sequence $\boldsymbol{x}$ is mapped to a binary codeword $\boldsymbol{c}_{s_i} \in \{+1, -1\}$ of length M_{Rx} that conveys the zero-crossing information according to $\boldsymbol{c}_{\text{map}}$. To guarantee that the codeword $\boldsymbol{c}_{s_i}$ corresponding to the input symbol x_i fulfills the assignment given by $\boldsymbol{c}_{\text{map}}$, the state of the last sample of the previous symbol interval $\boldsymbol{c}_{s_{i-1}}$ termed ρ_{i-1} must be taken into account. This means that the mapping assignment can be processed for $\rho_{i-1} = 1$ or $\rho_{i-1} = -1$, which results in two possible codewords per each symbol x_i. In terms of sample sequence patterns, Table 3.2 shows the structure of $\boldsymbol{c}_s$ depending on ρ.

As explained, the codeword $\boldsymbol{c}_{\text{s}}$ depends on the last sample of $\boldsymbol{c}_{\text{s}_{i-1}}$. Hence, a predefined pilot signal $p_{\text{b}} \in \{1, -1\}$ is required to enable the mapping of the first transmit symbol of the sequence $\boldsymbol{x}$, which means that $p_{\text{b}} = \rho_0$ for x_1. Finally, the desired binary output pattern $\boldsymbol{c}_{\text{out}}$ with length $NM_{\text{Rx}} + 1$ which yields the zero-crossings in the desired intervals for a sequence of N Nyquist intervals is constructed sequentially by concatenating all the segments $\boldsymbol{c}_{\text{s}_i}$, where the first sample of $\boldsymbol{c}_{\text{out}}$ corresponds to p_{b}. The construction of $\boldsymbol{c}_{\text{out}}$ with TI ZX modulation is shown in Fig. 3.1 for $M_{\text{Rx}} = 3$. Note that $\boldsymbol{c}_{\text{out}}$ can also be constructed with RLL sequences [14], which then requires a different sequence detector.

Table 3.1: Zero-crossing assignment $\boldsymbol{c}_{\text{map}}$

$\boldsymbol{c}_{\text{map}}$	
symbol	Zero-crossing assignment
b_1	No zero-crossing
b_2	Zero-crossing in the M_{Rx} interval
b_3	Zero-crossing in the $M_{\text{Rx}}-1$ interval
$\vdots$	$\vdots$
$b_{R_{\text{in}}-1}$	Zero-crossing in the second interval
$b_{R_{\text{in}}}$	Zero-crossing in the first interval

Table 3.2: Sequence patterns $\boldsymbol{c}_{\text{s}}$

	$\boldsymbol{c}_{s_i}$	
symbol	$\rho_{i-1}=1$	$\rho_{i-1}=-1$
b_1	$1_1 \quad 1_2 \cdots \quad 1_{M_{\text{Rx}}-1} \quad 1_{M_{\text{Rx}}}$	$-1_1 \; -1_2 \cdots -1_{M_{\text{Rx}}-1} \; -1_{M_{\text{Rx}}}$
b_2	$1_1 \quad 1_2 \cdots \quad 1_{M_{\text{Rx}}-1} \; -1_{M_{\text{Rx}}}$	$-1_1 \; -1_2 \cdots -1_{M_{\text{Rx}}-1} \quad 1_{M_{\text{Rx}}}$
b_3	$1_1 \quad 1_2 \cdots -1_{M_{\text{Rx}}-1} \; -1_{M_{\text{Rx}}}$	$-1_1 \; -1_2 \cdots \quad 1_{M_{\text{Rx}}-1} \quad 1_{M_{\text{Rx}}}$
$\vdots$	$\vdots$	$\vdots$
$b_{R_{\text{in}}-1}$	$1_1 \; -1_2 \cdots -1_{M_{\text{Rx}}-1} \; -1_{M_{\text{Rx}}}$	$-1_1 \quad 1_2 \quad \cdots 1_{M_{\text{Rx}}-1} \quad 1_{M_{\text{Rx}}}$
$b_{R_{\text{in}}}$	$-1_1 \; -1_2 \cdots -1_{M_{\text{Rx}}-1} \; -1_{M_{\text{Rx}}}$	$1_1 \quad 1_2 \quad \cdots 1_{M_{\text{Rx}}-1} \quad 1_{M_{\text{Rx}}}$

3.2 Gray Coding for Time-Instance Zero-Crossing Modulation

The proposed bit mapping scheme based on Gray coding for TI ZX modulation implies that symbols with near or consecutive zero-crossings differ only in one bit from another. Table 3.3 shows the Gray mapping for $M_{\text{Rx}}=3$, where each binary tuple is mapped on one symbol. The sequence segment $\boldsymbol{c}_{\text{s}}$ is presented for each symbol depending on ρ. For cases when R_{in} is not a power of 2 as in the case of $M_{\text{Rx}}=2$, the mapping from bits to symbols can be based on sequences of symbols to reduce the conversion loss. In the illustrated example in Table 3.4 for $M_{\text{Rx}}=2$, the conversion loss corresponds to $(1.5-\log_2 3) \approx 0.085$ bits per symbol. The total number of transmitted bits in N Nyquist intervals for $M_{\text{Rx}}=3$ is $N_{\text{b}}=2N$, whereas for $M_{\text{Rx}}=2$, $N_{\text{b}}=3N/2$ bits per user per dimension are transmitted. For an input bit sequence $\boldsymbol{x}_{\text{b}}$ of length N_{b} and $M_{\text{Rx}}=2$, the construction of the $\boldsymbol{c}_{\text{out}}$ sequence is presented in Algorithm 1.

Algorithm 1 Construction of the $\boldsymbol{c}_{\text{out}}$ sequence algorithm for $M_{\text{Rx}} = 2$ given p_{b}

1: Partition $\boldsymbol{x}_{\text{b}}$ into $N_{\text{b}}/3$ segments $\rightarrow \boldsymbol{x}_{\text{bs}_i}$
2: Map $\boldsymbol{x}_{\text{bs}_1} \rightarrow \boldsymbol{c}_{\text{s}_1}$ with Table 3.4 and p_{b}
3: $\boldsymbol{c}_{\text{out}}$ = concatenate $[p_{\text{b}}, \boldsymbol{c}_{\text{s}_1}]$
4: **for** $i = 2 : 1 : N/2$
5: Map $\boldsymbol{x}_{\text{bs}_i} \rightarrow \boldsymbol{c}_{\text{s}_i}$ with Table 3.4 and ρ_{i-1} (last sample of $\boldsymbol{c}_{\text{s}_{i-1}}$)
6: $\boldsymbol{c}_{\text{out}}$ = concatenate $[\boldsymbol{c}_{\text{out}}, \boldsymbol{c}_{\text{s}_i}]$
end

Table 3.3: *Gray code* for $M_{\text{Rx}} = 3$

$M_{\text{Rx}} = 3$		
Gray code	$\boldsymbol{c}_{\text{s}}$ $(\rho_{i-1} = 1)$	$\boldsymbol{c}_{\text{s}}$ $(\rho_{i-1} = -1)$
00	$1 \quad 1 \quad 1$	$-1 \; -1 \; -1$
01	$1 \quad 1 \; -1$	$-1 \; -1 \quad 1$
11	$1 \; -1 \; -1$	$-1 \quad 1 \quad 1$
10	$-1 \; -1 \; -1$	$1 \quad 1 \quad 1$

Table 3.4: Proposed *Gray code* for $M_{\text{Rx}} = 2$

$M_{\text{Rx}} = 2$		
Gray Code	$[\boldsymbol{c}_{\text{s},2i}, \boldsymbol{c}_{\text{s},2i+1}]$ $\rho_{2i-1} = 1$	$[\boldsymbol{c}_{\text{s},2i}, \boldsymbol{c}_{\text{s},2i+1}]$ $\rho_{2i-1} = -1$
000	$1 \quad 1 \quad 1 \quad 1$	$-1 \; -1 \; -1 \; -1$
001	$1 \quad 1 \quad 1 \; -1$	$-1 \; -1 \; -1 \quad 1$
011	$1 \quad 1 \; -1 \; -1$	$-1 \; -1 \quad 1 \quad 1$
010	$1 \; -1 \; -1 \; -1$	$-1 \quad 1 \quad 1 \quad 1$
110	$1 \; -1 \; -1 \quad 1$	$-1 \quad 1 \quad 1 \; -1$
111	$-1 \; -1 \; -1 \quad 1$	$1 \quad 1 \quad 1 \; -1$
101	$-1 \; -1 \; -1 \; -1$	$1 \quad 1 \quad 1 \quad 1$
100	$-1 \; -1 \quad 1 \quad 1$	$1 \quad 1 \; -1 \; -1$

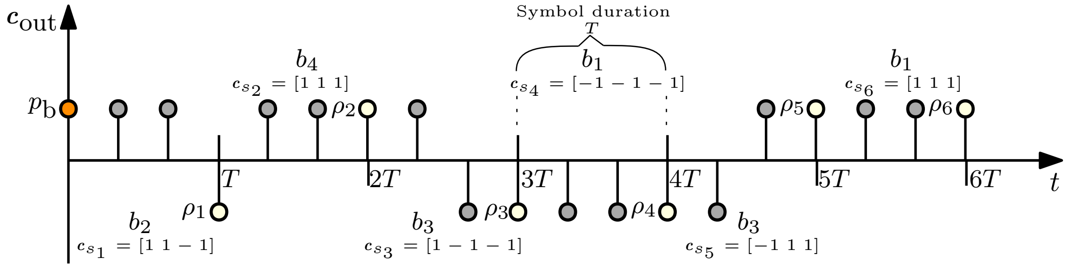

Figure 3.1: Example of the construction of $\boldsymbol{c}_{\text{out}}$ for $M_{\text{Rx}} = 3$.

3.3 Detection

The described detection process is considered for all proposed precoding methods, which will be presented later. The detection method should have low computational complexity. Hence, it is considered a detection technique based on the Hamming distance metric similar to that presented in [2]. Note that the in-phase and quadrature components of the received signal $\boldsymbol{z}_k$ are processed independently for all the users. For the detection process, the received signal $\boldsymbol{z}_k$ from (2-5) is considered. The TI ZX modulation implies a memory corresponding to the last sample of the previous symbol, denoted by ρ_{i-1} cf. Section 3.A. This memory property, defined by a single previous sample, does not imply a significant increase in the complexity of the receiver.

At the detector, the received signal $\boldsymbol{z}_R$ is divided into N overlapping subsequences of length $M_{\text{Rx}} + 1$ denoted as $\boldsymbol{z}_{b_i}$, where the first sample of $\boldsymbol{z}_{b_i}$ corresponds to the last sample of the previous subsequence $\boldsymbol{z}_{b_{i-1}}$. Subsequently, the backward mapping process is carried out $\overleftarrow{d} : \boldsymbol{z}_{b_i} \to \mathcal{X}_{\text{in}}$. In a noise free environment, all the subsequences $\boldsymbol{z}_{b_i}$ meet the requirements imposed in $\boldsymbol{c}_{\text{map}}$ so the detection is done only considering the backward mapping process and Table 3.1. All the valid subsequences for $\boldsymbol{z}_{b_{i-1}}$ are collected in the set $\mathcal{C}_{\text{det}}$ such that $\boldsymbol{z}_{b_i} \subseteq \mathcal{C}_{\text{det}}$. Table 3.5 shows the set $\mathcal{C}_{\text{det}}$ for $M_{\text{Rx}} = 3$ in a noise-free environment. The detection of the first symbol is done taking into account the pilot sample p_{b}. Fig. 3.2 shows an example of the construction of the subsequences $\boldsymbol{z}_{b_i}$ taking into account the pilot sample p_{b} and the last sample of the previous subsequence $\hat{\rho}_{i-1}$.

The backward mapping process described above is sufficient for establishing a unique detection in the noiseless environment allowing a perfect recovery of the input sequence $\boldsymbol{x}$. However, the noise can alter the received sequence $\boldsymbol{z}_R$ such that $\boldsymbol{z}_{b_i}$ can correspond to invalid segments. This means that $\boldsymbol{z}_{b_i} \nsubseteq \mathcal{C}_{\text{det}}$. Therefore, additional decision rules are defined considering the Hamming-distance metric [2]. In the presence of noise, the subsequence

Table 3.5: $\mathcal{C}_{\text{det}}$ for $M_{\text{Rx}} = 3$

$\mathcal{C}_{\text{det}}$								
symbol	$\boldsymbol{c}_{\text{det}}$							
	$\rho = 1$				$\rho = -1$			
b_1	1	1	1	1	-1	-1	-1	-1
b_2	1	1	1	-1	-1	-1	-1	1
b_3	1	1	-1	-1	-1	-1	1	1
b_4	1	-1	-1	-1	-1	1	1	1

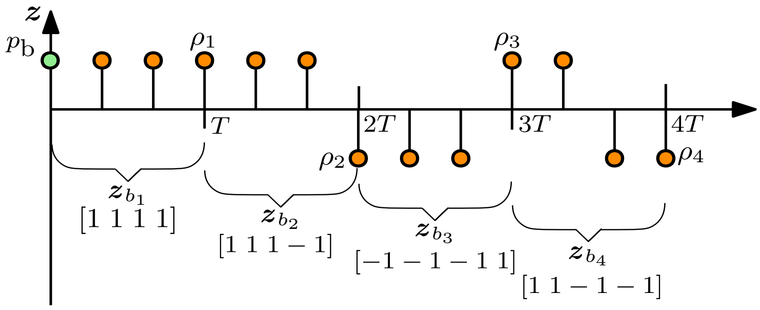

Figure 3.2: Representation of the $\boldsymbol{z}_{b,i}$ subsequences.

$\boldsymbol{z}_{b_i}$ is compared with all the valid subsequences from $\mathcal{C}_{\text{det}}$ with respect to the Hamming-distance. The codeword with the minimum Hamming-distance $\boldsymbol{c}$ is selected as the valid code segment and the backward mapping process is carried out. With this, the i-th symbol is detected according to

$$\widehat{x_i} = \overleftarrow{d}\left(\boldsymbol{c}\right), \quad \text{where} \quad \boldsymbol{c} = \arg\min_{\boldsymbol{c}_{\text{det}}} \ \text{Hamming}\left(\boldsymbol{z}_{b_i}, \boldsymbol{c}_{\text{det}}\right), \tag{3-1}$$

where Hamming $\left(\boldsymbol{z}_{b_i}, \boldsymbol{c}_{\text{det}}\right) = \sum_{n=1}^{M_{\text{Rx}}+1} \frac{1}{2} \left|\boldsymbol{z}_{b_i,n} - \boldsymbol{c}_{\text{det},n}\right|$, with $\boldsymbol{z}_{b_i,n}$ and $\boldsymbol{c}_{\text{det},n}$ being the nth element of the subsequence z_{b_i} and $\boldsymbol{c}_{\text{det}}$, respectively. Note that the mapping process does not incur error propagation, since if the last sample of the previous Nyquist interval ρ is detected wrong, it only affects the corresponding and subsequent Nyquist interval.

4
Optimization Based Precoding Methods

This chapter describes the precoding methods developed for the proposed TI ZX modulation.

4.1
MMDDT Criterion

When processing samples prior to detection, it is known that samples close to the decision threshold are more sensitive to perturbations. In this regard, MMDDT considers maximizing the minimum distance to the decision threshold, denoted as γ, as the optimization criterion. The maximization of γ is performed in the desired direction induced by $\boldsymbol{c}_{\text{out}}$. These techniques are presented in the following. First, the optimization problem is a direct formulation of the MMDDT precoding problem, which corresponds to a quadratically constrained quadratic program. The second strategy relies on an equivalent problem formulation which implies minimization of the transmit energy while taking the minimum distance to the decision threshold as a constraint, followed by scaling to the desired transmit energy. Another strategy to approach the MMDDT criterion in space and time involves using spatial ZF precoding and appropriately scaled, quality of service constrained temporal precoding, which further reduces the computational complexity. The existing technique based on the MMDDT criterion presented in [46], which yields the temporal precoding vector for user k for in-phase or quadrature component reads as

$$\begin{aligned} \min_{\boldsymbol{r}_{k\mathcal{R}/\mathcal{J}}} \quad & \boldsymbol{a}^{\mathrm{T}} \boldsymbol{r}_{k\mathcal{R}/\mathcal{J}} \\ \text{subject to:} \quad & \boldsymbol{B}_k \boldsymbol{r}_{k\mathcal{R}/\mathcal{J}} \preceq \mathbf{0} \\ & \boldsymbol{r}_{k\mathcal{R}/\mathcal{J}}^{\mathrm{T}} \boldsymbol{W}^{\mathrm{T}} \boldsymbol{W} \boldsymbol{r}_{k\mathcal{R}/\mathcal{J}} \leq \frac{1}{2} E_{\mathrm{Tx}}, \end{aligned} \tag{4-1}$$

where

$$
\begin{aligned}
\boldsymbol{r}_{k\mathcal{R}/\mathcal{J}} &= \left[\boldsymbol{p}^{T}_{\mathrm{x}_{k\mathcal{R}/\mathcal{J}}}, \gamma\right]^{\mathrm{T}} \\
\boldsymbol{a} &= \left[\boldsymbol{0}_{1\times N_{\mathrm{q}}}, -1\right]^{\mathrm{T}} \\
\boldsymbol{B}_k &= -\left[\beta \boldsymbol{C}_k \boldsymbol{V}\boldsymbol{U}, \boldsymbol{1}_{N_{\mathrm{tot}}\times 1}\right] \\
\boldsymbol{C}_k &= \operatorname{diag}\left(\boldsymbol{c}_{\mathrm{out}_{k\mathcal{R}/\mathcal{J}}}\right) \\
\boldsymbol{W} &= \left[\boldsymbol{G}^{T}_{\mathrm{Tx}}\boldsymbol{U}, \boldsymbol{0}_{N_{\mathrm{tot}}\times 1}\right],
\end{aligned}
\tag{4-2}
$$

and β refers to the real-valued beamforming gain [53]. The second constraint accounts for the transmit energy constraint considering $\frac{E_0}{E_{\mathrm{Tx}}} = N_{\mathrm{u}}$ and E_0 as the total transmit energy [47].

4.1.1 MMDDT Criterion in Space and Time

The proposed techniques based on MMDDT in space and time have been implemented considering stacked vector notation.

4.1.1.1 Joint MMDDT

For the joint MMDDT precoding process, each sequence $\boldsymbol{x}_k$ is forwarded to the TI ZX modulator for mapping to the desired output pattern $\boldsymbol{c}_{\mathrm{out}_k}$. In the $\boldsymbol{c}_{\mathrm{out}}$ stacking block, all the $\boldsymbol{c}_{\mathrm{out}_k}$ patterns are stacked for further processing. The corresponding real-valued representation of the stacked vector $\boldsymbol{c}_{\mathrm{out}}$ is a column vector of length $2N_{\mathrm{u}}N_{\mathrm{tot}}$, which reads as

$$
\boldsymbol{c}_{\mathrm{out}_R} = \left[\mathcal{R}\left\{\boldsymbol{c}_{\mathrm{out}_1}\right\}^T, \cdots, \mathcal{R}\left\{\boldsymbol{c}_{\mathrm{out}_{N_{\mathrm{u}}}}\right\}^T, \mathcal{J}\left\{\boldsymbol{c}_{\mathrm{out}_1}\right\}^T, \cdots, \mathcal{J}\left\{\boldsymbol{c}_{\mathrm{out}_{N_{\mathrm{u}}}}\right\}^T\right]^T .
\tag{4-3}
$$

The $\boldsymbol{c}_{\mathrm{out}_R}$ sequence serves as input to compute the space-time precoding vector $\boldsymbol{p}_{\mathrm{x}_R}$, which is the solution of a convex optimization problem. The waveform design optimization is addressed through the precoding optimization to maximize the minimum distance to the decision threshold of the received signal, termed γ. In the proposed maximization problem, all the users are addressed simultaneously, which is different from the approach used in [2,47]. Considering the maximum total transmit energy per block E_0, the corresponding equivalent optimization problem can be expressed in the epigraph form, cf. [54, Sec. 4.1.3], with

$$
\begin{aligned}
&\text{minimize}_{\boldsymbol{r}_R} \quad && \boldsymbol{a}^T \boldsymbol{r}_R \\
&\text{subject to:} \quad && \boldsymbol{B}\boldsymbol{r}_R \preceq \boldsymbol{0} \\
& && \left(\boldsymbol{W}\boldsymbol{r}_R\right)^T \left(\boldsymbol{W}\boldsymbol{r}_R\right) \leq E_0,
\end{aligned}
\tag{4-4}
$$

where

$$
\begin{aligned}
\boldsymbol{r}_R &= \left[\boldsymbol{p}_{x_R}^T, \gamma\right]^T, & \boldsymbol{a} &= \left[\boldsymbol{0}_{1\times 2N_\text{t}N_\text{q}}, -1\right]^T \\
\boldsymbol{B} &= \left[-\boldsymbol{C}\boldsymbol{H}_{\text{eff}_R}, \boldsymbol{1}_{2N_\text{tot}N_\text{u}\times 1}\right], & \boldsymbol{C} &= \text{diag}\left(\boldsymbol{c}_{\text{out}_R}\right) \\
\boldsymbol{W} &= \left[\boldsymbol{A}, \boldsymbol{0}_{6N_\text{tot}N_\text{t}\times 1}\right], & \boldsymbol{A} &= \left(\boldsymbol{I}_{2N_\text{t}} \otimes \boldsymbol{G}_\text{Tx}^T \boldsymbol{U}\right).
\end{aligned}
$$

The optimization problem in (4-4) has a linear objective, a quadratic, and a linear constraint, which is a particular case of the convex quadratically constrained quadratic program (QCQP), cf. [54, Sec. 4.4]. In the formulation of the convex optimization problem in (4-4), the objective function corresponds to the maximization of the minimum distance to the decision threshold of the received signal in the noise free case, where the vector $\boldsymbol{r}_R$ contains the temporal precoding vector of all the users and the distance to the decision threshold γ, which corresponds to its last entry. The first constraint addresses the optimization problem to maximize the minimum distance to the decision threshold in the desired direction induced by $\boldsymbol{c}_{\text{out}_R}$ considering the effective channel $\boldsymbol{H}_{\text{eff}_R}$. The second constraint with $\boldsymbol{W}$ accounts for the maximum transmit energy constraint. In the following, the precoding vector corresponding to the optimal solution in (4-4) is denoted by $\boldsymbol{p}_{\text{x}R_\text{joint}}$. Note that for a given problem, the optimal precoding vector $\boldsymbol{p}_{\text{x}R_\text{joint}}$ scales proportionally with $\sqrt{E_0}$ and γ in terms of $\boldsymbol{p}_{\text{x}R_\text{joint}} \propto \sqrt{E_0} \propto \gamma$. In other words, optimal precoding vectors with different power constraints can be readily extracted from the solution in (4-4). Therefore, an equivalent problem formulation to (4-4) is given by a reverse problem formulation in terms of a power minimization problem for a given positive scalar value for γ. The corresponding problem formulation is described as follows

$$
\begin{aligned}
&\text{minimize}_{r_{\text{p}_R}} \quad && \left(\boldsymbol{A}\boldsymbol{r}_{\text{p}_R}\right)^T \left(\boldsymbol{A}\boldsymbol{r}_{\text{p}_R}\right) \\
&\text{subject to:} \quad && \boldsymbol{B}_\text{opt}\boldsymbol{r}_{\text{p}_R} \preceq -\gamma\boldsymbol{1},
\end{aligned}
\tag{4-5}
$$

where $\boldsymbol{B}_\text{opt} = -\boldsymbol{C}\boldsymbol{H}_{\text{eff}_R}$. The problem formulation in (4-5) corresponds to a convex quadratic program given that $\boldsymbol{A}^T\boldsymbol{A}$ is positive semi-definite. In this case, the precoding vector $\boldsymbol{p}_{\text{x}_R}$ is a scaled version of the optimization variable in terms of $\boldsymbol{r}_{\text{p}_R} = \alpha\boldsymbol{p}_{\text{x}_R}$. The solution to the problem in (4-4) can be obtained by scaling the solution of (4-5) such that the total power constraint holds with equality. Taking into account the power constraint $\left(\boldsymbol{W}\boldsymbol{r}_R\right)^\text{T}\left(\boldsymbol{W}\boldsymbol{r}_R\right) = E_0$ and the power of the scaled version $\left(\boldsymbol{A}\boldsymbol{r}_{\text{p}_R}\right)^\text{T}\left(\boldsymbol{A}\boldsymbol{r}_{\text{p}_R}\right) = E$, it is possible to extract $\boldsymbol{p}_{\text{x}R_\text{joint}}$ from $\boldsymbol{r}_{\text{p}_R}$ with the scaling factor given by $\alpha = \sqrt{E/E_0}$. With this, the precoding vector reads as $\boldsymbol{p}_{\mathrm{x}_{R_{\mathrm{joint}}}} = \boldsymbol{r}_{\mathrm{p}_R}/\alpha$.

4.1.1.2 Joint MMDDT ZF

An approximate solution for the problem in (4-4) can be obtained with a lower computational complexity considering that spatial ZF precoding [55] is employed and that the convex optimization problem is solved separately per user and dimension for a given positive scalar value of γ and scaling due to the total power constraint as the final step.

The conventional spatial ZF precoding matrix [56] is defined as

$$\boldsymbol{P}_{\mathrm{sp}} = c_{\mathrm{zf}} \boldsymbol{P}_{\mathrm{zf}} \quad \text{with} \quad \boldsymbol{P}_{\mathrm{zf}} = \boldsymbol{H}^H \left(\boldsymbol{H}\boldsymbol{H}^H \right)^{-1}, \tag{4-6}$$

where the ZF scaling factor is expressed as

$$c_{\mathrm{zf}}^2 = \left(N_{\mathrm{u}} / \mathrm{trace} \left(\left(\boldsymbol{H}\boldsymbol{H}^H \right)^{-1} \right) \right). \tag{4-7}$$

The optimization problem per user and dimension for a given minimum distance γ, like considered as a quality of service constraint in [57], can be expressed as a convex quadratic program given by

$$\begin{aligned} &\text{minimize}_{\boldsymbol{r}_{\mathrm{zf}_{k\mathcal{R}/\mathcal{J}}}} && (\boldsymbol{W}\boldsymbol{r}_{\mathrm{zf}_{k\mathcal{R}/\mathcal{J}}})^T (\boldsymbol{W}\boldsymbol{r}_{\mathrm{zf}_{k\mathcal{R}/\mathcal{J}}}) \\ &\text{subject to:} && \boldsymbol{B}_k \boldsymbol{r}_{\mathrm{zf}_{k\mathcal{R}/\mathcal{J}}} \preceq -\gamma \boldsymbol{a}, \end{aligned} \tag{4-8}$$

where

$$\begin{aligned} \boldsymbol{B}_k &= -\beta \left(\boldsymbol{C}_k \boldsymbol{V} \boldsymbol{U} \right) \\ \boldsymbol{C}_k &= \mathrm{diag} \left(\boldsymbol{c}_{\mathrm{out}_{k\mathcal{R}/\mathcal{J}}} \right) \\ \boldsymbol{a} &= \left[\boldsymbol{1}_{M_{\mathrm{Rx}} N + 1 \times 1} \right]. \end{aligned}$$

In (4-8) β acts as an effective channel gain that results from the channel and the ZF precoding $\beta \boldsymbol{I} = \boldsymbol{H}\boldsymbol{P}_{\mathrm{sp}}$. The subscript $\mathcal{R}/\mathcal{J}$ denotes that the problem is solved separately for the in-phase and quadrature component of the signal and the corresponding complex representation is denoted by $\boldsymbol{r}_{\mathrm{zf}_k} = \boldsymbol{r}_{\mathrm{zf}_{\mathrm{k}\mathcal{R}}} + j \boldsymbol{r}_{\mathrm{zf}_{\mathrm{k}\mathcal{J}}}$.

The constraint in (4-8) ensures that the noise free received signal after quantization is equal to $\boldsymbol{c}_{\mathrm{out}_{k\mathcal{R}/\mathcal{J}}}$. The symbol $\preceq$ in (4-8) constrains each element of the vector $\boldsymbol{B}_k \boldsymbol{r}_{\mathrm{zf}_{k\mathcal{R}/\mathcal{J}}}$ to be less than or equal to $-\gamma$ such that the minimum distance of the samples of the received signal to the decision threshold is equal to γ. Implicitly, the optimization problem shapes the waveform $y(t)$ at the receiver, which is described in the discrete model by $\beta \boldsymbol{V}\boldsymbol{U}\boldsymbol{p}_{\mathrm{x}_k}$ for the noiseless case. The total transmit energy considering the temporal and spatial precoding can be computed as

$$E_{\mathrm{Tx}} = \mathrm{trace}\left(\boldsymbol{P}_{\mathrm{sp}}\boldsymbol{R}_{\mathrm{x_{Tx}}}\boldsymbol{R}^{\mathrm{H}}_{\mathrm{x_{Tx}}}\boldsymbol{P}^{\mathrm{H}}_{\mathrm{sp}}\right), \tag{4-9}$$

where the matrix $\boldsymbol{R}_{\mathrm{x_{Tx}}}$ is given by

$$\boldsymbol{R}_{\mathrm{x_{Tx}}} = \left[(\boldsymbol{G}^{\mathrm{T}}_{\mathrm{Tx}}\boldsymbol{U}\boldsymbol{r}_{\mathrm{zf}_1})^{\mathrm{T}}; (\boldsymbol{G}^{\mathrm{T}}_{\mathrm{Tx}}\boldsymbol{U}\boldsymbol{r}_{\mathrm{zf}_2})^{\mathrm{T}}; \cdots ; (\boldsymbol{G}^{\mathrm{T}}_{\mathrm{Tx}}\boldsymbol{U}\boldsymbol{r}_{\mathrm{zf}_{N_\mathrm{u}}})^{\mathrm{T}}\right]. \tag{4-10}$$

An appropriate temporal precoding matrix that fulfills the total energy constraint with equality can be found via scaling the complex matrix defined as $\boldsymbol{P}_{\mathrm{x_{temp}}} = \frac{1}{\alpha_{zf}}\left[\boldsymbol{r}^{T}_{\mathrm{zf}_1}; \boldsymbol{r}^{T}_{\mathrm{zf}_2}; \cdots ; \boldsymbol{r}^{T}_{\mathrm{zf}_{N_\mathrm{u}}}\right]$. Taking into account E_{Tx} and the desired transmit energy E_0, the scaling factor is given by $\alpha_{zf} = \sqrt{E_{\mathrm{Tx}}/E_0}$. After defining the matrix $\boldsymbol{P}_{\mathrm{x_{st}}} = \boldsymbol{P}_{\mathrm{sp}}\boldsymbol{P}_{\mathrm{x_{temp}}}$ it is vectorized as $\boldsymbol{p}_{\mathrm{x_{stk}}} = \mathrm{vec}(\boldsymbol{P}^{T}_{\mathrm{x_{st}}})$. Finally, the corresponding real-valued notation $\boldsymbol{p}_{\mathrm{x}_{\mathrm{stk}_R}}$ serves as an approximate solution for the problem in (4-4) such that $\boldsymbol{p}_{\mathrm{x}_{\mathrm{stk}_R}} \approx \boldsymbol{p}_{\mathrm{x}_{R_{\mathrm{joint}}}}$.

4.1.2 Numerical Results

This section presents the numerical evaluation of the proposed MMDDT TI ZX precoding techniques, in terms of the uncoded BER. The proposed precoding methods are compared with the state-of-the-art method in terms of quantization precoding [2]. The simulations were carried out for different sets of signaling rate (M_{Tx}/T) and sampling rate (M_{Rx}/T). For all the evaluated configurations, $g_{\mathrm{Tx}}(t)$ is an RC filter and the receive filter $g_{\mathrm{Rx}}(t)$ is an RRC filter, where the roll-off factors are $\epsilon_{\mathrm{Tx}} = \epsilon_{\mathrm{Rx}} = 0.22$, as in [2]. The bandwidth is defined with $W_{\mathrm{Rx}} = W_{\mathrm{Tx}} = (1+\epsilon_{\mathrm{Tx}})/T_{\mathrm{s}}$, wherein the simulations it is considered $T = T_{\mathrm{s}}$. A Rayleigh fading model is considered for the channel matrix $\boldsymbol{H}$, whose entries are i.i.d. zero-mean complex Gaussian distributed with unit variance. The noise samples are complex Gaussian with zero mean and variance σ_n^2. Moreover, in all the evaluated scenarios, the BS is equipped with $N_{\mathrm{t}} = 8$ antennas, $N_{\mathrm{u}} = 2$ users, $N = 30$ Nyquist intervals, and maximum energy constraint E_0. The SNR is defined by the ratio between the transmit power and the noise power in the occupied bandwidth. With noise spectral density N_0, the SNR can be defined as

$$\mathrm{SNR} = \frac{E_0/(NT)}{N_0(1+\epsilon_{\mathrm{Tx}})/T} = \frac{E_0}{NN_0(1+\epsilon_{\mathrm{Tx}})}. \tag{4-11}$$

Note that (4-11) can also be interpreted as the common receive SNR (in the occupied frequency band) for the case of uncorrelated signals at the transmit antennas.

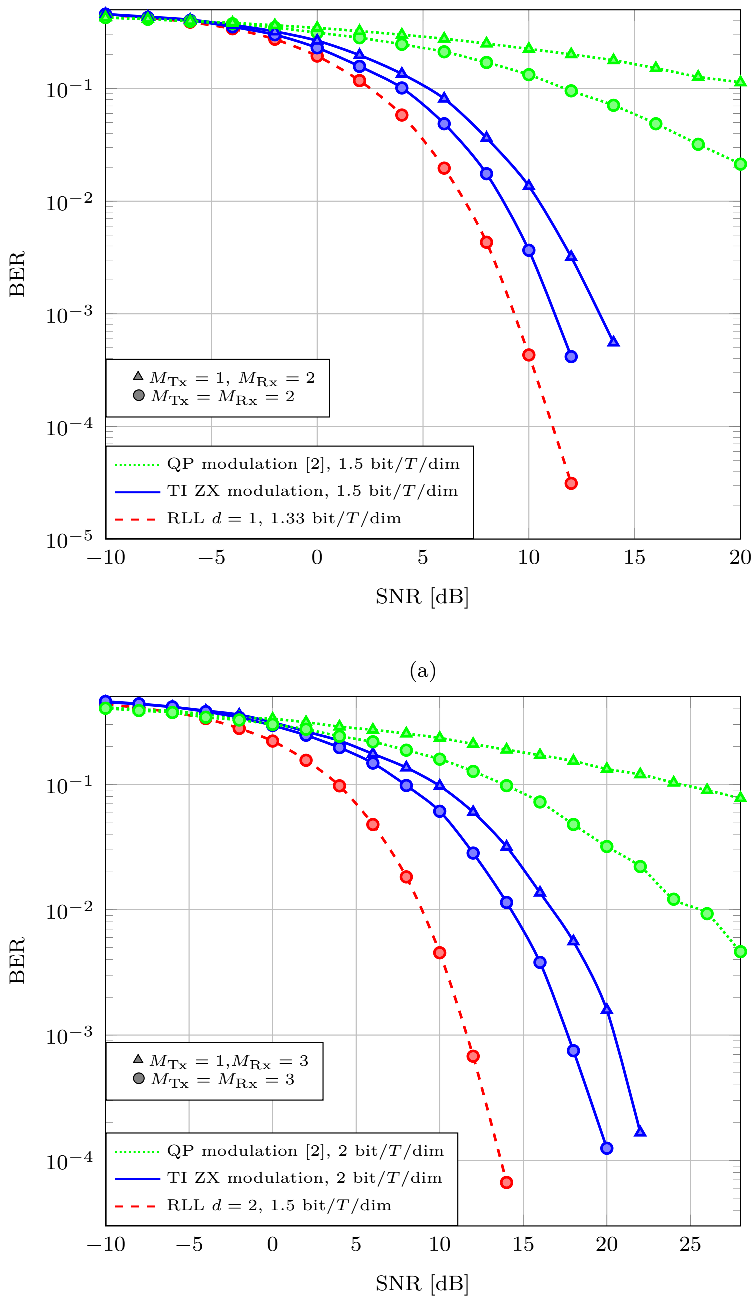

(a)

(b)

Figure 4.1: BER comparison of the considered modulations. In (a) for $M_{\text{Rx}} = 2$ and in (b) for $M_{\text{Rx}} = 3$.

A BER comparison between TI ZX modulation, QP modulation [2] and RLL modulation [14] is presented, where the established precoding methods are considered with per user per dimension MMDDT in combination with spatial ZF precoding [47], [2].

The TI ZX modulation and QP modulation approaches are evaluated with the same rate and under the same simulation environment for different sets. The considered modulations result in different data rate: For TI ZX with $M_{\mathrm{Rx}} = 3$, 2 bit/T/dim and with $M_{\mathrm{Rx}} = 2$, 1.5 bit/T/dim. In the case of RLL sequences for $M_{\mathrm{Rx}} = 2$ and parameter $d = 1$, 1.33 bit/T/dim are considered and for $M_{\mathrm{Rx}} = 3$ and $d = 2$, 1.5 bit/T/dim. With this, the throughput for TI ZX is higher than the throughput for RLL and QPSK.

Fig. 4.1 compares the TI ZX modulation, QP modulation [2] and RLL sequences in terms of the BER. It can be observed that the TI ZX modulation yields better performance than QP modulation, which can be explained by the fact that TI ZX modulation sequences contain on average, a smaller number of zero-crossings in comparison with sequences constructed with QP modulation [2]. In the presence of appropriate bandlimitation, the QP method with its relatively large number of zero-crossings, indirectly yields a lower performance in the waveform optimization. Note that, without bandlimitation, QP modulation [2] and the proposed TI ZX modulation can be equivalent in terms of γ or MSE as shown in [47, Fig. 3] and [48, Fig. 3], where the effect of bandlimitation is investigated. On the other hand, RLL mapping achieves a lower BER than TI ZX and QP modulation approaches. However, the proposed TI ZX yields a higher data rate and its detection scheme has lower complexity than the Viterbi detector for RLL sequences [51]. Note that sequence construction with 4-ASK symbols [11, 13, 14] has a lower computational complexity than the proposed modulation approach but would result in out-of-band radiation.

The BER comparison of the MMDDT based precoding techniques is shown in Fig. 4.2. It can be observed that in the high SNR regime, the established MMDDT ZF precoding technique is outperformed significantly by the precoders considering the MMDDT criterion jointly in space and time. Moreover, Fig. 4.2 shows that the alternative formulation of the joint MMDDT with (4-5) yields an equivalent performance to the direct joint MMDDT formulation (4-4). A complexity performance trade-off is found in the total MMDDT ZF (4-8), which yields a better BER performance than the MMDDT ZF while having the lowest computational complexity among all the methods, as confirmed in Table 4.1.

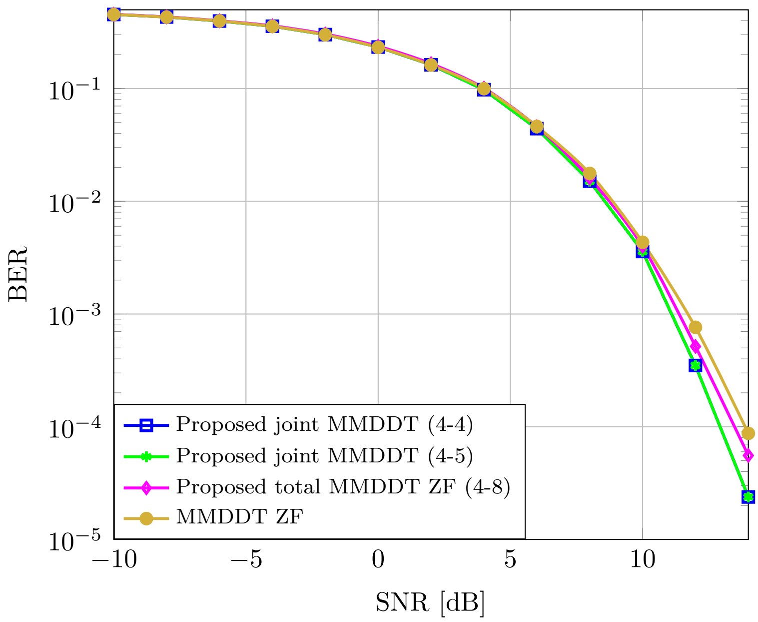

Figure 4.2: BER vs. SNR for Joint MMDDT and total MMDDT ZF with $M_{\text{Rx}} = M_{\text{Tx}} = 2$, considering the proposed TI ZX modulation.

4.2 MMSE Criterion in Space and Time

The general MMSE precoding problem with TI ZX modulation is formulated as

$$\begin{aligned} \text{minimize}_{f>0,\boldsymbol{p}_{\text{x}}} \quad & \mathrm{E}\{\|f(\boldsymbol{H}_{\text{eff}}\boldsymbol{p}_{\text{x}} + \boldsymbol{G}_{\text{Rx,eff}}\boldsymbol{n}) - \boldsymbol{c}_{\text{out}}\|_2^2\} \\ \text{subject to:} \quad & \boldsymbol{p}_{\text{x}}^H \boldsymbol{A}^H \boldsymbol{A} \boldsymbol{p}_{\text{x}} \leq E_0 \end{aligned} \tag{4-12}$$

with $\boldsymbol{A} = \boldsymbol{I}_{N_{\text{t}}} \otimes \boldsymbol{G}_{\text{Tx}}^T \boldsymbol{U}$. Note that the scaling factor f is essential for the MMSE problem formulation, however f does not need to be included in the system model because scaling at the receiver does not change the output of the 1-bit quantization. The sequence $\boldsymbol{c}_{\text{out}}$ is obtained by stacking in a column vector the $\boldsymbol{c}_{\text{out}_k}$ patterns expressed as $\boldsymbol{c}_{\text{out}} = [\boldsymbol{c}_{\text{out}_1}^T, \boldsymbol{c}_{\text{out}_2}^T, \cdots, \boldsymbol{c}_{\text{out}_k}^T, \cdots, \boldsymbol{c}_{\text{out}_{N_{\text{u}}}}^T]^T$. It can be shown that the MSE optimal solution of $\boldsymbol{p}_{\text{x}}$ corresponds to a maximum total transmit energy E_0. The linear MMSE precoder minimizes the mean square error between the received signal $\boldsymbol{z}$ and the desired output pattern $\boldsymbol{c}_{\text{out}}$ with transmit energy E_0. By exploiting the knowledge that the optimal precoding vector must fulfill the total energy constraint with equality, the optimization problem in (4-12) can be solved in closed form, e.g., by a strategy similar to what is presented in [58]. With this, the optimal solution of (4-12) is given by

$$\boldsymbol{p}_{\mathrm{x_{MSE}}} = f^{-1}\left(\boldsymbol{H}_{\mathrm{eff}}^{H}\boldsymbol{H}_{\mathrm{eff}} + E_0{}^{-1}\mathrm{trace}\{\boldsymbol{G}_{\mathrm{Rx,eff}}^{H}\boldsymbol{C}_n\boldsymbol{G}_{\mathrm{Rx,eff}}\}\boldsymbol{A}^{H}\boldsymbol{A}\right)^{-1}\boldsymbol{H}_{\mathrm{eff}}^{H}\boldsymbol{c}_{\mathrm{out}}, \tag{4-13}$$

where the scaling factor is defined by $f = \left\|\boldsymbol{c}_{\mathrm{out}}^{H}\boldsymbol{\Delta}\right\|_2/\sqrt{E_0}$ and $\boldsymbol{C}_n = \mathbb{E}\left[\boldsymbol{n}\boldsymbol{n}^{H}\right]$ corresponds to the noise covariance matrix. The derivation of (4-13) and the description of the matrix $\boldsymbol{\Delta}$ are provided in Appendix A.1. Using (4-13), the MSE of the received signal samples can be expressed as

$$\begin{aligned} MSE =& \mathrm{trace}\{\boldsymbol{H}_{\mathrm{eff}}\boldsymbol{X}\boldsymbol{H}_{\mathrm{eff}}^{H}\mathrm{E}\{\boldsymbol{c}_{\mathrm{out}}\boldsymbol{c}_{\mathrm{out}}^{H}\}\boldsymbol{H}_{\mathrm{eff}}\boldsymbol{X}^{H}\boldsymbol{H}_{\mathrm{eff}}^{H}\} \\ &- 2\mathrm{Re}\{\mathrm{trace}\{\boldsymbol{H}_{\mathrm{eff}}\boldsymbol{X}\boldsymbol{H}_{\mathrm{eff}}^{H}\mathrm{E}\{\boldsymbol{c}_{\mathrm{out}}\boldsymbol{c}_{\mathrm{out}}^{H}\}\}\} + 2N_{\mathrm{tot}} \\ &+ (1/E_0)\mathrm{trace}\{\boldsymbol{\Delta}^{H}\mathrm{E}\{\boldsymbol{c}_{\mathrm{out}}\boldsymbol{c}_{\mathrm{out}}^{H}\}\boldsymbol{\Delta}\}\mathrm{trace}\{\boldsymbol{G}_{\mathrm{Rx,eff}}\boldsymbol{C}_n\boldsymbol{G}_{\mathrm{Rx,eff}}^{H}\}, \end{aligned} \tag{4-14}$$

where $\boldsymbol{X} = \left(\boldsymbol{H}_{\mathrm{eff}}^{H}\boldsymbol{H}_{\mathrm{eff}} + E_0^{-1}\mathrm{trace}\{\boldsymbol{G}_{\mathrm{Rx,eff}}\boldsymbol{C}_n\boldsymbol{G}_{\mathrm{Rx,eff}}^{H}\}\boldsymbol{A}^{H}\boldsymbol{A}\right)^{-1}$.

4.2.1 MMSE With Active Constellation Extension

The MSE cost function in the proposed system also penalizes waveforms where the received signal has amplitude larger than 1 per dimension, which is not a disadvantage for detection performance. This issue corresponds to a relatively poor BER performance for high SNR. Allowing for the case that the amplitude of the received signal can be larger than 1 the MMSE problem can be reformulated using the active constellation extension [49]. The ACE corresponds to an extension of $\boldsymbol{c}_{\mathrm{out}}$ to constellation point with relaxation in amplitude which can be larger or equal to 1.

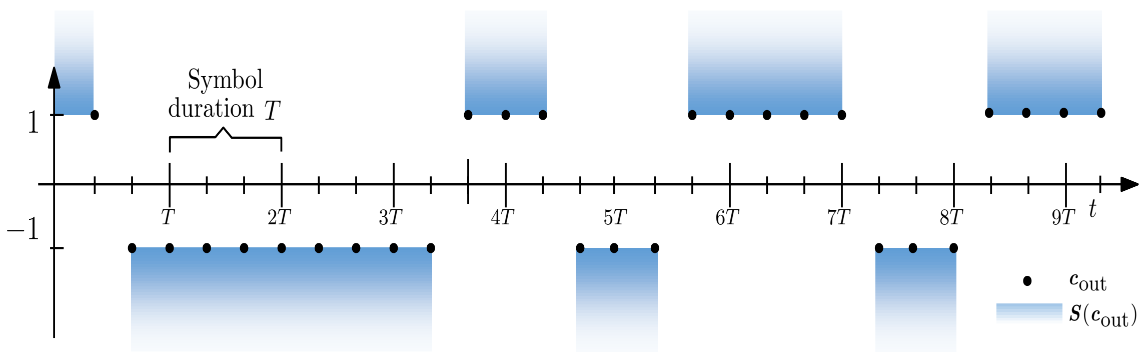

Figure 4.3: Active constellation extension example for a given $\boldsymbol{c}_{\mathrm{out}}$.

It is considered that the constellation points $\boldsymbol{s}$ in the region $\mathcal{S}(\boldsymbol{c}_{\mathrm{out}})$ are chosen with the MSE criterion. An example of the ACE is shown in Fig. 4.3, where the constellation region $\mathcal{S}(\boldsymbol{c}_{\mathrm{out}})$ is determined by $\boldsymbol{c}_{\mathrm{out}}$. Using $\boldsymbol{s} \in \mathcal{S}(\boldsymbol{c}_{\mathrm{out}})$, the extension of (4-12) can be formulated as

$$\begin{aligned} \text{minimize}_{\boldsymbol{s},f>0,\boldsymbol{p}_{\text{x}}} \quad & \text{E}\{\|f\boldsymbol{H}_{\text{eff}}\boldsymbol{p}_{\text{x}} - \boldsymbol{s}\|_2^2\} + f^2\text{trace}\{\boldsymbol{G}_{\text{Rx,eff}}\boldsymbol{C}_{\text{n}}\boldsymbol{G}_{\text{Rx,eff}}^H\} \\ \text{subject to:} \quad & \boldsymbol{p}_{\text{x}}^H\boldsymbol{A}^H\boldsymbol{A}\boldsymbol{p}_{\text{x}} \leq E_0 \\ & \boldsymbol{s} \in \mathcal{S}(\boldsymbol{c}_{\text{out}}). \end{aligned} \tag{4-15}$$

In order to approach the solution for the problem in (4-15) two strategies are developed in the following in terms of the MMSE ACE and iterative MMSE ACE.

4.2.1.1 Optimal MMSE ACE

The proposed optimal MMSE ACE formulates the problem in (4-15) as a convex optimization problem for jointly solving the problem with respect to f, $\boldsymbol{s}$, and $\boldsymbol{p}_{\text{x}}$. Rewriting (4-15) with real-valued notation yields

$$\begin{aligned} \text{minimize}_{\boldsymbol{s}_R,f>0,\boldsymbol{p}_{\text{x}_R}} \quad & \text{E}\{\|f(\boldsymbol{H}_{\text{eff}_R}\boldsymbol{p}_{\text{x}_R}) - \boldsymbol{s}_R\|_2^2\} + f^2\text{trace}\{\boldsymbol{G}_{\text{Rx,eff}_R}\boldsymbol{C}_{\text{n}_R}\boldsymbol{G}_{\text{Rx,eff}_R}^T\} \\ \text{subject to:} \quad & \boldsymbol{p}_{\text{x}_R}^T\boldsymbol{A}_R^T\boldsymbol{A}_R\boldsymbol{p}_{\text{x}_R} \leq E_0 \\ & \boldsymbol{C}\boldsymbol{s}_R \succeq \boldsymbol{1} \end{aligned} \tag{4-16}$$

where $\boldsymbol{C} = \text{diag}(\boldsymbol{c}_{\text{out}_R})$. By introducing $\boldsymbol{p}_{\text{fx}_R} = \boldsymbol{p}_{\text{x}_R}f$, (4-16) can be rewritten as

$$\begin{aligned} \text{minimize}_{\boldsymbol{s}_R,f>0,\boldsymbol{p}_{\text{fx}_R}} \quad & \text{E}\{\|\boldsymbol{H}_{\text{eff}_R}\boldsymbol{p}_{\text{fx}_R} - \boldsymbol{s}_R\|_2^2\} + f^2\text{trace}\{\boldsymbol{G}_{\text{Rx,eff}_R}\boldsymbol{C}_{\text{n}_R}\boldsymbol{G}_{\text{Rx,eff}_R}^T\} \\ \text{subject to:} \quad & \boldsymbol{p}_{\text{fx}_R}^T\boldsymbol{A}_R^T\boldsymbol{A}_R\boldsymbol{p}_{\text{fx}_R} \leq f^2E_0 \\ & \boldsymbol{C}\boldsymbol{s}_R \succeq \boldsymbol{1}. \end{aligned} \tag{4-17}$$

Considering the stacked vector $\boldsymbol{\nu} = \left[\boldsymbol{p}_{\text{fx}_R}^T, \boldsymbol{s}_R^T, f\right]^T$ the problem in (4-17) can be expressed as

$$\begin{aligned} \text{minimize}_{\boldsymbol{\nu}} \quad & \boldsymbol{\nu}^T\boldsymbol{\Omega}\boldsymbol{\nu} \\ \text{subject to:} \quad & \|\boldsymbol{R}\boldsymbol{\nu}\|_2 \leq \sqrt{E_0}\boldsymbol{\delta}^T\boldsymbol{\nu} \\ & \boldsymbol{\delta}^T\boldsymbol{\nu} > 0 \\ & \boldsymbol{\Lambda}\boldsymbol{\nu} \succeq \boldsymbol{1}, \end{aligned} \tag{4-18}$$

where

$$\begin{aligned}
\boldsymbol{\Omega} &= \boldsymbol{\Theta}^T\boldsymbol{\Theta} + \boldsymbol{\Xi} \\
\boldsymbol{\Theta} &= [\boldsymbol{H}_{\mathrm{eff}_R}, \boldsymbol{0}_{2N_\mathrm{u}N_\mathrm{tot}\times 2N_\mathrm{u}N_\mathrm{tot}+1}] - \left[\boldsymbol{0}_{2N_\mathrm{u}N_\mathrm{tot}\times 2N_\mathrm{q}N_\mathrm{t}}, \boldsymbol{I}_{2N_\mathrm{u}N_\mathrm{tot}}, \boldsymbol{0}_{2N_\mathrm{u}N_\mathrm{tot}\times 1}\right] \\
\boldsymbol{\Xi} &= \mathrm{diag}\left(\left[\boldsymbol{0}_{1\times 2N_\mathrm{q}N_\mathrm{t}+2N_\mathrm{tot}N_\mathrm{u}}, \mathrm{trace}\{\boldsymbol{G}_{\mathrm{Rx,eff}_R}\boldsymbol{C}_{\mathrm{n}_R}\boldsymbol{G}^T_{\mathrm{Rx,eff}_R}\}\right]\right) \\
\boldsymbol{R} &= [\boldsymbol{A}_R, \boldsymbol{0}_{6N_\mathrm{t}N_\mathrm{tot}\times 2N_\mathrm{u}N_\mathrm{tot}+1}] \\
\boldsymbol{\delta} &= \left[\boldsymbol{0}_{1\times 2N_\mathrm{q}N_\mathrm{t}+2N_\mathrm{tot}N_\mathrm{u}}, 1\right]^T \\
\boldsymbol{\Lambda} &= \left[\boldsymbol{0}_{2N_\mathrm{tot}N_\mathrm{u}\times 2N_\mathrm{q}N_\mathrm{t}}, \boldsymbol{C}, \boldsymbol{0}_{2N_\mathrm{tot}N_\mathrm{u}\times 1}\right].
\end{aligned}$$

Considering $\boldsymbol{L} = \sqrt{\boldsymbol{\Omega}}$ the objective function in (4-18) becomes $\boldsymbol{\nu}^T\boldsymbol{L}\boldsymbol{L}^T\boldsymbol{\nu} = \left\|\boldsymbol{L}^T\boldsymbol{\nu}\right\|_2^2$. Then, by considering the 2-norm, an equivalent optimization problem as in (4-18) is given by

$$\begin{aligned}
\text{minimize}_{\boldsymbol{\nu}} \quad & \left\|\boldsymbol{L}^T\boldsymbol{\nu}\right\|_2 \\
\text{subject to:} \quad & \|\boldsymbol{R}\boldsymbol{\nu}\|_2 \le \sqrt{E_0}\boldsymbol{\delta}^T\boldsymbol{\nu} \\
& \boldsymbol{\delta}^T\boldsymbol{\nu} > 0 \\
& \boldsymbol{\Lambda}\boldsymbol{\nu} \succeq \boldsymbol{1}.
\end{aligned} \tag{4-19}$$

By considering the epigraph form, the problem in (4-19) can be expressed as a SOCP in standard form. By introducing $\eta \ge \left\|\boldsymbol{L}^T\boldsymbol{\nu}\right\|_2$, the objective function in (4-19) can be replaced by η. Using stacked vector notation with $\boldsymbol{\xi} = [\eta, \boldsymbol{\nu}]$, an equivalent problem to (4-19) is given by

$$\begin{aligned}
\text{minimize}_{\boldsymbol{\xi}} \quad & \boldsymbol{\theta}^T\boldsymbol{\xi} \\
\text{subject to:} \quad & \|\boldsymbol{\Gamma}^T\boldsymbol{\xi}\|_2 \le \boldsymbol{\theta}^T\boldsymbol{\xi} \\
& \|\boldsymbol{D}\boldsymbol{\xi}\|_2 \le \sqrt{E_0}\boldsymbol{\psi}^T\boldsymbol{\xi} \\
& \boldsymbol{\psi}^T\boldsymbol{\xi} > 0 \\
& \boldsymbol{\Phi}\boldsymbol{\xi} \succeq \boldsymbol{1},
\end{aligned} \tag{4-20}$$

Algorithm 2 Proposed iterative MMSE ACE algorithm

1: Calculate $\boldsymbol{p}_\mathrm{x}$and $f \rightarrow$ by (4-13) for a given $\boldsymbol{c}_\mathrm{out}$ vector
repeat
2: Calculate $\boldsymbol{s}_\mathrm{p} = f\boldsymbol{H}_\mathrm{eff}\boldsymbol{p}_\mathrm{x}$
3: Extract samples from $\boldsymbol{s}_\mathrm{p}$ such that $\rightarrow \boldsymbol{s}_\mathrm{aux} = \left\{\boldsymbol{s}_{\mathrm{p}_i} \mid \left|\boldsymbol{s}_{\mathrm{p}_i}\right| < 1\right\}$
4: Bring $\boldsymbol{s}_\mathrm{aux}$ to -1 or 1 according to $\boldsymbol{c}_\mathrm{out}$
5: Generate $\boldsymbol{s}, \rightarrow \boldsymbol{s} = \left\{\boldsymbol{s}_\mathrm{p} \mid \left|\boldsymbol{s}_{\mathrm{p}_i}\right| < 1 = \boldsymbol{s}_{\mathrm{aux}_i}\right\}$
6: Calculate $\boldsymbol{p}_\mathrm{x}$ and $f \rightarrow$ by (4-13) with $\boldsymbol{s}$ instead of $\boldsymbol{c}_\mathrm{out}$
until convergence criterion triggers

where

$$
\begin{aligned}
\boldsymbol{D} \quad & = [\mathbf{0}_{6N_\mathrm{t}N_\mathrm{tot}\times 1}, \boldsymbol{R}] \\
\boldsymbol{\Gamma} \quad & = \left[\mathbf{0}_{1\times 2N_\mathrm{q}N_\mathrm{t}+2N_\mathrm{tot}N_\mathrm{u}+1}; \left[\mathbf{0}_{1\times 2N_\mathrm{q}N_\mathrm{t}+2N_\mathrm{tot}N_\mathrm{u}+1}, \boldsymbol{L}\right]\right] \\
\boldsymbol{\psi} \quad & = \left[\mathbf{0}_{1\times 2N_\mathrm{q}N_\mathrm{t}+2N_\mathrm{tot}N_\mathrm{u}+1}, 1\right]^T \\
\boldsymbol{\theta} \quad & = \left[1, \mathbf{0}_{1\times 2N_\mathrm{q}N_\mathrm{t}+2N_\mathrm{tot}N_\mathrm{u}+1}\right]^T \\
\boldsymbol{\Phi} \quad & = [\mathbf{0}_{2N_\mathrm{tot}N_\mathrm{u}\times 1}, \boldsymbol{\Lambda}] .
\end{aligned}
$$

4.2.1.2
Iterative MMSE ACE Algorithm

The iterative MMSE ACE algorithm is proposed as an alternative approach to finding an approximate solution for the problem in (4-15) with an iterative strategy and reduced complexity. The initial step to find $\boldsymbol{s} \in S(\boldsymbol{c}_\mathrm{out})$ is to solve the MMSE problem using (4-13) considering $\boldsymbol{c}_\mathrm{out}$. With the corresponding precoding vector $\boldsymbol{p}_\mathrm{x}$, the auxiliary vector $\boldsymbol{s}_\mathrm{p}$ is calculated by $\boldsymbol{s}_\mathrm{p} = f\boldsymbol{H}_\mathrm{eff}\boldsymbol{p}_\mathrm{x}$. Note that the vector $\boldsymbol{s}_\mathrm{p}$ can include samples with small amplitudes, i.e., $-1 < \boldsymbol{s}_{\mathrm{p}_i} < 1$. In this case, such samples are forced to the corresponding samples given in $\boldsymbol{c}_\mathrm{out} \in \{1, -1\}$. Accordingly, the vector $\boldsymbol{s}$ is determined by $\boldsymbol{s}_\mathrm{p}$ and $\boldsymbol{c}_\mathrm{out}$ jointly. Subsequently, the problem in (4-15) is solved like in (4-13) with the fixed vector $\boldsymbol{s}$ instead of $\boldsymbol{c}_\mathrm{out}$. The process is repeated until a convergence criterion is reached, e.g., a maximum number of iterations. The process is summarized in Algorithm 2.

4.2.2
Iterative MMSE Gradient Descent Method

This section introduces the collaborative work presented in the study [50]. For this method the considered system model is presented in Fig. 4.4, which changes slightly concerning the system model presented in Section. 2, since

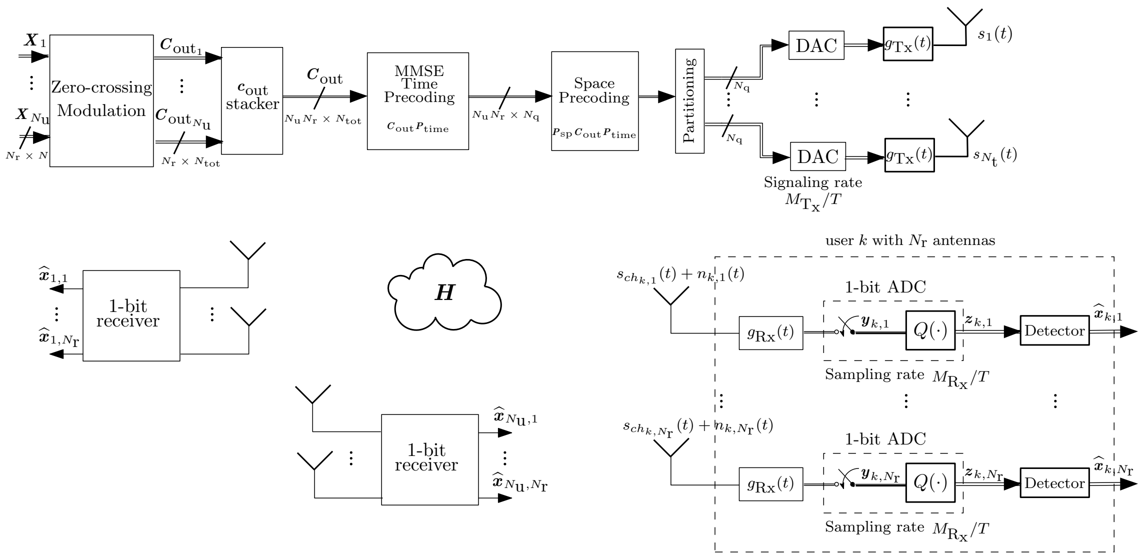

Figure 4.4: Multiuser MIMO system model for the Iterative Gradient Descent method.

spatial and temporal precoders are defined separately and multiantenna users are taking into account.

Considering N_{u} users with N_{r} receive antennas and defining the matrices $\boldsymbol{C}_{\text{out}} = [\boldsymbol{c}_{\text{out},1}; \ldots; \boldsymbol{c}_{\text{out},N_{\text{u}}}]$, the spatial precoding matrix $\boldsymbol{P}_{\text{space}}$ and the temporal precoding matrix $\boldsymbol{P}_{\text{time}}$, the unquantized received signals can be expressed with a stacked vector notation in terms of a matrix with dimensions $N_{\text{u}}N_{\text{r}} \times N_{\text{tot}}$ by

$$\begin{aligned} \boldsymbol{Y} &= \boldsymbol{H}\boldsymbol{P}_{\text{space}}\boldsymbol{C}_{\text{out}}\boldsymbol{P}_{\text{time}}\boldsymbol{U}^T\boldsymbol{V}^T + \boldsymbol{N}\boldsymbol{G}_{\text{Rx}}^T, \\ [\boldsymbol{Y}_1; \ldots; \boldsymbol{Y}_{N_{\text{u}}}] &= [\boldsymbol{H}_1; \ldots; \boldsymbol{H}_{N_{\text{u}}}]\boldsymbol{P}_{\text{space}}\boldsymbol{C}_{\text{out}}\boldsymbol{P}_{\text{time}}\boldsymbol{U}^T\boldsymbol{V}^T + [\boldsymbol{N}_1; \ldots; \boldsymbol{N}_{N_{\text{u}}}]\boldsymbol{G}_{\text{Rx}}^T, \end{aligned} \tag{4-21}$$

where $\boldsymbol{H}_k \in \mathbb{C}^{N_{\text{u}} \times N_{\text{t}}}$ and $\boldsymbol{N}_k \in \mathbb{C}^{N_{\text{r}} \times 3N_{\text{tot}}}$ contains i.i.d. complex Gaussian noise samples with zero mean and variance $\sigma_n^2 = N_0$.

The aim is to find an *optimal* $\boldsymbol{P}_{\text{space}}$ with dimensions $N_{\text{t}} \times N_{\text{u}}N_{\text{r}}$ and an *optimal* $\boldsymbol{P}_{\text{time}}$ with dimensions $N_{\text{tot}} \times N_{\text{q}}$, that minimizes the MSE which is denoted as ϵ in the sequel. With the MMSE criterion and an instantaneous power constraint, the optimization problem can be cast as

$$\begin{aligned} \min_{f,\boldsymbol{P}_{\text{time}},\boldsymbol{P}_{\text{space}}} \quad & \mathrm{E}\{\|f\boldsymbol{Y} - \boldsymbol{C}_{\text{out}}\|_F^2\} \\ \text{subject to:} \quad & \|\boldsymbol{P}_{\text{space}}\boldsymbol{C}_{\text{out}}\boldsymbol{P}_{\text{time}}\boldsymbol{U}^T\boldsymbol{G}_{\text{Tx}}\|_F^2 \leq E_0. \end{aligned} \tag{4-22}$$

The derivative of the objective function in (4-22) with respect to (w.r.t.)

$\boldsymbol{P}^*_{\text{space}}$ is given by

$$\begin{aligned}\frac{\partial\epsilon}{\partial\boldsymbol{P}^*_{\text{space}}} =& f^2\boldsymbol{H}^H\boldsymbol{H}\boldsymbol{P}_{\text{space}}\boldsymbol{C}_{\text{out}}\boldsymbol{P}_{\text{time}}\boldsymbol{U}^T\boldsymbol{V}^T\boldsymbol{V}\boldsymbol{U}\boldsymbol{P}^H_{\text{time}}\boldsymbol{C}^H_{\text{out}}\\ &- f\boldsymbol{H}^H\boldsymbol{C}_{\text{out}}\boldsymbol{V}\boldsymbol{U}\boldsymbol{P}^H_{\text{time}}\boldsymbol{C}^H_{\text{out}}.\end{aligned}\tag{4-23}$$

The derivative w.r.t. $\boldsymbol{P}^*_{\text{time}}$ is given by

$$\begin{aligned}\frac{\partial\epsilon}{\partial\boldsymbol{P}^*_{\text{time}}} =& f^2\boldsymbol{C}^H_{\text{out}}\boldsymbol{P}^H_{\text{space}}\boldsymbol{H}^H\boldsymbol{H}\boldsymbol{P}_{\text{space}}\boldsymbol{C}_{\text{out}}\boldsymbol{P}_{\text{time}}\boldsymbol{U}^T\boldsymbol{V}^T\boldsymbol{V}\boldsymbol{U}\\ &- f\boldsymbol{C}^H_{\text{out}}\boldsymbol{P}^H_{\text{space}}\boldsymbol{H}^H\boldsymbol{C}_{\text{out}}\boldsymbol{V}\boldsymbol{U}.\end{aligned}\tag{4-24}$$

Taking the derivative of ϵ w.r.t. f and equating it to zero yields

$$\begin{aligned}f =& (\text{trace}\{\boldsymbol{H}\boldsymbol{P}_{\text{space}}\boldsymbol{C}_{\text{out}}\boldsymbol{P}_{\text{time}}\boldsymbol{U}^T\boldsymbol{V}^T\boldsymbol{C}^H_{\text{out}}\}\\ &+ \text{trace}\{\boldsymbol{C}_{\text{out}}\boldsymbol{V}\boldsymbol{U}\boldsymbol{P}^H_{\text{time}}\boldsymbol{C}^H_{\text{out}}\boldsymbol{P}^H_{\text{space}}\boldsymbol{H}^H\})/\\ &(2(\|\boldsymbol{H}\boldsymbol{P}_{\text{space}}\boldsymbol{C}_{\text{out}}\boldsymbol{P}_{\text{time}}\boldsymbol{U}^T\boldsymbol{V}^T\|^2_F\\ &+ \text{trace}\{\boldsymbol{G}_{\text{Rx}}\boldsymbol{R}_{\boldsymbol{N}}\boldsymbol{G}^T_{\text{Rx}}\})).\end{aligned}\tag{4-25}$$

Based on the instantaneous power constraint in (4-22), it can be defined $\boldsymbol{Q} = \boldsymbol{C}_{\text{out}}\boldsymbol{P}_{\text{time}}\boldsymbol{U}^T\boldsymbol{G}_{\text{Tx}}$, $\boldsymbol{A} = \boldsymbol{P}_{\text{space}}\boldsymbol{C}_{\text{out}}$, and $\boldsymbol{B} = \boldsymbol{U}^T\boldsymbol{G}_{\text{Tx}}$. With this, the power constraint can be further expressed as

$$\|\boldsymbol{P}_{\text{space}}\boldsymbol{Q}\|^2_F = \|\boldsymbol{A}\boldsymbol{P}_{\text{time}}\boldsymbol{B}\|^2_F \leq E_0.\tag{4-26}$$

Hence, the spatial- and time-domain filters can be normalized to satisfy the instantaneous power constraint with equality as

$$\hat{\boldsymbol{P}}_{\text{space}} = \boldsymbol{P}_{\text{space}}\cdot\sqrt{E_0}\|\boldsymbol{P}_{\text{space}}\boldsymbol{Q}\|^{-1}_F\tag{4-27}$$

$$\hat{\boldsymbol{P}}_{\text{time}} = \boldsymbol{P}_{\text{time}}\cdot\sqrt{E_0}\|\boldsymbol{A}\boldsymbol{P}_{\text{time}}\boldsymbol{B}\|^{-1}_F.\tag{4-28}$$

Using the introduced gradient expressions and normalizations from above a projected gradient descent algorithm is proposed as described in Algorithm 3.

For the initialization, we use a spatial zero-forcing precoder with scaling factor expressed as

$$c_{\text{zf}} = \sqrt{N_{\text{r}}N_{\text{u}}/\text{trace}\{(\boldsymbol{H}\boldsymbol{H}^H)^{-1}\}}.\tag{4-29}$$

Then, the maximum transmit power can be expressed without the spatial

Algorithm 3 Proposed Projected Gradient Descent

$i \leftarrow 0$
Set μ_s and μ_t
Initialize $\boldsymbol{P}_\mathrm{space}[i] \leftarrow$ Spatial ZF
Initialize $\boldsymbol{P}_\mathrm{time}[i],\ f[i] \leftarrow$ Closed-form MMSE (4-39), (4-40)
repeat
  Update Precoding matrices:
  Calculate $\boldsymbol{Q}[i] = \boldsymbol{C}_\mathrm{out}\boldsymbol{P}_\mathrm{time}[i]\boldsymbol{U}^T\boldsymbol{G}_\mathrm{Tx}$
  Calculate $\partial\epsilon/\partial\boldsymbol{P}^*_\mathrm{space}[i]$ by (4-23)
  $\boldsymbol{P}_\mathrm{space}[i+1] \leftarrow \boldsymbol{P}_\mathrm{space}[i] - \mu_\mathrm{s}\cdot\partial\epsilon/\partial\boldsymbol{P}^*_\mathrm{space}[i]$
  Normalize $\boldsymbol{P}_\mathrm{space}[i+1]$ due to (4-27)
  Calculate $\boldsymbol{A}[i] = \boldsymbol{P}_\mathrm{space}[i+1]\boldsymbol{C}_\mathrm{out}$
  Calculate $\partial\epsilon/\partial\boldsymbol{P}^*_\mathrm{time}[i]$ by (4-24)
  $\boldsymbol{P}_\mathrm{time}[i+1] \leftarrow \boldsymbol{P}_\mathrm{time}[i] - \mu_\mathrm{t}\cdot\partial\epsilon/\partial\boldsymbol{P}^*_\mathrm{time}[i]$
  Normalize $\boldsymbol{P}_\mathrm{time}[i+1]$ due to (4-28)
  Update f
  Calculate $f[i+1]$ by (4-25)
  $i \leftarrow i+1$
until convergence criterion triggers

precoding as

$$E_0 = \mathrm{trace}\{\boldsymbol{C}_\mathrm{out}\boldsymbol{P}_\mathrm{time}\boldsymbol{U}^T\boldsymbol{G}_\mathrm{Tx}\boldsymbol{G}_\mathrm{Tx}^T\boldsymbol{U}\boldsymbol{P}_\mathrm{time}^H\boldsymbol{C}_\mathrm{out}^H\}. \tag{4-30}$$

Based on the ZF-precoding matrix the unquantized received signal is described by

$$\boldsymbol{Y} = c_\mathrm{zf}\boldsymbol{C}_\mathrm{out}\boldsymbol{P}_\mathrm{time}\boldsymbol{U}^T\boldsymbol{V}^T + \boldsymbol{N}\boldsymbol{G}_\mathrm{Rx}^T. \tag{4-31}$$

With this, the temporal MMSE problem can be cast as

$$\begin{aligned} \min_{f,\boldsymbol{P}_\mathrm{time}} \quad & \mathrm{E}\{\|f\boldsymbol{Y} - \boldsymbol{C}_\mathrm{out}\|_F^2\} \\ \text{subject to:} \quad & \|\boldsymbol{C}_\mathrm{out}\boldsymbol{P}_\mathrm{time}\boldsymbol{U}^T\boldsymbol{G}_\mathrm{Tx}\|_F^2 \leq E_0, \end{aligned} \tag{4-32}$$

which is a similar problem as solved in [59]. By denoting the new MSE expression by ϵ_T, the Lagrangian function reads as

$$\begin{aligned} &L(\boldsymbol{P}^*_\mathrm{time}, \boldsymbol{P}_\mathrm{time}, f) = \\ &\epsilon_\mathrm{T} + \lambda(\mathrm{trace}\{\boldsymbol{C}_\mathrm{out}^H\boldsymbol{C}_\mathrm{out}\boldsymbol{P}_\mathrm{time}\boldsymbol{U}^T\boldsymbol{G}_\mathrm{Tx}\boldsymbol{G}_\mathrm{Tx}^T\boldsymbol{U}\boldsymbol{P}_\mathrm{time}^H\} - E_0). \end{aligned} \tag{4-33}$$

The derivative w.r.t. $\boldsymbol{P}_{\text{time}}^*$ yields

$$\begin{aligned}\frac{\partial L}{\partial \boldsymbol{P}_{\text{time}}^*} =& f^2\ c_{\text{zf}}^2\ \boldsymbol{C}_{\text{out}}^H \boldsymbol{C}_{\text{out}} \boldsymbol{P}_{\text{time}} \boldsymbol{U}^T \boldsymbol{V}^T \boldsymbol{V} \boldsymbol{U} \\ &- f\ c_{\text{zf}}\ \boldsymbol{C}_{\text{out}}^H \boldsymbol{C}_{\text{out}} \boldsymbol{V} \boldsymbol{U} \\ &+ \lambda \boldsymbol{C}_{\text{out}}^H \boldsymbol{C}_{\text{out}} \boldsymbol{P}_{\text{time}} \boldsymbol{U}^T \boldsymbol{G}_{\text{Tx}} \boldsymbol{G}_{\text{Tx}}^T \boldsymbol{U}.\end{aligned} \tag{4-34}$$

By equating it to zero implies

$$\begin{aligned}\frac{c_{\text{zf}}}{f}\ \boldsymbol{C}_{\text{out}}^H \boldsymbol{C}_{\text{out}} \boldsymbol{V} \boldsymbol{U} =& c_{\text{zf}}^2 \boldsymbol{C}_{\text{out}}^H \boldsymbol{C}_{\text{out}} \boldsymbol{P}_{\text{time}} \boldsymbol{U}^T \boldsymbol{V}^T \boldsymbol{V} \boldsymbol{U} \\ &+ \frac{\lambda}{f^2} \boldsymbol{C}_{\text{out}}^H \boldsymbol{C}_{\text{out}} \boldsymbol{P}_{\text{time}} \boldsymbol{U}^T \boldsymbol{G}_{\text{Tx}} \boldsymbol{G}_{\text{Tx}}^T \boldsymbol{U},\end{aligned} \tag{4-35}$$

and

$$\frac{c_{\text{zf}}}{f}\ \boldsymbol{V} \boldsymbol{U} = c_{\text{zf}}^2 \boldsymbol{P}_{\text{time}} \boldsymbol{U}^T \boldsymbol{V}^T \boldsymbol{V} \boldsymbol{U} + \frac{\lambda}{f^2} \boldsymbol{P}_{\text{time}} \boldsymbol{U}^T \boldsymbol{G}_{\text{Tx}} \boldsymbol{G}_{\text{Tx}}^T \boldsymbol{U}.$$

The latter can be rearranged such that the structure of the optimal precoding matrix can be determined as

$$\boldsymbol{P}_{\text{time}} = \frac{c_{\text{zf}}}{f}\ \boldsymbol{V} \boldsymbol{U} (\ c_{\text{zf}}^2 \boldsymbol{U}^T \boldsymbol{V}^T \boldsymbol{V} \boldsymbol{U} + \frac{\lambda}{f^2} \boldsymbol{U}^T \boldsymbol{G}_{\text{Tx}} \boldsymbol{G}_{\text{Tx}}^T \boldsymbol{U})^{-1}.$$

The derivative w.r.t. f yields

$$\begin{aligned}\frac{\partial L}{\partial f} =& 2 f c_{\text{zf}}^2 \|\boldsymbol{V} \boldsymbol{U} \boldsymbol{P}_{\text{time}}^H \boldsymbol{C}_{\text{out}}^H\|_F^2 \\ &- c_{\text{zf}}\ 2\text{Re}\{\text{trace}\{\boldsymbol{C}_{\text{out}}^H \boldsymbol{C}_{\text{out}} \boldsymbol{V} \boldsymbol{U} \boldsymbol{P}_{\text{time}}^H\}\} \\ &+ 2f\ \text{trace}\{\boldsymbol{G}_{\text{Rx}} \boldsymbol{R}_{\boldsymbol{N}} \boldsymbol{G}_{\text{Rx}}^T\}.\end{aligned} \tag{4-36}$$

Equation it to zero yields

$$\begin{aligned}&\frac{c_{\text{zf}}}{f}\ \ \text{trace}\{\boldsymbol{C}_{\text{out}}^H \boldsymbol{C}_{\text{out}} \boldsymbol{V} \boldsymbol{U} \boldsymbol{P}_{\text{time}}^H\} = \\ &c_{\text{zf}}^2 \|\boldsymbol{C}_{\text{out}} \boldsymbol{P}_{\text{time}} \boldsymbol{U}^T \boldsymbol{V}^T\|_F^2 + \text{trace}\{\boldsymbol{G}_{\text{Rx}} \boldsymbol{R}_{\boldsymbol{N}} \boldsymbol{G}_{\text{Rx}}^T\},\end{aligned} \tag{4-37}$$

where the real part operator has been skipped due to the structure of the optimal $\boldsymbol{P}_{\text{time}}$. After multiplication from the right with $\boldsymbol{P}_{\text{time}}$ and applying the trace operator, (4-35) is equal to (4-37). Putting together the right hand sides yields

$$\frac{\lambda}{f^2} = \frac{\text{trace}\{\boldsymbol{G}_{\text{Rx}} \boldsymbol{R}_{\boldsymbol{N}} \boldsymbol{G}_{\text{Rx}}^T\}}{\text{trace}\{\boldsymbol{C}_{\text{out}}^H \boldsymbol{C}_{\text{out}} \boldsymbol{P}_{\text{time}} \boldsymbol{U}^T \boldsymbol{G}_{\text{Tx}} \boldsymbol{G}_{\text{Tx}}^T \boldsymbol{U} \boldsymbol{P}_{\text{time}}^H\}}, \tag{4-38}$$

where it is considered that the power constraint holds with equality such that $\mathrm{trace}\{\boldsymbol{C}_{\mathrm{out}}^{H}\boldsymbol{C}_{\mathrm{out}}\boldsymbol{P}_{\mathrm{time}}\boldsymbol{U}^{T}\boldsymbol{G}_{\mathrm{Tx}}\boldsymbol{G}_{\mathrm{Tx}}^{T}\boldsymbol{U}\boldsymbol{P}_{\mathrm{time}}^{H}\} = E_0$. With this, the temporal precoding matrix reads as

$$\boldsymbol{P}_{\mathrm{time}} = f^{-1}\, c_{\mathrm{zf}}\, \boldsymbol{V}\boldsymbol{U}\boldsymbol{\Gamma}^{-1}, \tag{4-39}$$

with $\boldsymbol{\Gamma} = c_{\mathrm{zf}}^{2}\boldsymbol{U}^{T}\boldsymbol{V}^{T}\boldsymbol{V}\boldsymbol{U} + \frac{\mathrm{trace}\{\boldsymbol{G}_{\mathrm{Rx}}\boldsymbol{R}_{\boldsymbol{N}}\boldsymbol{G}_{\mathrm{Rx}}^{T}\}}{E_0}\boldsymbol{U}^{T}\boldsymbol{G}_{\mathrm{Tx}}\boldsymbol{G}_{\mathrm{Tx}}^{T}\boldsymbol{U}$. Inserting (4-39) into the power constraint (4-30) yields

$$f = c_{\mathrm{zf}} E_0^{-\frac{1}{2}}\, \|\boldsymbol{C}_{\mathrm{out}}\, \boldsymbol{V}\boldsymbol{U}\boldsymbol{\Gamma}^{-1}\boldsymbol{U}^{T}\boldsymbol{G}_{\mathrm{Tx}}\|_F. \tag{4-40}$$

4.2.3 Numerical Results

This section presents the numerical evaluation of the proposed MMSE TI ZX precoding techniques, in terms of the MSE. The simulations were carried out for different sets of signaling rate (M_{Tx}/T) and sampling rate (M_{Rx}/T). For all the evaluated configurations, $g_{\mathrm{Tx}}(t)$ is an RC filter and the receive filter $g_{\mathrm{Rx}}(t)$ is an RRC filter, where the roll-off factors are $\epsilon_{\mathrm{Tx}} = \epsilon_{\mathrm{Rx}} = 0.22$, as in [2]. The bandwidth is defined with $W_{\mathrm{Rx}} = W_{\mathrm{Tx}} = (1+\epsilon_{\mathrm{Tx}})/T_{\mathrm{s}}$, wherein the simulations it is considered $T = T_{\mathrm{s}}$. A Rayleigh fading model is considered for the channel matrix $\boldsymbol{H}$, whose entries are i.i.d. zero-mean complex Gaussian distributed with unit variance. The noise samples are complex Gaussian with zero mean and variance σ_n^2. Moreover, in all the evaluated scenarios, the BS is equipped with $N_{\mathrm{t}} = 8$ antennas, $N_{\mathrm{u}} = 2$ users, $N = 30$ Nyquist intervals, and maximum energy constraint E_0. The SNR is defined as in (4-11).

Fig. 4.5 shows a performance comparison among the conventional MMSE precoding (4-12), the optimal MMSE ACE (4-15) and the iterative MMSE ACE considering different numbers of maximum iterations $i_{\max}$ (Algorithm 2). In Fig. 4.5, the configuration $M_{\mathrm{Rx}} = M_{\mathrm{Tx}} = 2$ is considered. It is observed that when increasing the number of iterations, the iterative MMSE ACE precoding approaches the MMSE ACE performance. The proposed MMSE precoding techniques are compared for different sets in Fig. 4.6, with $i_{\max} = 30$ for the iterative MMSE ACE. As expected, a substantial improvement can be achieved with ACE compared to the MMSE precoder, especially at high SNR. Based on Fig. 4.5 and Fig. 4.6, one can conclude that the iterative MMSE ACE in general, yields a performance close to the optimal MMSE ACE at low and medium SNR.

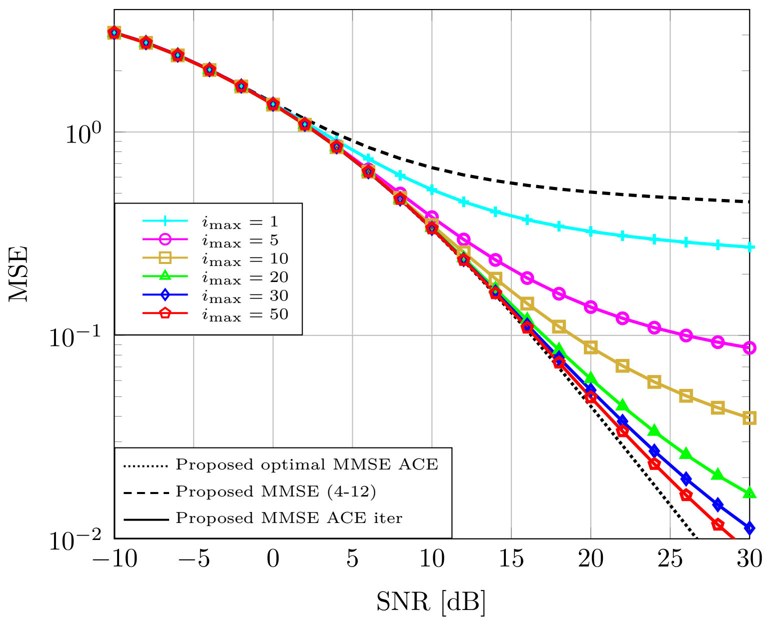

Figure 4.5: Comparison between the optimal MMSE ACE and the iterative MMSE ACE for different number of iterations for $M_{\mathrm{Rx}} = M_{\mathrm{Tx}} = 2$.

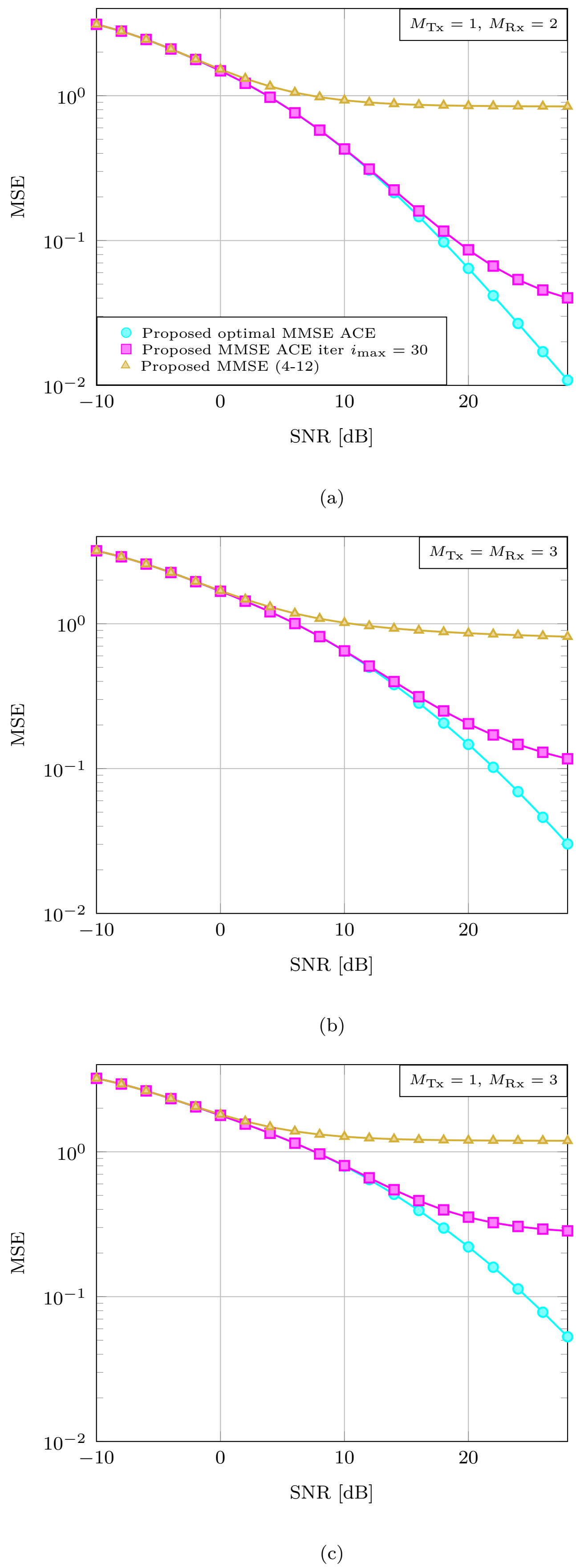

Figure 4.6: MSE comparison for different configurations. In (a) $M_{\mathrm{Rx}} = 2$, $M_{\mathrm{Tx}} = 1$. In (b) $M_{\mathrm{Rx}} = M_{\mathrm{Tx}} = 3$. In (c) $M_{\mathrm{Rx}} = 3$, $M_{\mathrm{Tx}} = 1$.

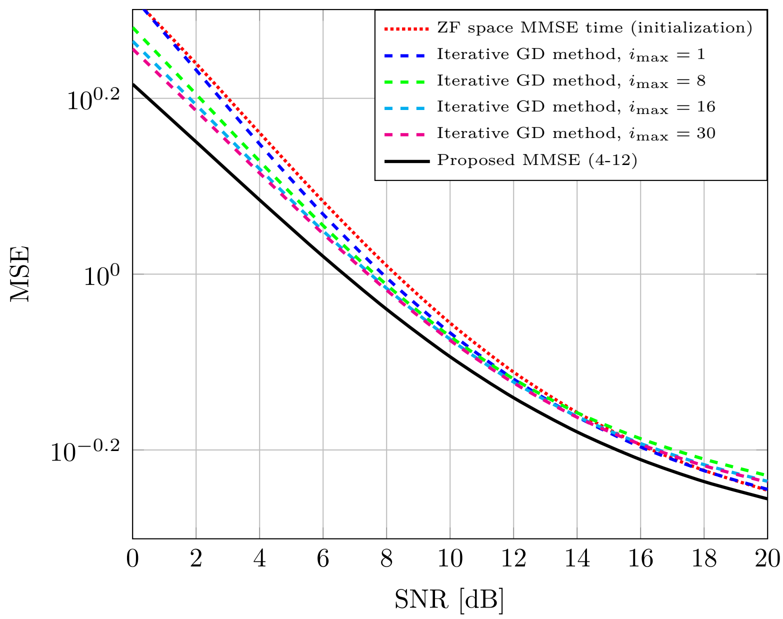

Figure 4.7: MSE cost function for different precoding strategies.

For the numerical evaluation of the iterative MMSE gradient descent method it was considered a system with $N_\mathrm{u} = 2$ users with $N_\mathrm{r} = 2$ antennas and $N_\mathrm{t} = 5$ base station antennas. Each transmit block consists of $N = 50$ symbols. The signaling and sampling rate are chosen as $M_\mathrm{Rx} = M_\mathrm{Tx} = 2$. The step size for the proposed projected gradient descent algorithm equals $\mu_\mathrm{t} = 10^{-7}$ and $\mu_\mathrm{s} = 10^{-3}$. In Fig. 4.7 the proposed iterative spatial temporal MMSE precoding algorithm is compared with the joint space time MMSE precoder [48] in terms of the MSE, which confirms that the MSE decreases with the iterations. The computational complexity of the precoder in [48] is on the order of $\mathcal{O}((N_\mathrm{t} N_\mathrm{q})^3)$. With $\mathcal{O}((N_\mathrm{r} N_\mathrm{u})^3 + N_\mathrm{q}^3 + i_{\max}(2 N_\mathrm{tot} N_\mathrm{u} N_\mathrm{r} N_\mathrm{q}) + N_\mathrm{tot}(N_\mathrm{u} N_\mathrm{r})^2) + N_\mathrm{tot} N_\mathrm{t} N_\mathrm{r} N_\mathrm{u} + N_\mathrm{t}^2 N_\mathrm{r} N_\mathrm{u} + (N_\mathrm{r} N_\mathrm{u})^2 N_\mathrm{t} + N_\mathrm{tot} N_\mathrm{t} N_\mathrm{r} N_\mathrm{u} + N_\mathrm{tot} N_\mathrm{t} N_\mathrm{q} + N_\mathrm{t}^2 N_\mathrm{r} N_\mathrm{u} + N_\mathrm{tot} N_\mathrm{t} N_\mathrm{r} N_\mathrm{u} + N_\mathrm{q}^2 N_\mathrm{r} N_\mathrm{u} + N_\mathrm{tot} N_\mathrm{q} N_\mathrm{r} N_\mathrm{u})$, which is approximately $\mathcal{O}(N_\mathrm{q}^3)$ for small $i_{\max}$, the proposed method has significantly lower computational complexity, in comparison to the method in [48]. Fig. 4.8 illustrates the uncoded bit error rate. The different precoding methods are compared in combination with the zero-crossing approach and the forward mapping approach presented in [2]. The results show a significant benefit for the zero-crossing approach. Finally, it is shown that the proposed iterative approach has a comparable bit error rate to the closed form approach in [48] while having significantly lower computational complexity.

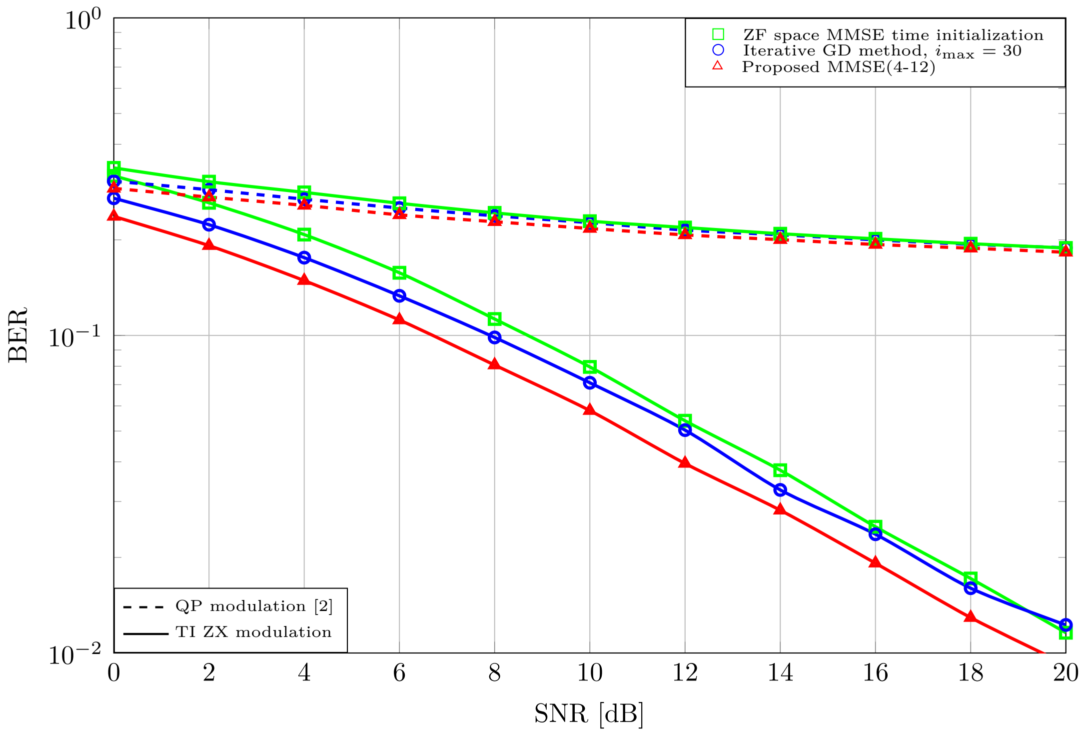

Figure 4.8: BER performance comparison.

4.3 Performance Comparison Between the Optimization Based Precoding Methods

This section presents a performance comparison between the proposed precoding techniques based on the MMDDT and MMSE approaches in terms of the BER, PSD, time offset analysis, and computational complexity.

4.3.1 BER Performance and PSD Evaluation

In Fig. 4.9 and Fig. 4.10, a performance comparison between the considered precoders in terms of BER is shown. Fig. 4.9 compares the performance of the precoders for $M_{\mathrm{Rx}} = M_{\mathrm{Tx}} = 2$. In addition, a conventional QPSK modulated signal is presented as a reference. Fig. 4.10 shows the simulation results for other configurations. The joint MMDDT precoder has the best performance at high SNR among all the evaluated precoding methods. In general, it can be observed that the conventional MMSE criterion corresponds to performance degradation in the high SNR region. In contrast, the MMDDT precoding approaches correspond to performance degradation in the low SNR region. It is demonstrated that a performance trade-off can be obtained with the MMSE ACE, which has a good performance at low and high SNR region. The BER results align with the previously shown MSE results, confirming that the MSE is an appropriate design criterion. Fig. 4.11 shows simulation results in terms of normalized PSD for all the precoding techniques. The results were simulated for $M_{\mathrm{Rx}} = M_{\mathrm{Tx}} = 2$, employing $\mathrm{PSD}_{\mathrm{dB}} = 10\log_{10}\left[\mathrm{E}\{\left|F_i(\sqrt{3N_{\mathrm{tot}}})^{(-1)}\right|^2\}\right]$, where F_i is the discrete Fourier transform of the signal per transmit antenna given by $\boldsymbol{s}_i = \boldsymbol{G}_{\mathrm{Tx}}^{\mathrm{T}}\boldsymbol{U}\boldsymbol{p}_{\mathrm{x}_i}$.

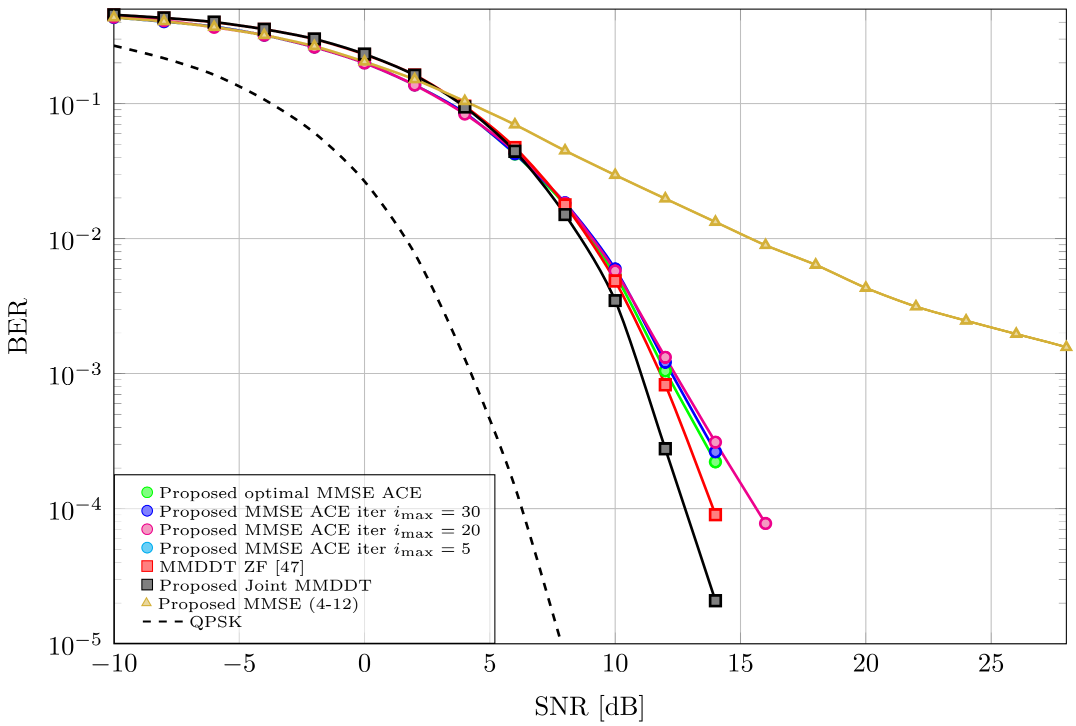

Figure 4.9: BER vs. SNR for $M_{\mathrm{Rx}} = M_{\mathrm{Tx}} = 2$.

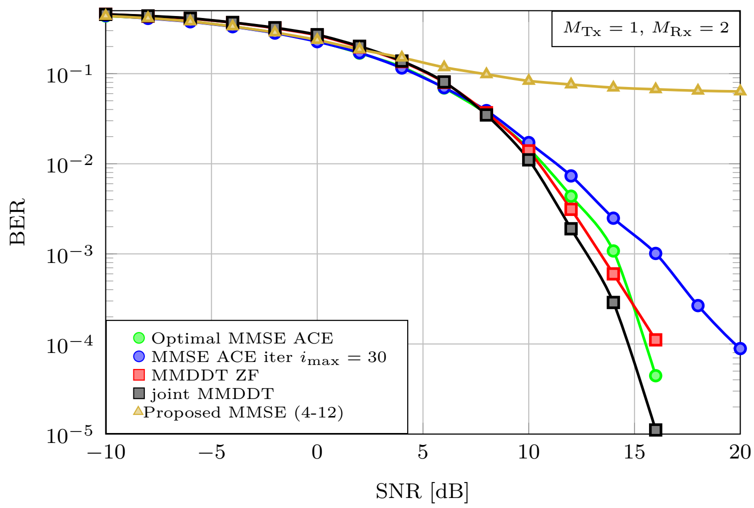

(a)

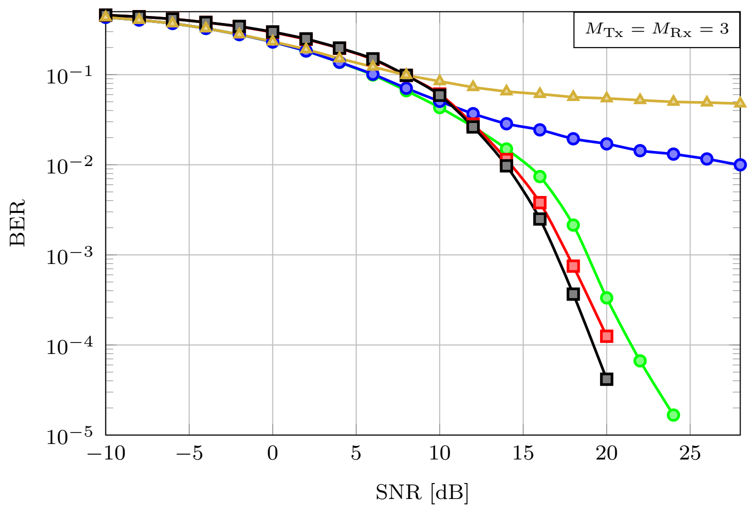

(b)

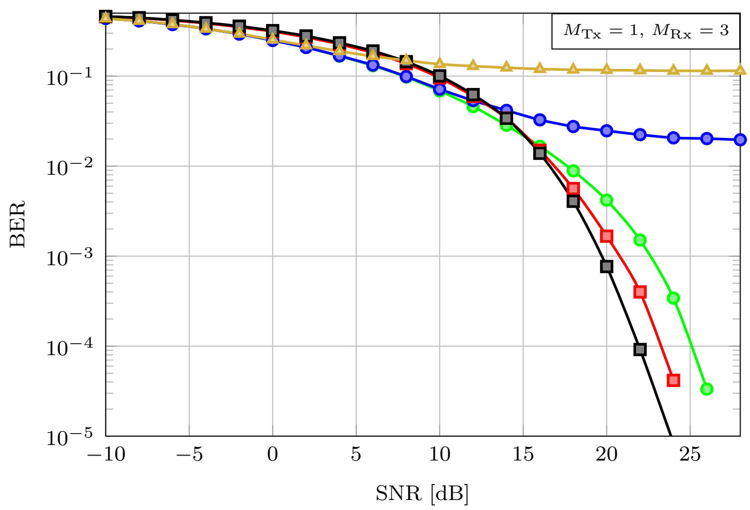

(c)

Figure 4.10: BER vs. SNR for different configurations. In (a) $M_{\mathrm{Rx}} = 2$, $M_{\mathrm{Tx}} = 1$. In (b) $M_{\mathrm{Rx}} = M_{\mathrm{Tx}} = 3$. In (c) $M_{\mathrm{Rx}} = 3$, $M_{\mathrm{Tx}} = 1$.

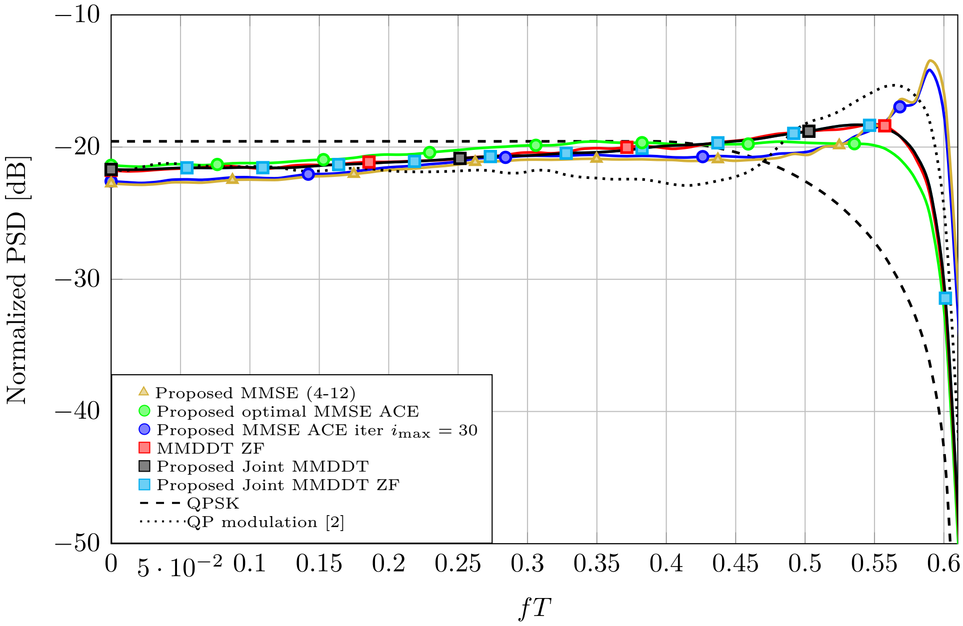

Figure 4.11: Power spectral density for $M_{\text{Rx}} = M_{\text{Tx}} = 2$.

4.3.2 Time Offset Analysis

In addition, simulation results are presented with sampling time offset τ at the receiver. In this context, the received signal has a sub-sampling time offset τ, and the impulse response $v(t)$ becomes $v_{\text{offset}}(t)$, whose discrete-time representation is given by matrix $\mathbf{V}_{\text{offset}}$

$$\mathbf{V}_{\text{offset}} = \tag{4-41}$$

$$\begin{bmatrix} v\left(\tau\right) & v\left(\frac{T}{M_{\text{Rx}}}+\tau\right) & \cdots & v\left(TN+\tau\right) \\ v\left(-\frac{T}{M_{\text{Rx}}}+\tau\right) & v\left(\tau\right) & \cdots & v\left(T\left(N-\frac{1}{M_{\text{Rx}}}\right)+\tau\right) \\ \vdots & \vdots & \ddots & \vdots \\ v\left(-TN+\tau\right) & v\left(T\left(-N+\frac{1}{M_{\text{Rx}}}\right)+\tau\right) & \cdots & v\left(\tau\right) \end{bmatrix}_{N_{\text{tot}}\times N_{\text{tot}}} .$$

The received signal at user k taking into account the sub-sampling time offset is described by

$$\boldsymbol{z}_{k_{\text{offset}}} = Q_1\left(\left(\boldsymbol{h}_k \otimes \boldsymbol{I}_{N_{\text{tot}}}\right)\left(\boldsymbol{I}_{N_{\text{t}}} \otimes \mathbf{V}_{\text{offset}}\boldsymbol{U}\right)\boldsymbol{p}_{\text{x}} + \left(\boldsymbol{I}_{N_{\text{u}}N_{\text{r}}} \otimes \boldsymbol{G}_{\text{Rx}}\right)\boldsymbol{n}\right), \tag{4-42}$$

where $\boldsymbol{p}_{\text{x}}$ relies on the impulse response $v(t)$. In the detection process $v(t)$ is also considered. Using the described configuration, BER simulations have been carried out for different sampling time offsets as shown in Fig. 4.12. Note that for the proposed iterative MMSE $i_{max} = 30$. From Fig. 4.12, it is possible to observe that the MMDDT based precoding techniques are the most robust against the effects of sampling offset in high SNR regions.

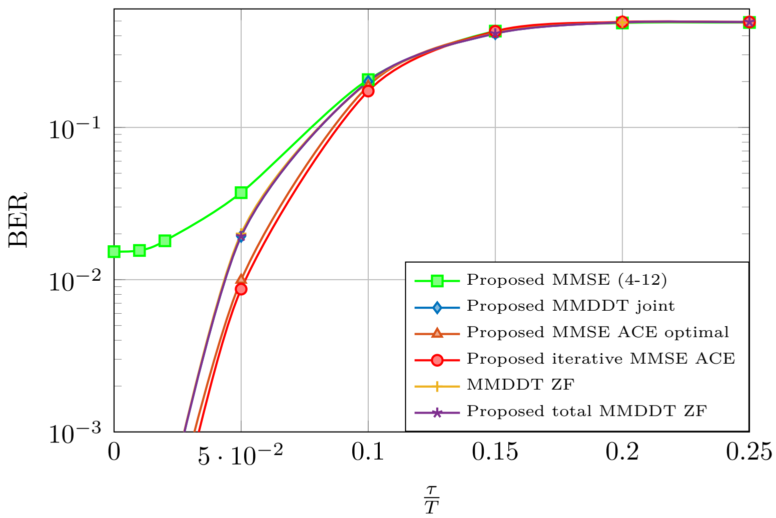

(a)

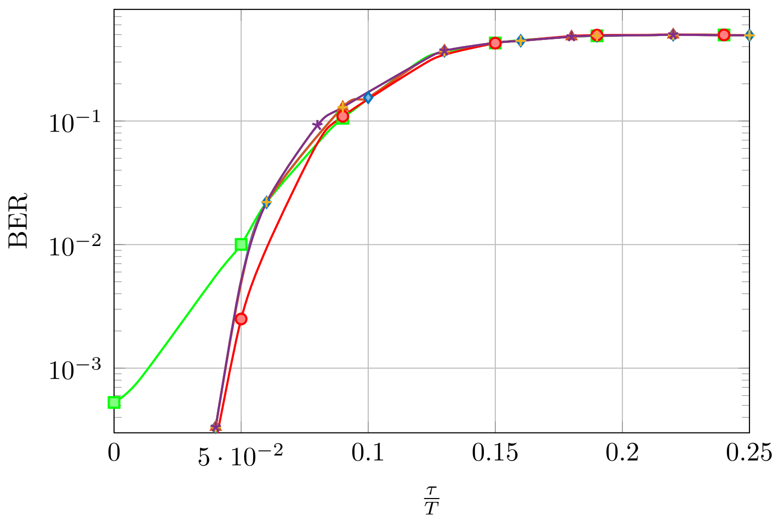

(b)

Figure 4.12: BER vs. time delay for $M_{\mathrm{Rx}} = M_{\mathrm{Tx}} = 2$ considering different values of SNR. In (a) for SNR [dB] = 10 and in (b) for SNR [dB] = 30.

4.3.3 Computational Complexity Evaluation

In this section, the computational complexity of the proposed methods is evaluated. Table 4.1 lists the optimization problem associated with each method, algorithm and complexity order.

The MMDDT ZF precoding technique, the joint MMDDT and the total MMDDT ZF are quadratically constrained quadratic programs solved with interior point methods. Unlike joint MMDDT, MMDDT ZF and total

Table 4.1: Computational Complexity analysis

Method	Problem	Algorithm	Complexity Order
MMDDT ZF [47] [2]	QCQP and matrix inversion	Interior point methods and Gauss–Jordan elimination	$\mathcal{O}\left(2N_{\mathrm{u}}(N_{\mathrm{q}}+1)^{3.5}+N_{\mathrm{t}}^3\right)$
Proposed joint MMDDT (4-5)	QCQP	Interior point methods	$\mathcal{O}\left((2N_{\mathrm{q}}N_{\mathrm{t}})^{3.5}\right)$
Proposed total MMDDT ZF	QCQP and matrix inversion	Interior point methods and Gauss–Jordan elimination	$\mathcal{O}\left(2N_{\mathrm{u}}(N_{\mathrm{q}})^{3.5}+N_{\mathrm{t}}^3\right)$
Proposed optimal MMSE ACE	SOCP	Interior point methods	$\mathcal{O}\left((2N_{\mathrm{q}}N_{\mathrm{t}}+2N_{\mathrm{u}}N_{\mathrm{tot}}+2)^{3.5}\right)$
Proposed iterative MMSE ACE	Matrix inversion	Gauss–Jordan elimination	$\mathcal{O}\left((N_{\mathrm{q}}N_{\mathrm{t}})^3+i_{\max}(N_{\mathrm{u}}N_{\mathrm{tot}}+(N_{\mathrm{q}}N_{\mathrm{t}})^3)\right)$
Proposed MMSE	Matrix inversion	Gauss–Jordan elimination	$\mathcal{O}\left((N_{\mathrm{q}}N_{\mathrm{t}})^3\right)$

MMDDT ZF are solved separately for the in-phase and quadrature components and each user stream. With this, the complexity scales linearly twice by the number of users. As a result, the MMDDT ZF and the proposed total MMDDT ZF are the precoders with the lowest complexity. Moreover, the proposed optimal MMSE ACE corresponds to a SOCP which can be solved with interior point methods. The proposed iterative MMSE ACE and the proposed MMSE involve a matrix inversion problem that corresponds to cubic complexity. The complexity results are presented in Fig. 4.13. In Fig. 4.13 (a) the precoding techniques are evaluated in terms of the number of transmit antennas N_{t}, where $i_{\max}=30$ and $M_{\mathrm{Tx}}=M_{\mathrm{Rx}}=2$. Fig. 4.13 (a) confirms that MMDDT ZF and the proposed total MMDDT ZF are the precoders with the lowest complexity among all the evaluated precoders, while MMSE ACE optimal and joint MMDDT are the precoders with relatively high complexity. The proposed conventional MMSE precoder has the lowest complexity among all the considered MMSE-based techniques. In Fig. 4.13 (b), a complexity comparison between the optimal MMSE ACE and iterative MMSE ACE is shown in terms of the number of iterations and different values for M_{Tx} and M_{Rx}, where the BS is equipped with $N_{\mathrm{t}}=8$ antennas and $N_{\mathrm{u}}=2$ users. It can be seen that the proposed iterative MMSE ACE yields a significantly lower complexity in comparison with the proposed optimal MMSE ACE even when the number of iterations $i_{\max}$ is high.

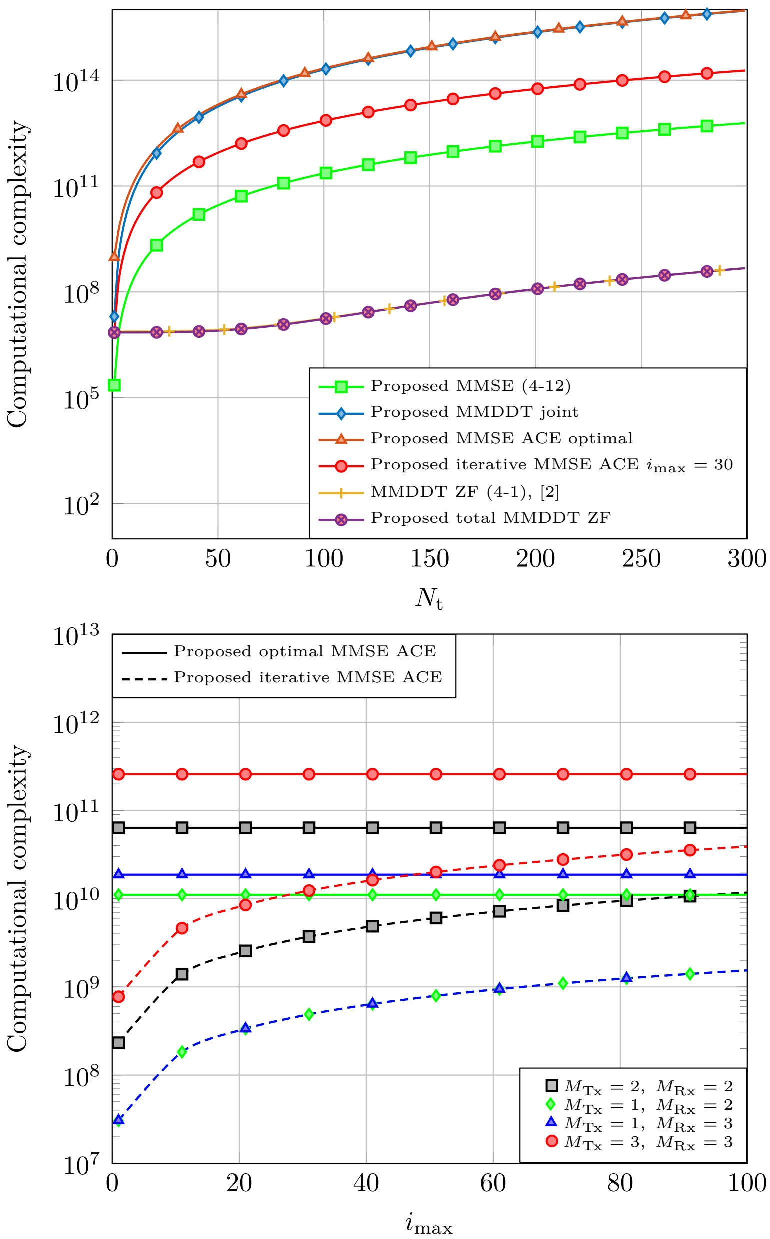

(b)

Figure 4.13: Computational complexity. (a) vs. the number of transmit antennas. (b) comparison between the optimal and iterative MMSE ACE.

4.4 Zero-Crossing Waveform Comparison

This section presents a comparison between the mappings with the TI ZX modulation, and the RLL sequence-based mapping derived in [60]. This part of the thesis corresponds to the collaborative study [51].

In this analysis, the multi-user MIMO downlink scenario shown in Fig. 2.1 with the spatio-temporal MMSE precoder from (4-12) is considered.

Furthermore, instead of using the soft-input soft-output RLL decoder from [60], a low-complexity minimum Hamming distance Viterbi algorithm for RLL sequence decoding is presented. Finally, a simple SE lower bound, which depends on the system's uncoded BER is derived. The description of the RLL mapping derived in [60] is explained in detail in Appendix A.4.

4.4.1
Spectral Efficiency

In this section, we obtain a lower bound on the SE for the considered system model.

First, we evaluate the average mutual information $\lim_{I_\mathrm{b}\to\infty} \frac{1}{I_\mathrm{b}} I\left(\boldsymbol{x}_k; \hat{\boldsymbol{x}}_k\right)$, where $\boldsymbol{x}_k \in \{0,1\}^{I_\mathrm{b}}$ and $\hat{\boldsymbol{x}}_k \in \{0,1\}^{I_\mathrm{b}}$ denote the transmitted bit sequence and its estimate at the kth user, both of length I_b. In the following, we drop the index k for ease of notation. If the sequence $\boldsymbol{x}$ is i. i. d., then it holds $H\left(\boldsymbol{x}\right) = \sum_{n=1}^{I_\mathrm{b}} H\left(x_n\right)$ [61, Th. 2.6.6], where $H(\cdot)$ denotes entropy. Hence, we obtain

$$\begin{aligned} \frac{1}{I_\mathrm{b}} I\left(\boldsymbol{x}; \hat{\boldsymbol{x}}\right) &\overset{(a)}{\geq} \frac{1}{I_\mathrm{b}} \sum_{n=1}^{I_\mathrm{b}} H\left(x_n\right) - \frac{1}{I_\mathrm{b}} \sum_{n=1}^{I_\mathrm{b}} H\left(x_n | \hat{x}_n\right) \\ &= 1 - \frac{1}{I_\mathrm{b}} \sum_{n=1}^{I_\mathrm{b}} H_\mathrm{b}\left(\Pr(x_n \neq \hat{x}_n)\right) \\ &\overset{(b)}{\geq} 1 - H_\mathrm{b}\left(\frac{1}{I_\mathrm{b}} \sum_{n=1}^{I_\mathrm{b}} \Pr(x_n \neq \hat{x}_n)\right) \triangleq \bar{I}_\mathrm{LB}, \end{aligned} \tag{4-43}$$

where the inequality (a) is due to the chain rule for information [61, Th. 2.5.2], due to independent x_n, and due to the fact that conditioning cannot increase entropy [61, Th. 2.6.5]. The last step, i. e., (b), is due to Jensen's inequality [61, Th. 2.6.2]. Furthermore, $H_\mathrm{b}(\cdot)$ denotes binary entropy (cf. [61, eq. (2.1)]) and $\frac{1}{I_\mathrm{b}} \sum_{n=1}^{I_\mathrm{b}} \Pr(x_n \neq \hat{x}_n)$ corresponds to the uncoded BER.

Using (4-43), a lower bound on the SE can be obtained as

$$\mathrm{SE}_\mathrm{LB} = \frac{2 \cdot \Xi \cdot \bar{I}_\mathrm{LB}}{1 + \epsilon_\mathrm{Tx}}, \tag{4-44}$$

where the factor 2 in the numerator is due to complex signaling and Ξ denotes the transmission rate of the considered mapping in bit per Nyquist interval per real signaling dimension (cf. 4.2). Furthermore, ϵ_Tx denotes the roll-off of the RC transmit filter. Note that in contrast to [21, 62, 63], the SE lower bound in (4-44) is evaluated w. r. t. a strictly band-limited channel. Defining the uncoded

Table 4.2: Considered zero-crossing mapping configurations.

Number of Nyquist intervals per block $N = 30$				
Precoding	$M_{\mathrm{Tx}} = M_{\mathrm{Rx}}$	I_{b}	O_{s}	Ξ [bit/T/dim]
TI ZX	2	45	60	1.5
TI ZX	3	60	90	2
RLL $d = 1$, [60, Table I]	2	40	60	1.33
RLL $d = 2$, [60, Table II]	3	45	90	1.5

BER as ϖ, the lower bound in the mutual information $\bar{I}_{\mathrm{LB}}$ is calculated as

$$\bar{I}_{\mathrm{LB}} = 1 - H_{\mathrm{b}}(\varpi) \tag{4-45}$$

$$= 1 - (-\varpi \log_2(\varpi) - (1-\varpi)\log_2(1-\varpi)) \tag{4-46}$$

Note that ϖ is calculated numerically. For practical design, in this study, the uncoded BER has been considered to obtain a lower bound on spectral efficiency. However, alternative methods like the one presented in [20] have been developed to calculate the lower bound on the spectral efficiency for mappings with zero-crossing information.

4.4.2 Numerical Results

Here, we compare the performance of the considered ZX mappings numerically. Simulation parameters are listed in Table 4.2, where I_{b} and O_{s} denote the number of input bits and output symbols per block of N Nyquist intervals. For the RLL mapping, we always choose $d = M_{\mathrm{Tx}} - 1$. The SNR is defined as in (4-11).

Simulation results are obtained for a system with $N_{\mathrm{t}} = 8$ transmit antennas and $N_{\mathrm{u}} = 2$ single-antenna users. The entries of $\boldsymbol{H}$ are i. i. d. zero-mean complex Gaussian distributed with unit variance. The noise samples in $\boldsymbol{n}$ are complex Gaussian with zero mean and variance σ_n^2. The receive and the transmit filters are chosen as a root-raised cosine and RC, respectively; each with roll-off factor $\epsilon_{\mathrm{Rx}} = \epsilon_{\mathrm{Tx}} = 0.22$. Parameters are chosen similarly to [2]. Furthermore, for all numerical evaluations, it holds $M_{\mathrm{Rx}} = M_{\mathrm{Tx}}$.

First, we evaluate the uncoded BER for all ZX mapping configurations from Table 4.2 in Fig 4.14 Comparing the time-instance ZX mapping with $M_{\mathrm{Tx}} = 2$ and the RLL ZX mapping with $M_{\mathrm{Tx}} = 3$, which both achieve the same transmission rate (cf. Table 4.2), we notice that for SNR above approx. 10dB, the RLL ZX mapping achieves a substantially lower uncoded BER. Note that the remaining configurations are difficult to compare, as they result in different transmission rates (cf. Table 4.2).

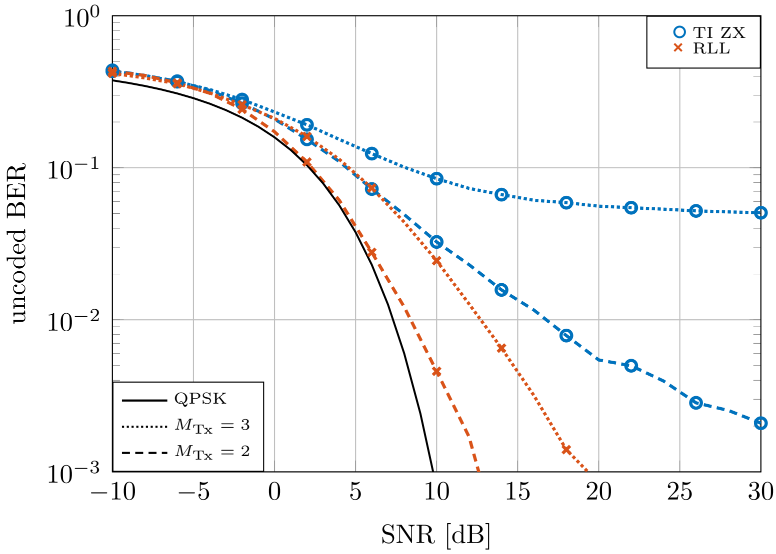

Figure 4.14: Uncoded BER.

In Fig 4.15 we evaluate the SE lower bound given in (4-44). For SNR below 0dB, all schemes show a similar performance. The RLL ZX mappings achieve the highest SE for all considered SNR. However, the encoding and decoding complexity of the RLL ZX mappings is also higher. For SNR below and above 10dB, the highest SE is achieved using the RLL mapping with $M_{\mathrm{Tx}} = 2$ and $M_{\mathrm{Tx}} = 3$, respectively. Surprisingly, the TI ZX mapping achieves a higher SE for $M_{\mathrm{Tx}} = 2$ as for $M_{\mathrm{Tx}} = 3$. This could be caused by increased ISI in case of higher M_{Tx}.

Finally, for $M_{\mathrm{Tx}} = 2$, we compare the SE lower bound for the ZX mappings to QP [2]. QP involves zero-forcing spatial precoding and per user MMDDT codebook optimization [2], i. e., temporal precoding; its performance is depicted in Fig. 4.16 Because MMDDT precoding is known to outperform MMSE precoding at high SNR, whereas MMSE precoding is better at low SNR, we also consider a modified version of QP here: We optimize a single codebook for all users w. r. t. the MSE criterion and then employ MMSE precoding. This scheme is denoted as QP w/ MMSE in Fig. 4.16 The ZX mappings achieve a significantly higher SE as QP with MMSE precoding for SNR > 0dB. This demonstrates the effectiveness of signaling in the time-domain, i. e., encoding the information in the ZX, as compared to signaling in the amplitude-domain, e. g., using QP, for systems employing 1-bit quantization and oversampling. QP achieves the highest SE at high SNR, which is also partly due to MMDDT precoding. However, in practice, the complexity of QP is prohibitive as it involves optimization and transmission of a codebook for each user and channel realization [2].

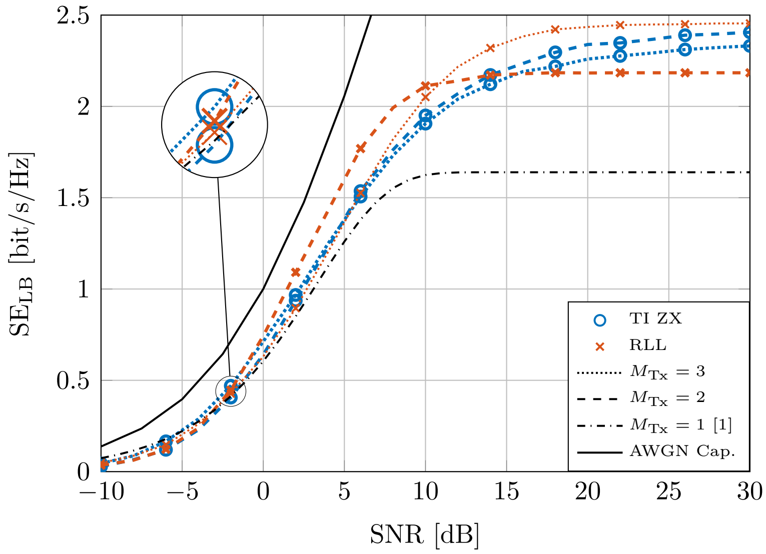

Figure 4.15: Lower bound on the SE for a bandlimited channel. All ZX mappings achieve a substantially higher SE as compared to standard QPSK signaling with 1-bit quantization [1].

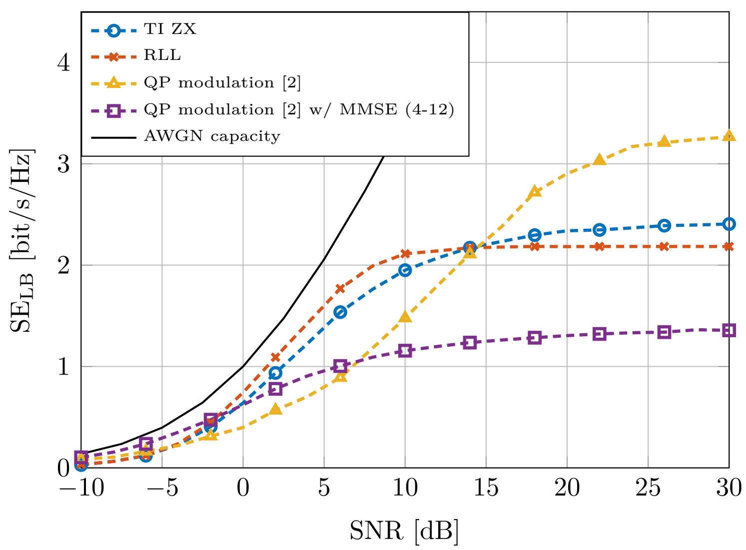

Figure 4.16: Comparison SE lower bound of the considered ZX mappings to QP modulation [2]

5
Proposed State Machine-based Waveform Design With TI ZX Modulation

In this part of the study, we propose a TI ZX waveform design for multiuser MIMO systems in downlink scenarios with 1-bit quantization and oversampling where a predefined level of out-of-band radiation is tolerated. The proposed waveform design considers the novel TI ZX modulation and follows a similar idea as presented in [26]. The proposed method conveys the information into the time-instances of zero-crossings but instead of considering sequences of samples, input bits are mapped into waveform segments according to the TI ZX mapping rules. The temporal precoding vector is then used with a simple pulse shaping filter. The optimal set of coefficients is computed with an optimization problem which is formulated to maximize the minimum distance to the decision threshold, constrained with some tolerated out-of-band radiation.

A multiuser MIMO downlink scenario with N_{u} single antenna users and N_{t} transmit antennas at the BS, is also considered as shown in Fig. 5.1. The input sequence of bits for user k is mapped into the sequences of symbols $\boldsymbol{x}_k$, such that transmission blocks of N symbols (N Nyquist intervals) are considered. The input sequence for user k is mapped using the TI ZX mapping and the set of coefficients $\mathcal{G}$ which yields the temporal precoding vector $\boldsymbol{s}_{g_k} \in \mathbb{C}^{N_{\mathrm{tot}}}$, where $N_{\mathrm{tot}} = M_{\mathrm{Rx}} N$ and M_{Rx}/T denotes the sampling rate and T refers to the symbol duration. Moreover, the transmit filter $g_{\mathrm{Tx}}(t)$ and receive filter $g_{\mathrm{Rx}}(t)$ are presented, where the combined waveform is given by $v(t) = (g_{\mathrm{Tx}} * g_{\mathrm{Rx}})(t)$. Furthermore 1-bit quantization is applied at the receivers. The channel matrix $\boldsymbol{H} \in \mathbb{C}^{N_{\mathrm{u}} \times N_{\mathrm{t}}}$ is known at the base station and is considered to be frequency-flat fading as typically assumed for narrowband IoT systems [2]. Then, stacking the temporal precoding vector of all the N_{u} users, the temporal precoding vector $\boldsymbol{s}_g$ is otained such that $\boldsymbol{s}_g = \left[\boldsymbol{s}_{g_1}^T, \boldsymbol{s}_{g_2}^T, \cdots, \boldsymbol{s}_{g_k}^T, \cdots, \boldsymbol{s}_{g_{N_{\mathrm{u}}}}^T\right]^T$.

The received signal $\boldsymbol{z} \in \mathbb{C}^{N_{\mathrm{tot}} N_{\mathrm{u}}}$ can be expressed by stacking the received samples of the N_{u} users as follows:

$$\begin{aligned} \boldsymbol{z} &= Q_1\left(\left(\boldsymbol{H}\boldsymbol{P}_{\mathrm{sp}} \otimes \boldsymbol{I}_{N_{\mathrm{tot}}}\right)\left(\boldsymbol{I}_{N_{\mathrm{u}}} \otimes \boldsymbol{V}\right)\boldsymbol{s}_{\mathrm{g}} + \left(\boldsymbol{I}_{N_{\mathrm{u}}} \otimes \boldsymbol{G}_{\mathrm{Rx}}\right)\boldsymbol{n}\right) \\ &= Q_1\left(\left(\boldsymbol{H}\boldsymbol{P}_{\mathrm{sp}} \otimes \boldsymbol{V}\right)\boldsymbol{s}_{\mathrm{g}} + \left(\boldsymbol{I}_{N_{\mathrm{u}}} \otimes \boldsymbol{G}_{\mathrm{Rx}}\right)\boldsymbol{n}\right) \\ &= Q_1\left(\boldsymbol{H}_{\mathrm{eff}}\boldsymbol{s}_{\mathrm{g}} + \boldsymbol{G}_{\mathrm{Rx,eff}}\boldsymbol{n}\right), \end{aligned} \tag{5-1}$$

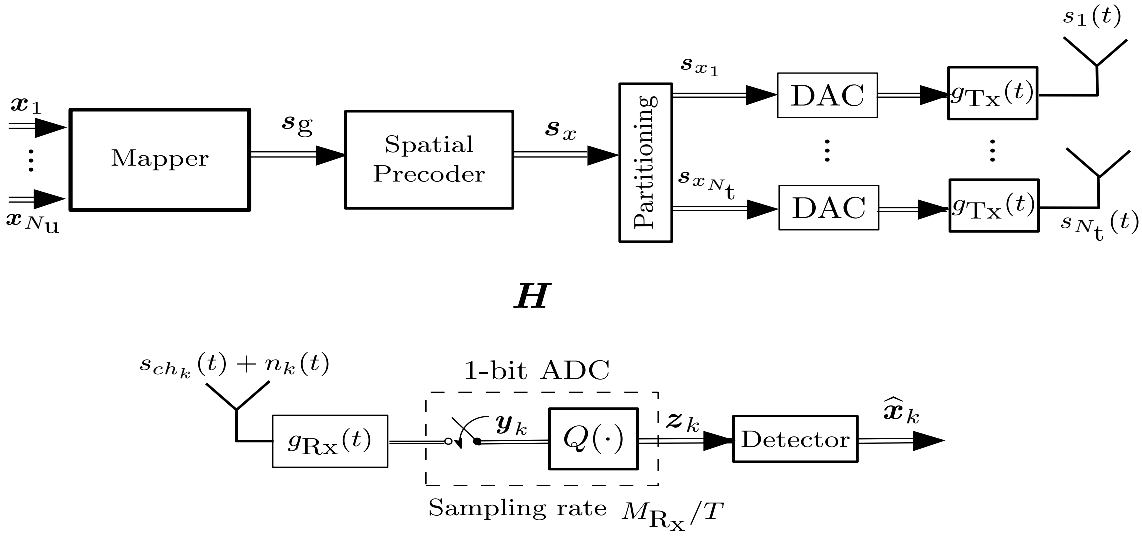

Figure 5.1: Considered multi-user MIMO downlink system model.

where, $\boldsymbol{n} \in \mathbb{C}^{3N_{\mathrm{tot}}N_{\mathrm{u}}}$ denotes a vector with zero-mean complex Gaussian noise samples with variance σ_n^2. The matrix $\boldsymbol{P}_{\mathrm{sp}}$ denotes the spatial zero-forcing precoder.

5.1 Waveform Design Optimization

The proposed waveform design, suitable for systems with 1-bit quantization and oversampling, considers the TI ZX modulation, in conjunction with the optimization of a set of coefficients. It means that instead of considering binary sequences of samples, the proposed waveform is built by concatenating segment sequences of coefficients that contain zero-crossings at the desired time-instances according to $\boldsymbol{c}_{\mathrm{map}}$.

The proposed waveform design relies on the transmit and receive filters $g_{\mathrm{Tx}}(t)$ and $g_{\mathrm{Rx}}(t)$ which preserve the zero-crossing time-instance. Different to the classic TI ZX, the sequence is no longer binary but is defined by the set of coefficients $\boldsymbol{\mathcal{G}}$ so that each symbol x_i drawn from the set $\mathcal{X}_{\mathrm{in}}$ is mapped into a codeword $\boldsymbol{g}_i$ with M_{Rx} different coefficients which convey the information into the time-instances of zero-crossings. As in the original TI ZX modulation, it is considered that sequences are constructed for real and imaginary parts independently. In the following, a real-valued process is described.

The set of optimal coefficients $\boldsymbol{\mathcal{G}}$ with dimensions $n_{\mathrm{s}} \times q$ is defined in terms of $\boldsymbol{\mathcal{G}} = \{\boldsymbol{G}_+; \boldsymbol{G}_-\}$ where $\boldsymbol{G}_- = -\boldsymbol{G}_+$, such that they both convey the same zero-crossings information. In this context, $\boldsymbol{G}_+$ is associated to $\rho = 1$ and $\boldsymbol{G}_-$ is associated to $\rho = -1$.

Considering bit sequences as input and the Gray coding for TI ZX modulation shown in Table 3.3 and Table 3.4, q is established such that

$q = 3$ for $M_{\text{Rx}} = 3$ and $q = 4$ for $M_{\text{Rx}} = 2$, where q denotes the length of the codeword when Gray coding is considered. In the same way, $n_s = 8$ for $M_{\text{Rx}} = 3$ and $n_s = 16$ for $M_{\text{Rx}} = 2$, where n_s represents the number of different codewords. By considering the symmetry in $\mathcal{G}$, we define the reduced matrices $\boldsymbol{G}_{+/-} = \left[\boldsymbol{g}^T_{1_{+/-}}; \boldsymbol{g}^T_{2_{+/-}}; \cdots ; \boldsymbol{g}^T_{\frac{n_s}{2}_{+/-}}\right]$, where $\boldsymbol{g}_{i_{+/-}} = \left[g_{i,1_{+/-}}, g_{i,2_{+/-}}, \cdots g_{i,q_{+/-}}\right]$ and $\rho = \operatorname{sgn}(g_{i,q})$.

In this context the set $\mathcal{G}$ is shown in Table 5.1 for $M_{\text{Rx}} = 3$ and the matrix $\boldsymbol{G}_+ = -\boldsymbol{G}_-$ for $M_{\text{Rx}} = 3$ is described as

$$\boldsymbol{G}_+ = -\boldsymbol{G}_- = \begin{pmatrix} g_{1,1} & g_{1,2} & g_{1,3} \\ g_{2,1} & g_{2,2} & -g_{2,3} \\ g_{3,1} & -g_{3,2} & -g_{3,3} \\ -g_{4,1} & -g_{4,2} & -g_{4,3} \end{pmatrix} \tag{5-2}$$

Table 5.1: Set of optimal coefficients $\mathcal{G}$ for $M_{\text{Rx}} = 3$.

$\mathcal{G}$		
$g_{1,1}$	$g_{1,2}$	$g_{1,3}$
$g_{2,1}$	$g_{2,2}$	$-g_{2,3}$
$g_{3,1}$	$-g_{3,2}$	$-g_{3,3}$
$-g_{4,1}$	$-g_{4,2}$	$-g_{4,3}$
$-g_{1,1}$	$-g_{1,2}$	$-g_{1,3}$
$-g_{2,1}$	$-g_{2,2}$	$g_{2,3}$
$-g_{3,1}$	$g_{3,2}$	$g_{3,3}$
$g_{4,1}$	$g_{4,2}$	$g_{4,3}$

Then, as initially established, the symbol x_i is mapped in the segment $\boldsymbol{g}_{i_{+/-}}$. The pilot sample ρ_{b} is required for the encoding and decoding processes of the first symbol x_1. Finally, the input sequence of symbols $\boldsymbol{x}_k$ is mapped in the sequence $\boldsymbol{s}_{g_k}$ with length N_{tot} by concatenating all the segments $\boldsymbol{g}_{i_{+/-}}$ such that, $\boldsymbol{s}_{g_k} = [\boldsymbol{g}_0^T, \ldots, \boldsymbol{g}_{N-1}^T]^T$. Note that the pilot sample ρ_{b} is predefined and known at the receivers, hence not included in the precoding vector $\boldsymbol{s}_{g_k}$.

5.1.1 Autocorrelation for TI ZX Modulation

In this section, it is described how to compute the autocorrelation function of the TI ZX modulated signal, considering the set of coefficients $\mathcal{G}$ which conveys the information into the time-instances of zero-crossings.

To obtain the autocorrelation function, the TI ZX modulation system is converted to a finite-state machine where the current output values are determined only by its current state which corresponds to an equivalent Moore machine [45]. For $M_{\mathrm{Rx}} = 3$, one symbol in terms of two bits is mapped in one output pattern, so $n_{\mathrm{s}} = 8$ different states are presented. While for $M_{\mathrm{Rx}} = 2$ sequences of symbols are considered in terms of mapping three bits segments in four samples, such that there are $n_{\mathrm{s}} = 16$ different states. Table 5.2 and Table 5.3 provide the equivalent Moore machine for $M_{\mathrm{Rx}} = 3$ and $M_{\mathrm{Rx}} = 2$, respectively. The states with positive subscripts represent sequences for $\rho = 1$ and states with negative subscripts represent sequences for $\rho = -1$.

Considering a symmetric machine, the matrix $\mathbf{\Gamma}$ is defined with m different positive coefficients, where $m = 12$ for $M_{\mathrm{Rx}} = 3$ and $m = 32$ for $M_{\mathrm{Rx}} = 2$.

The state transition probability matrix $\boldsymbol{Q}$ of the equivalent Moore machine, with dimensions $n_{\mathrm{s}} \times n_{\mathrm{s}}$ is defined for i.i.d. input bits, all valid state transitions have equal probability p with $p = 1/4$ for $M_{\mathrm{Rx}} = 3$ and $p = 1/8$ for $M_{\mathrm{Rx}} = 2$. Furthermore, the vector $\boldsymbol{\pi} = (1/n_{\mathrm{s}})\mathbf{1}$ of length n_{s} corresponds to the stationary distribution of the equivalent Moore machine, which implies $\boldsymbol{\pi}^T \boldsymbol{Q} = \boldsymbol{\pi}^T$. Then, the matrix $\mathbf{\Gamma}$ with dimensions $n_{\mathrm{s}} \times M_{\mathrm{Rx}}$ for $M_{\mathrm{Rx}} = 3$ and $n_{\mathrm{s}} \times 2M_{\mathrm{Rx}}$ for $M_{\mathrm{Rx}} = 2$ is defined which contains the Moore machine's output $\boldsymbol{g}_{i_{+/-}}$. The block-wise correlation matrix of the TI ZX mapping output is given by [64, eq. 3.46]

$$\boldsymbol{R}_{\boldsymbol{g}}^{\kappa} = \mathrm{E}\{\boldsymbol{g}_{\kappa'} \boldsymbol{g}_{\kappa'+\kappa}^{T}\} = \mathbf{\Gamma}^T \mathbf{\Pi} \boldsymbol{Q}^{|\kappa|} \mathbf{\Gamma}. \tag{5-3}$$

Then, the average autocorrelation function $\boldsymbol{r}_g$ of the TI ZX modulation output sequence can be obtained as [64, eq. 3.39]

$$\boldsymbol{r}_{\boldsymbol{g}}[kq+l] = \frac{1}{q} \left(\sum_{i=1}^{q-l} \left[\boldsymbol{R}_{\boldsymbol{g}}^{k}\right]_{i,l+i} + \sum_{i=q-l+1}^{q} \left[\boldsymbol{R}_{\boldsymbol{g}}^{k+1}\right]_{i,l+i-q} \right), \tag{5-4}$$

for $k \in \mathbb{Z}$, $0 \leq l \leq q-1$.

Table 5.2: Equivalent Moore machine for TI ZX mapping for $M_{\mathrm{Rx}} = 3$.

Current state	next state 00	01	11	10	output $\boldsymbol{g}_i$
1_+	1_+	2_+	3_+	4_+	$g_{1,1} \quad g_{1,2} \quad g_{1,3}$
2_+	1_-	2_-	3_-	4_-	$g_{2,1} \quad g_{2,2} \quad -g_{2,3}$
3_+	1_-	2_-	3_-	4_-	$g_{3,1} \quad -g_{3,2} \quad -g_{3,3}$
4_+	1_-	2_-	3_-	4_-	$-g_{4,1} \quad -g_{4,2} \quad -g_{4,3}$
1_-	1_-	2_-	3_-	4_-	$-g_{1,1} \quad -g_{1,2} \quad -g_{1,3}$
2_-	1_+	2_+	3_+	4_+	$-g_{2,1} \quad -g_{2,2} \quad g_{2,3}$
3_-	1_+	2_+	3_+	4_+	$-g_{3,1} \quad g_{3,2} \quad g_{3,3}$
4_-	1_+	2_+	3_+	4_+	$g_{4,1} \quad g_{4,2} \quad g_{4,3}$

Table 5.3: Equivalent Moore machine for TI ZX mapping for $M_{\mathrm{Rx}} = 2$.

Current state	next state 000	001	011	010	110	111	101	100	output $\boldsymbol{g}_i$
1_+	1_+	2_+	3_+	4_+	5_+	6_+	7_+	8_+	$g_{1,1} \quad g_{1,2} \quad g_{1,3} \quad g_{1,4}$
2_+	1_-	2_-	3_-	4_-	5_-	6_-	7_-	8_-	$g_{2,1} \quad g_{2,2} \quad g_{2,3} \quad -g_{2,4}$
3_+	1_-	2_-	3_-	4_-	5_-	6_-	7_-	8_-	$g_{3,1} \quad g_{3,2} \quad -g_{3,3} \quad -g_{3,4}$
4_+	1_-	2_-	3_-	4_-	5_-	6_-	7_-	8_-	$g_{4,1} \quad -g_{4,2} \quad -g_{4,3} \quad -g_{4,4}$
5_+	1_+	2_+	3_+	4_+	5_+	6_+	7_+	8_+	$g_{5,1} \quad -g_{5,2} \quad -g_{5,3} \quad g_{5,4}$
6_+	1_+	2_+	3_+	4_+	5_+	6_+	7_+	8_+	$-g_{6,1} \quad -g_{6,2} \quad -g_{6,3} \quad g_{6,4}$
7_+	1_-	2_-	3_-	4_-	5_-	6_-	7_-	8_-	$-g_{7,1} \quad -g_{7,2} \quad -g_{7,3} \quad -g_{7,4}$
8_+	1_+	2_+	3_+	4_+	5_+	6_+	7_+	8_+	$-g_{8,1} \quad -g_{8,2} \quad g_{8,3} \quad g_{8,4}$
1_-	1_-	2_-	3_-	4_-	5_-	6_-	7_-	8_-	$-g_{1,1} \quad -g_{1,2} \quad -g_{1,3} \quad -g_{1,4}$
2_-	1_+	2_+	3_+	4_+	5_+	6_+	7_+	8_+	$-g_{2,1} \quad -g_{2,2} \quad -g_{2,3} \quad g_{2,4}$
3_-	1_+	2_+	3_+	4_+	5_+	6_+	7_+	8_+	$-g_{3,1} \quad -g_{3,2} \quad g_{3,3} \quad g_{3,4}$
4_-	1_+	2_+	3_+	4_+	5_+	6_+	7_+	8_+	$-g_{4,1} \quad g_{4,2} \quad g_{4,3} \quad g_{4,4}$
5_-	1_-	2_-	3_-	4_-	5_-	6_-	7_-	8_-	$-g_{5,1} \quad g_{5,2} \quad g_{5,3} \quad -g_{5,4}$
6_-	1_-	2_-	3_-	4_-	5_-	6_-	7_-	8_-	$g_{6,1} \quad g_{6,2} \quad g_{6,3} \quad -g_{6,4}$
7_-	1_+	2_+	3_+	4_+	5_+	6_+	7_+	8_+	$g_{7,1} \quad g_{7,2} \quad g_{7,3} \quad g_{7,4}$
8_-	1_-	2_-	3_-	4_-	5_-	6_-	7_-	8_-	$g_{8,1} \quad g_{8,2} \quad -g_{8,3} \quad -g_{8,4}$

5.1.2 Waveform Design

As the signs of the coefficients are predefined by the TI ZX modulation, we optimize the amplitude of the coefficients in the optimization process by introducing the matrix $\boldsymbol{G}$. Let $\boldsymbol{G}$ be a matrix such that $\boldsymbol{G}_{i,j} = \left|\boldsymbol{G}_{+_{i,j}}\right| = \left|\boldsymbol{G}_{-_{i,j}}\right|$. Then, the matrix $\boldsymbol{G}$, is vectorized such that $\boldsymbol{g}_u = \mathrm{vec}(\boldsymbol{G})$. The vector $\boldsymbol{g}_u$ is later optimized such that with this optimal vector the set $\boldsymbol{\mathcal{G}}$ is shaped to construct the temporal precoding vector $\boldsymbol{s}_g$. The autocorrelation function is calculated with (5-4) and the PSD is calculated by

$$S(f) = S_x(f) \left| G_{\mathrm{Tx}}(f) \right|^2, \tag{5-5}$$

where $G_{\mathrm{Tx}}(f)$ refers to the transfer function of the transmit filter g_{Tx} and $S_x(f)$ to the PSD of the transmit sequence

$$S_x(f) = \frac{M_{\mathrm{Rx}}}{T} \sum_{l=-\infty}^{\infty} c_l e^{j2\pi \frac{lT}{M_{\mathrm{Rx}}} f}, \tag{5-6}$$

where c_l denotes the l-th element of the autocorrelation function from (5-4). By defining a critical frequency f_c and a power containment factor η, the inband power is defined as

$$\int_{-f_c}^{f_c} S(f) \mathrm{df} = \eta P, \tag{5-7}$$

where $P = \int_{-\infty}^{\infty} S(f)\mathrm{df}$. Then, when considering $g_{\mathrm{Rx}}(t)$ and $g_{\mathrm{Tx}}(t)$ as rectangular filters,

$$g_{\mathrm{Rx}}(t) = g_{\mathrm{Tx}}(t) = \sqrt{\frac{1}{\frac{T}{M_{\mathrm{Rx}}}}} \mathrm{rect}\left(\frac{t}{\frac{T}{M_{\mathrm{Rx}}}} \right), \tag{5-8}$$

matrix $\boldsymbol{V}$ is as an identity matrix. The absolute value squared of the transfer function is given by

$$\left| G_{\mathrm{Tx}}(f) \right|^2 = \frac{T}{M_{\mathrm{Rx}}} \mathrm{sinc}^2 \left(f \frac{T}{M_{\mathrm{Rx}}} \right). \tag{5-9}$$

With this, (5-5) can be expressed as

$$S(f) = \mathrm{sinc}^2 \left(f \frac{T}{M_{\mathrm{Rx}}} \right) \sum_{l=-\infty}^{\infty} c_l e^{j2\pi \frac{lT}{M_{\mathrm{Rx}}} f}. \tag{5-10}$$

Samples close to the decision threshold are more noise-sensitive. Then, the maximization of the minimum distance to the decision threshold γ is considered as the optimization criterion. With this, an optimization problem that maximizes γ can be formulated as:

$$\begin{aligned} \mathrm{minimize}_{\boldsymbol{g}_u} \quad & -\gamma \\ \text{subject to} \quad & \boldsymbol{g}_u \succeq \gamma \mathbf{1} \\ & \|\boldsymbol{g}_u\|_2^2 \leq m \frac{E_0}{2N_{\mathrm{u}} N M_{\mathrm{Rx}}} \\ & \eta(\boldsymbol{g}_u, f_c) \geq \delta, \end{aligned} \tag{5-11}$$

where δ corresponds to the in band power target ratio. Assuming that the optimal solution for $\boldsymbol{g}_u$ fulfills the power constraint with equality, we can make the following statement. Using the optimal set of coefficients $\mathcal{G}$, the sequence $\boldsymbol{s}_{g_k}$ is constructed for each user. Then, the average total power of the complex transmit signal $\boldsymbol{s}_g$ is given by

$$\mathbb{E}\left\{\boldsymbol{s}_g^H \boldsymbol{A}^H \boldsymbol{A} \boldsymbol{s}_{\mathrm{g}}\right\} = E_0, \tag{5-12}$$

where $\boldsymbol{A} = \boldsymbol{I}_{N_{\mathrm{u}}} \otimes \boldsymbol{G}_{\mathrm{Tx}}^T$. Note that under the assumption in (5-8), $\boldsymbol{A}^H \boldsymbol{A}$ corresponds to the identity matrix of dimensions $N_{\mathrm{tot}} \times N_{\mathrm{tot}}$. Due to the last constraint in (5-11) the problem is non convex and it is difficult to find a solution directly.

When no spectral constraint is considered, the maximum value for γ, it is γ_M is reached, and it is obtained by solving the optimization problem

$$\begin{aligned} \text{minimize}_{\boldsymbol{g}_u} \quad & -\gamma \\ \text{subject to} \quad & \boldsymbol{g}_u \succeq \gamma \mathbf{1} \\ & \|\boldsymbol{g}_u\|_2^2 \leq m \frac{E_0}{2N_{\mathrm{u}} N M_{\mathrm{Rx}}}. \end{aligned} \tag{5-13}$$

The maximum values γ_M reached by solving (5-13) corresponds to $\gamma_M = \sqrt{\frac{E_0}{2N_{\mathrm{u}} N M_{\mathrm{Rx}}}}$.

The optimization problem in (5-11) can be solved more easily with fewer restrictions if it is considered that instead of maximizing γ, the power containment bandwidth factor η is maximized. Then, the next section explains in detail how to find sub-optimal solutions to the optimization problem in (5-11).

5.2 A Practical Waveform Design Optimization Strategy

This section describes the implementation of the solution to problem (5-11). Once the oversampling factor M_{Rx} has been defined, an initial vector $\boldsymbol{g}_u = \gamma \mathbf{1}$ of positive coefficients of length $m = 12$ is established. Then the matrix Q of the equivalent Moore machine, which defines the transition probability from one state to another, is established as shown below for

$M_{\mathrm{Rx}} = 3$.

$$\boldsymbol{Q} = \frac{1}{4}\begin{bmatrix} 1 & 1 & 1 & 1 & 0 & 0 & 0 & 0 \\ 0 & 0 & 0 & 0 & 1 & 1 & 1 & 1 \\ 0 & 0 & 0 & 0 & 1 & 1 & 1 & 1 \\ 0 & 0 & 0 & 0 & 1 & 1 & 1 & 1 \\ 0 & 0 & 0 & 0 & 1 & 1 & 1 & 1 \\ 1 & 1 & 1 & 1 & 0 & 0 & 0 & 0 \\ 1 & 1 & 1 & 1 & 0 & 0 & 0 & 0 \\ 1 & 1 & 1 & 1 & 0 & 0 & 0 & 0 \end{bmatrix}. \tag{5-14}$$

With the initial vector $\boldsymbol{g}_u$ the matrix $\boldsymbol{\Gamma}$ is shaped. Then the matrix $\boldsymbol{\Pi} = \mathrm{diag}(\boldsymbol{\pi})$ is defined. With a maximum value κ established, the average autocorrelation is calculated through equation (5-4).

To calculate the PSD in (5-10), a new variable $f_T = fT$ is introduced such that normalized vector $\boldsymbol{f}_T$ is defined as

$$\boldsymbol{f}_T = [0, 0.001, 0.002, \cdots, \lambda].$$

Then the double side average autocorrelation function is shaped by flipping the vector $\boldsymbol{r}_g$ in the left-right direction except for the first sample and concatenating with the original $\boldsymbol{r}_g$ vector. Then, $S(f) = S^{'}(\boldsymbol{f}_T)$ is calculated with (5-10) using the vector $\boldsymbol{f}_T$.

The approximate integral P_T of $S(f)$ is computed as:

$$P_T = \int_0^{\lambda/T} S(f)df \approx \frac{\Delta_f}{2}\sum_{n=1}^{N_f}(S^{'}(f_{T,n}) + S^{'}(f_{T,n+1})), \tag{5-15}$$

where $\Delta_f = \frac{\lambda}{N_f T}$ and $N_f + 1$ corresponds to the length of the vector $\boldsymbol{f}_T$. Then the critical frequency is set to f_c, and the approximate integral P_{f_c} of $S(f) = S^{'}(\boldsymbol{f}_{T_c})$ is calculated for a normalized frequency vector $\boldsymbol{f}_{T_c} = [0, 0.001, \cdots, f_c T]$. Then, the in-band power can be computed as follows

$$P_{f_c} = \int_0^{f_c} S(f)df \approx \frac{\Delta_{f_c}}{2}\sum_{n=1}^{N_c}(S^{'}(f_{T_c,n}) + S^{'}(f_{T_c,n+1})), \tag{5-16}$$

where $\Delta_{f_c} = \frac{f_c}{N_c T}$ and $N_c + 1$ corresponds to the length of the vector $\boldsymbol{f}_{T_c}$. Next, the power containment factor η is calculated as

$$\eta = \frac{P_{f_c}}{P_T}. \tag{5-17}$$

Algorithm 4 Proposed algorithm to solve (5-11)

1: Define a critical frequency f_c
2: Define $\gamma = \Delta_\gamma$
3: Define an in band power target ratio α
repeat
4: Initialize $\boldsymbol{g}_u = \gamma\mathbf{1}$
repeat
5: solve

$$\begin{aligned} \text{minimize}_{\boldsymbol{g}_u} \quad & -\eta(\boldsymbol{g}_u) \\ \text{subject to} \quad & \|\boldsymbol{g}_u\|_2^2 \leq m\frac{E_0}{2N_\mathrm{u}NM_\mathrm{Rx}} \\ & \boldsymbol{g}_u \succeq \gamma\mathbf{1}, \end{aligned}$$

until A feasible solution is found.
6: Increase γ, $\gamma = \gamma + \Delta_\gamma$ in (5-18)
until $\eta \leq \delta$.

With the latter, an equivalent optimization problem to (5-11) is expressed as:

$$\begin{aligned} \text{minimize}_{\boldsymbol{g}_u} \quad & -\eta(\boldsymbol{g}_u) \\ \text{subject to} \quad & \|\boldsymbol{g}_u\|_2^2 \leq m\frac{E_0}{2N_\mathrm{u}NM_\mathrm{Rx}} \\ & \boldsymbol{g}_u \succeq \gamma\mathbf{1}, \end{aligned} \tag{5-18}$$

where γ corresponds to the minimum value of $\boldsymbol{g}_u$. Practical solutions for the problem in (5-18) can be found by numerical local optimization. When the optimal value for $\eta > \delta$, then γ can be increased, in terms of $\gamma = \gamma + \Delta_\gamma$ and the process is repeated until $\eta \approx \delta$. The optimization strategy is summarized in Algorithm 4.

Finally, the detection process for the proposed waveform, follows the same process as for the existing TI ZX waveforms described in Section 3.3

5.3 Numerical Results

This section presents numerical results in terms of uncoded BER and normalized PSD for the proposed TI ZX state machine waveform design. Moreover, the proposed technique results are compared with other methods, namely TI ZX MMDDT and ZX transceiver design [26]. The system under consideration employs $N_\mathrm{t} = 8$ transmit antennas and $N_\mathrm{u} = 2$ single-antenna users for all the evaluated methods. The SNR is defined as follows:

$$\mathrm{SNR} = \frac{E_0 \mathrm{trace}\left(HH^H\right)}{NTN_0N_\mathrm{u}N_\mathrm{t}2f_c}, \tag{5-19}$$

where N_0 denotes the noise power spectral density. The bandwidth B is defined as $B = 2f_c$, where the critical frequency is set to $f_c = 0.65/T$. The entries of the channel matrix $\boldsymbol{H}$ are i.i.d. with $\mathcal{CN}(0,1)$.

The presented results for the TI ZX MMDDT method consider $M_{\mathrm{Rx}} = 3$ and the same data rate as for the proposed TI ZX state machine waveform design with $g_{\mathrm{Tx}}(t)$ as an RC filter and $g_{\mathrm{Rx}}(t)$ as an RRC filter with roll-off factors $\epsilon_{\mathrm{Tx}} = \epsilon_{\mathrm{Rx}} = 0.22$, with $f_c = (1 + \epsilon_{\mathrm{Tx}})/2T$. On the other hand, for the ZX transceiver design [26], $M_{\mathrm{Rx}} = 3$ is considered for the random and the Golay mapping methods. The truncation interval is set to $\zeta = 3$ and the number of bits per subinterval $n = 2$, and at the receiver an integrate-and-dump-filter is considered [26]. Table 5.4 presents the simulation parameters considered to solve the optimization problem in (5-18). On the other hand, Table 5.5 summarizes the simulation specifications for the proposed TI ZX waveform design and other methods from the literature, where I_{b} corresponds to the number of input bits per user and O_{s} represents the number of samples after the mapping process.

The optimal matrix $\boldsymbol{G}$ of positive coefficients is shown in Table 5.6 and Table 5.7 for $M_{\mathrm{Rx}} = 2$ and $M_{\mathrm{Rx}} = 3$, respectively, where the normalization $\frac{E_0}{N} = 1$ is considered for the problems in (5-11), (5-13) and (5-18). The input sequences of symbols $\boldsymbol{x}$ are mapped onto the temporal transmit vector $\boldsymbol{s}_g$ considering the set of coefficients in Table 5.6 and Table 5.7 where $N_{\mathrm{u}} = 1$ are considered and $\delta = 0.95$. Moreover, Δ_γ was set to $\Delta_\gamma = 0.1$ for $M_{\mathrm{Rx}} = 3$ and $\Delta_\gamma = 0.001$ for $M_{\mathrm{Rx}} = 2$. Fig. 5.2 illustrates an example for $M_{\mathrm{Rx}} = 3$, of how the sequence $\boldsymbol{s}_g$ is built taking into account the optimal coefficients $\boldsymbol{G}$ of Table 5.7. For Fig. 5.2, it is considered an example of the input sequence of bits $\boldsymbol{x}_k = [0, 0, 1, 0, 1, 0, 1, 1, 0, 1]$ and with the Gray coding shown in Table 3.3 two bits are mapped in one sequence $\boldsymbol{g}$. The pilot sample is set to $\rho_b = 1$ such that for the first binary tuple 00 the mapped sequence corresponds to $\boldsymbol{g}_{1_+} = [g_{1,1}, g_{1,2}, g_{1,3}] = [0.6592, 0.3531, 0.2237]$. To map the second binary tuple 10, the last sample of $\boldsymbol{g}_{1_+}$ needs to be taken into account, so that $\rho = \mathrm{sgn}\,(0.2237) = 1$, therefore the mapped sequence corresponds to $\boldsymbol{g}_{4_+} = [-g_{4,1}, -g_{4,2}, -g_{4,3}] = [-0.1823, -0.3117, -0.5094]$. The process is done for the whole sequence $\boldsymbol{x}_k$ and the final sequence $\boldsymbol{s}_g = \left[\boldsymbol{g}_{1_+}, \boldsymbol{g}_{4_+}, \boldsymbol{g}_{4_-}, \boldsymbol{g}_{3_+}, \boldsymbol{g}_{2_-}\right]$.

In Fig. 5.3 the influence of the bandwidth on γ is presented, which confirms that when higher amount of out-of-band radiation is allowed, the optimal γ reaches a higher value. For $M_{\mathrm{Rx}} = 3$ the maximum value for $\gamma_M = 1/\sqrt{6N_{\mathrm{u}}}$ where an 79% of in band radiation is reached. In the case of $M_{\mathrm{Rx}} = 2$ the maximum value for $\gamma_M = 1/(2\sqrt{N_{\mathrm{u}}})$, where an 83% of in band radiation is reached. It is also observed that the case with $M_{\mathrm{Rx}} = 2$ reaches a higher γ value than for $M_{\mathrm{Rx}} = 3$ when achieving the same in-band power. Then, Fig. 5.4 presents the BER results considering $\gamma_M = 0.35$ for $M_{\mathrm{Rx}} = 2$ and $\gamma_M = 0.28$ $M_{\mathrm{Rx}} = 3$. In the case of $M_{\mathrm{Rx}} = 2$, it shows a better performance

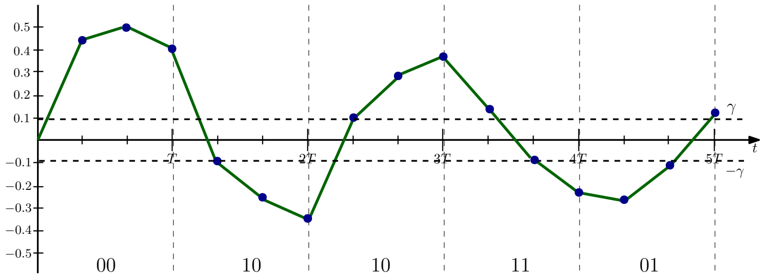

Figure 5.2: Mapping process for construction of $\boldsymbol{s}_g$ with the set of optimal coefficients $\boldsymbol{G}$ for $M_{\text{Rx}} = 3$.

since it is based on a higher γ_M value.

Numerical results are also presented in terms of BER for the proposed TI ZX state machine waveform design in Fig. 5.5 for $M_{\text{Rx}} = 2$ and $M_{\text{Rx}} = 3$. As expected for $M_{\text{Rx}} = 2$ a lower BER is achieved than for $M_{\text{Rx}} = 3$. In both cases, a target power containment factor $\delta = 0.95$ was reached. On the other hand, $\gamma = 0.07$ for $M_{\text{Rx}} = 3$ and $\gamma = 0.17$ for $M_{\text{Rx}} = 2$.

In Fig. 5.6 the BER is evaluated and compared with other methods form the literature for $M_{\text{Rx}} = 3$. The proposed TI ZX state machine waveform design achieves a lower BER than the TI ZX MMDDT while having a lower computational complexity. In this context, the complexity order for the proposed state machine waveform design is dominated by the spatial ZF precoder whose complexity in Big O nation is given by $\mathcal{O}\left(N_{\text{t}}^3\right)$. This is because the coefficients are optimized only once for any transmitted sequence of symbols. On the other hand, the complexity order for the TI ZX MMDDT is given by $\mathcal{O}\left(2N_{\text{u}}(N_{\text{tot}})^{3.5} + N_{\text{t}}^3\right)$. However, note that the proposed TI ZX state machine waveform design yields a low level of out-of-band-radiation as seen in Fig. 5.7. Additionally, the proposed method is compared with the transceiver design from [26]. The transceiver design method considers the nonuniform zero-crossing pattern with random and Golay mapping and power containment factor $\eta = 0.95$. The proposed TI ZX state machine BER performance is better than the transceiver design [26] when both allow the same level of out-of-band radiation since the concatenation of the codewords which conveys the zero-crossing information for TI ZX method is done considering the sign of the last coefficient of the previous Nyquist Interval. The latter implies a lower number of zero-crossings on average, which can be understood as a relaxation in the waveform design. The concatenation process for the TI ZX method is different from the method in [26] which does not consider the state of the previous Nyquist Interval.

Simulation results are presented also in terms of the normalized PSD.

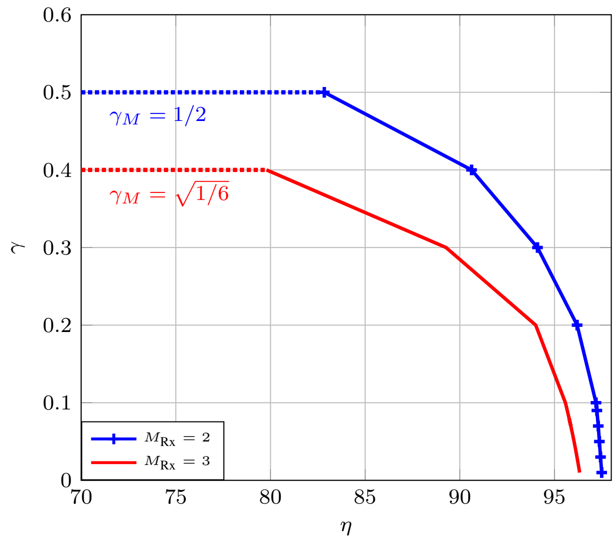

Figure 5.3: γ vs η with $N_{\mathrm{u}} = 1$.

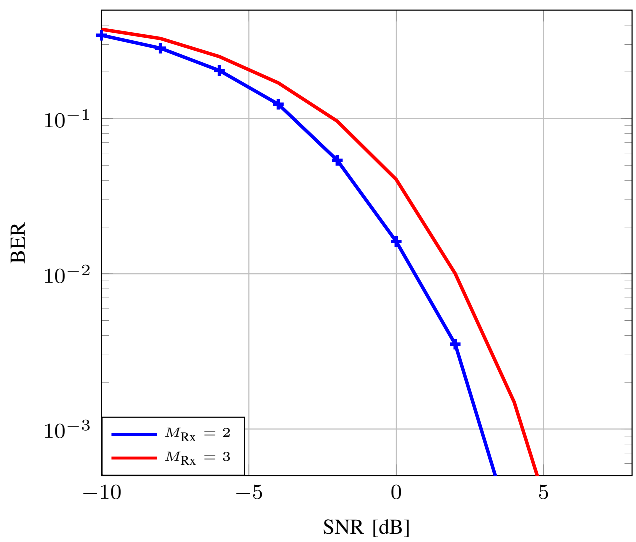

Figure 5.4: BER vs SNR for γ_M with $N_u = 2$.

In Fig. 5.7 the analytical and numerical PSD are compared for the proposed TI ZX state machine waveform design with $M_{\mathrm{Rx}} = 3$. The analytical PSD is calculated with (5-5) considering the autocorrelation function in (5-4). In Fig. 5.7, the normalized PSD of the proposed waveform design is also compared with the normalized PSD of the methods from the literature which is calculated by

$$\mathrm{PSD}_{\mathrm{dB}} = 10\log_{10}\left[O_{\mathrm{s}}^{(-1)}\mathrm{E}\{|F_i|^2\}\right], \tag{5-20}$$

where F_i is the discrete Fourier transform of the normalized temporal transmit signal per user.

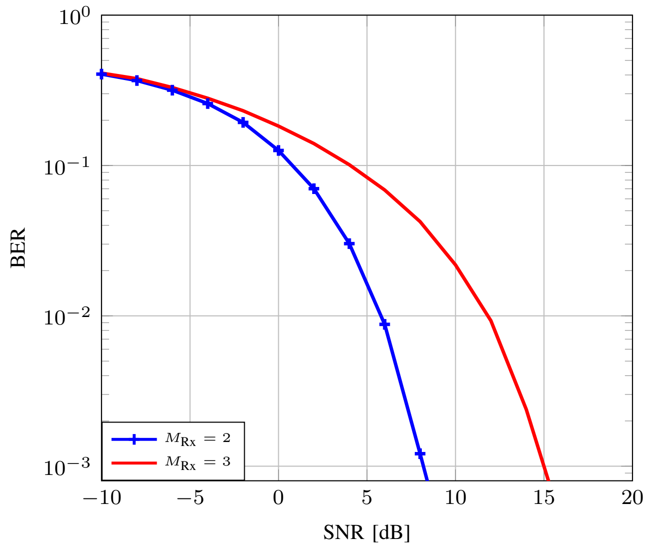

Figure 5.5: BER vs SNR for the proposed waveform with $\delta = 0.95$.

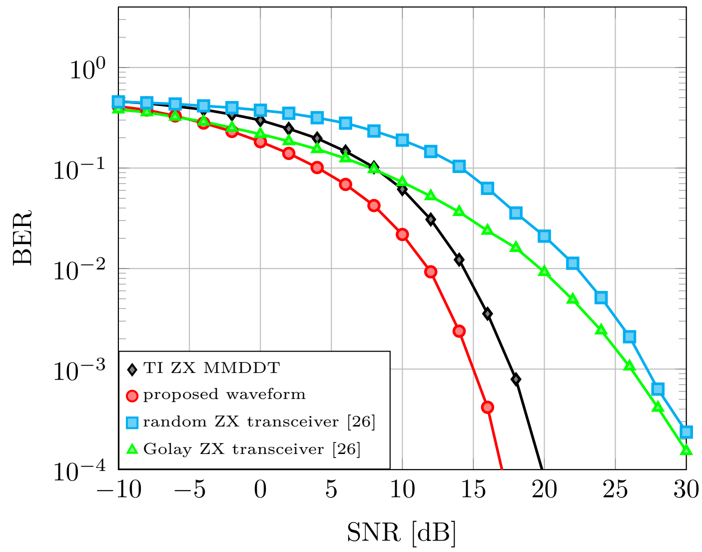

Figure 5.6: BER vs SNR for $M_{\mathrm{Rx}} = 3$ for all the considered methods.

Table 5.4: Parameters values

Parameter	**Value**
κ	400
f_c	$0.65/T$
λ	$2M_{\mathrm{Rx}}$
Δ_γ	0.01
δ	0.95

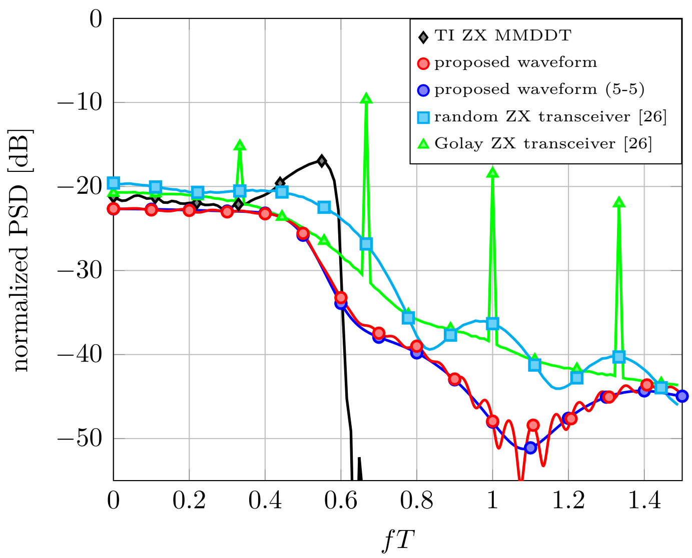

Figure 5.7: PSD for $M_{\mathrm{Rx}} = 3$.

Table 5.5: Simulation parameters

Method	M_{Rx}	Transmit Filter	Receive filter	I_{b}	O_{s}
TI ZX MMDDT	2	RC $\alpha = 0.22$	RRC $\alpha = 0.22$	45	61
	3			60	91
ZX transceiver design [26]	3	RC window $\alpha = 0.1$	Integrate-and-dump	180	270
TI ZX waveform design	2	Integrator $\frac{T}{M_{\mathrm{Rx}}}$	Integrator $\frac{T}{M_{\mathrm{Rx}}}$	45	60
	3			60	90

Table 5.6: Optimal set $\boldsymbol{G}$ for $M_{\mathrm{Rx}} = 2$ with $N_{\mathrm{u}} = 1$ and $\delta = 0.95$

$\boldsymbol{G}$					
$\boldsymbol{g}_1$	000	0.8176,	0.5430,	0.4428,	0.25
$\boldsymbol{g}_2$	001	0.25,	0.25,	0.25,	0.25
$\boldsymbol{g}_3$	011	0.19,	0.5461,	0.25,	0.25
$\boldsymbol{g}_4$	010	0.25,	0.5131,	0.6711,	0.25
$\boldsymbol{g}_5$	110	1.1826,	0.25,	0.25,	0.25
$\boldsymbol{g}_6$	111	0.25,	0.25,	0.7025,	0.25
$\boldsymbol{g}_7$	101	0.7287,	0.25,	0.3715,	0.4114
$\boldsymbol{g}_8$	100	0.25,	0.25,	0.462,	0.424

Table 5.7: Optimal set $\boldsymbol{G}$ for $M_{\mathrm{Rx}} = 3$ with $N_{\mathrm{u}} = 1$ and $\delta = 0.95$

$\boldsymbol{G}$				
$\boldsymbol{g}_1$	00	0.6592,	0.3531,	0.2237
$\boldsymbol{g}_2$	01	0.1,	0.6986,	0.1
$\boldsymbol{g}_3$	11	0.1,	0.3724,	0.5866
$\boldsymbol{g}_4$	10	0.1823	0.3117	0.5094

6
TI ZX for mmWave Channels

In this part of the study, we develop a precoding framework with the novel TI ZX modulation with the established mmWave channel model. We adopted different precoding techniques namely the MMSE precoding and the joint MMDDT precoding.

6.1
Precoding Framework

For the development of the precoding framework, the adopted system model is the one presented in Fig. 2.1. The channel is considered as a frequency-selective mmWave channel with impulse response in continuous time for user k defined as

$$\boldsymbol{h}_k(t) = \sum_{l=0}^{L_k-1} \alpha_{l,k} \boldsymbol{a}_{\mathrm{Tx}}^H(\theta_{l,k}) \delta(t - \tau_{l,k}), \tag{6-1}$$

where $\delta(t-\tau_{l,k})$ corresponds to the Dirac delta function, τ_l the delay of the l-th path, $\alpha_l \in \mathbb{C}$ is the channel coefficient on the l-th path and $\theta_{l,k}$ the angle of departure for the l-th path. The steering vector $\boldsymbol{a}_{\mathrm{Tx}}(\theta_{l,k}) \in \mathbb{C}^{N_\mathrm{t}}$ is defined as

$$\boldsymbol{a}_{\mathrm{Tx}}(\theta_{l,k}) = \frac{1}{\sqrt{N_\mathrm{t}}} \left[1, \cdots, e^{-j\pi(N_\mathrm{t}-1)\sin(\theta_{l,k})}\right]^T, \tag{6-2}$$

where the inter-element spacing is half-wavelength. Including the effects of pulse shaping filtering, the corresponding channel is represented as

$$\tilde{\boldsymbol{h}}_k(t) = \sum_{l=0}^{L_k-1} \alpha_{l,k} \boldsymbol{a}_{\mathrm{Tx}}^H(\theta_{l,k}) v(t - \tau_{l,k}). \tag{6-3}$$

The effects of pulse shaping filtering are given by the combined waveform determined by the transmit and receive filters which is described by $v(t) = g_{\mathrm{Tx}}(t) * g_{\mathrm{Rx}}(t)$. In discrete time, the combined waveform for the l-th path of user k is represented by the matrix $\mathbf{V}_{l,k}$ with size N_{tot} in equation (4-41). The received signal is quantized and vectorized such that the vector $\boldsymbol{z}_k \in \mathbb{C}^{N_{\mathrm{tot}}}$ is obtained. Considering a frequency selective channel with L_k number of channel

$$\mathbf{V}_{l,k} = \tag{6-4}$$
$$\begin{bmatrix} v\left(\tau_{l,k}\right) & v\left(\frac{T}{M_{\mathrm{Rx}}}+\tau_{l,k}\right) & \cdots & v\left(TN+\tau_{l,k}\right) \\ v\left(-\frac{T}{M_{\mathrm{Rx}}}+\tau_{l,k}\right) & v\left(\tau_{l,k}\right) & \cdots & v\left(T\left(N-\frac{1}{M_{\mathrm{Rx}}}\right)+\tau_{l,k}\right) \\ \vdots & \vdots & \ddots & \vdots \\ v\left(-TN+\tau_{l,k}\right) & v\left(T\left(-N+\frac{1}{M_{\mathrm{Rx}}}\right)+\tau_{l,k}\right) & \cdots & v\left(\tau_{l,k}\right) \end{bmatrix}$$

paths, the received signal for user k is described as

$$\boldsymbol{z}_k = Q_1\left(\boldsymbol{y}_k\right), \tag{6-5}$$

where

$$\begin{aligned} \boldsymbol{y}_k &= \sum_{l=0}^{L_k-1}\sum_{i=1}^{N_{\mathrm{t}}} \alpha_{l,k} a_{\mathrm{Tx}_i}(\theta_{l,k}) \boldsymbol{V}_{l,k}\boldsymbol{U}\boldsymbol{p}_{x_i} + \boldsymbol{G}_{\mathrm{Rx}}\boldsymbol{n}_k \\ &= \sum_{l=0}^{L_k-1} \alpha_{l,k}\left[a_{\mathrm{Tx}_1}(\theta_{l,k})\boldsymbol{V}_{l,k}\boldsymbol{U}, a_{\mathrm{Tx}_2}(\theta_{l,k})\boldsymbol{V}_{l,k}\boldsymbol{U}, \cdots,\right. \\ &\qquad \left. a_{\mathrm{Tx}_{N_{\mathrm{t}}}}(\theta_{l,k})\boldsymbol{V}_{l,k}\boldsymbol{U}\right]\left[\boldsymbol{p}_{x_1}^T, \cdots, \boldsymbol{p}_{x_{N_{\mathrm{t}}}}^T\right]^T + \boldsymbol{G}_{\mathrm{Rx}}\boldsymbol{n}_k \\ &= \sum_{l=0}^{L_k-1} \alpha_{l,k}\left(\boldsymbol{a}_{\mathrm{Tx}}^H(\theta_{l,k}) \otimes \boldsymbol{I}_{N_{\mathrm{tot}}}\right)\left(\boldsymbol{I}_{N_{\mathrm{t}}} \otimes \mathbf{V}_{l,k}\boldsymbol{U}\right)\boldsymbol{p}_{\mathrm{x}} \\ &\qquad + \boldsymbol{G}_{\mathrm{Rx}}\boldsymbol{n}_k, \end{aligned} \tag{6-6}$$

where the stacked vector $\boldsymbol{p}_{\mathrm{x}} = \left[\boldsymbol{p}_{\mathrm{x}_1}^T, \boldsymbol{p}_{\mathrm{x}_2}^T, \cdots, \boldsymbol{p}_{\mathrm{x}_i}^T, \cdots, \boldsymbol{p}_{\mathrm{x}_{N_{\mathrm{t}}}}^T\right]^T$ and $\boldsymbol{p}_{\mathrm{x}_i} \in \mathbb{C}^{N_{\mathrm{q}}}$ corresponds to the spatial and temporal precoding vector of the i-th transmit antenna and $\boldsymbol{n}_k \in \mathbb{C}^{3N_{\mathrm{tot}}}$ represents the complex Gaussian noise vector with zero mean and variance σ_n^2. Defining the matrix

$$\boldsymbol{H}_{\mathrm{eff}_k} = \sum_{l=0}^{L_k-1} \alpha_{l,k}\left(\boldsymbol{a}_{\mathrm{Tx}}^H(\theta_{l,k}) \otimes \boldsymbol{I}_{N_{\mathrm{tot}}}\right)\left(\boldsymbol{I}_{N_{\mathrm{t}}} \otimes \mathbf{V}_{l,k}\boldsymbol{U}\right) \tag{6-7}$$

equation (6-6) can be rewritten as

$$\boldsymbol{y}_k = \boldsymbol{H}_{\mathrm{eff}_k}\boldsymbol{p}_{\mathrm{x}} + \boldsymbol{G}_{\mathrm{Rx}}\boldsymbol{n}_{\boldsymbol{k}}. \tag{6-8}$$

Then, stacking the received sequences of the N_{u} user in the vector $\boldsymbol{z} = \left[\boldsymbol{z}_1^T, \boldsymbol{z}_2^T, \cdots, \boldsymbol{z}_i^T, \cdots, \boldsymbol{z}_{N_{\mathrm{u}}}^T\right]^T$ the received signal can be written as

$$\begin{aligned} \boldsymbol{z} &= Q_1\left(\boldsymbol{y}\right) \\ &= Q_1\left(\boldsymbol{H}_{\mathrm{eff}}\boldsymbol{p}_{\mathrm{x}} + \boldsymbol{G}_{\mathrm{Rx,eff}}\boldsymbol{n}\right), \end{aligned} \tag{6-9}$$

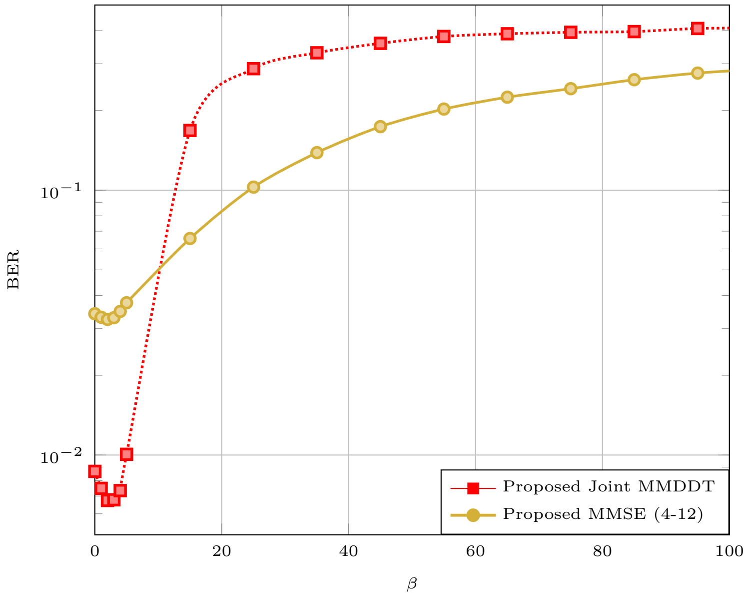

Figure 6.1: BER vs. β for $M_{\mathrm{Rx}} = M_{\mathrm{Tx}} = 2$, $L_k = 5$ and SNR = 20dB.

where

$$\begin{aligned} \boldsymbol{H}_{\mathrm{eff}} &= \left[\boldsymbol{H}_{\mathrm{eff}_1}, \boldsymbol{H}_{\mathrm{eff}_2}, \cdots, \boldsymbol{H}_{\mathrm{eff}_{N_\mathrm{u}}}\right]^H \\ \boldsymbol{G}_{\mathrm{Rx,eff}} &= \left(\boldsymbol{I}_{N_\mathrm{u}} \otimes \boldsymbol{G}_{\mathrm{Rx}}\right), \end{aligned} \tag{6-10}$$

and $\boldsymbol{n} = [\boldsymbol{n}_1, \boldsymbol{n}_2, \cdots, \boldsymbol{n}_k, \cdots, \boldsymbol{n}_{N_\mathrm{u}}]$.

The two considered precoding designs are the joint MMDDT from Section 4.1.1.1 and the general MMSE criterion in space and time from Section 4.2.

6.2 Numerical Results

The numerical evaluations of the precoding techniques joint MMDDT and MMSE considering signals transmitted over a frequency selective channel are presented in this section in terms of BER considering different parameters. The transmit filter $g_{\mathrm{Tx}}(t)$ is an RC filter and the receive filter $g_{\mathrm{Rx}}(t)$ is an RRC filter, where the roll-off factors are $\epsilon_{\mathrm{Tx}} = \epsilon_{\mathrm{Rx}} = 0.22$ [2]. The bandwidth is defined with $W_{\mathrm{Rx}} = W_{\mathrm{Tx}} = (1 + \epsilon_{\mathrm{Tx}})/T$. The BS is equipped with $N_\mathrm{t} = 8$ antennas, $N_\mathrm{u} = 2$ single antenna users, $N = 30$ transmit symbols, and maximum energy constraint E_0. The mmWave channel parameters are defined

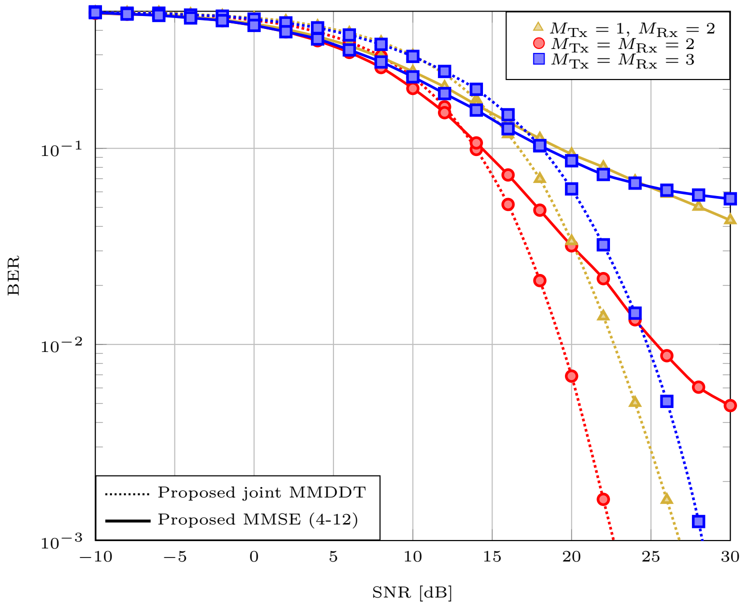

Figure 6.2: BER vs. SNR. for different sets of signaling and sampling rates with $L_k = 5$ and $\beta = 1.5$.

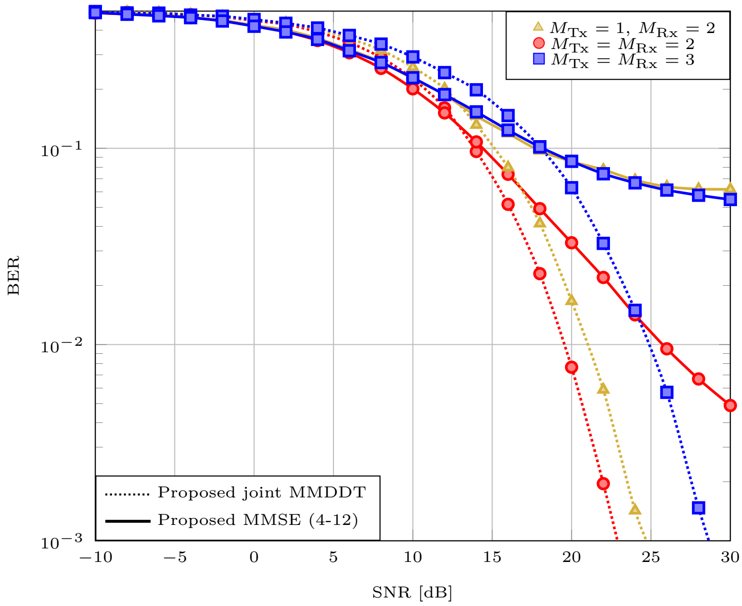

Figure 6.3: BER vs. SNR. for different sets of signaling and sampling rates with $L_k = 5$ and $\beta = 0$.

as follows

$$\alpha_{l,k} \sim \mathcal{CN}\left(0, \frac{1}{L_k}\right) \tag{6-11}$$

$$\theta_{l,k} \sim \text{uniform}\left(\left[\frac{-\pi}{2}, \frac{\pi}{2}\right]\right) \tag{6-12}$$

$$\tau_{l,k} \sim \text{uniform}\left([0, \beta T]\right). \tag{6-13}$$

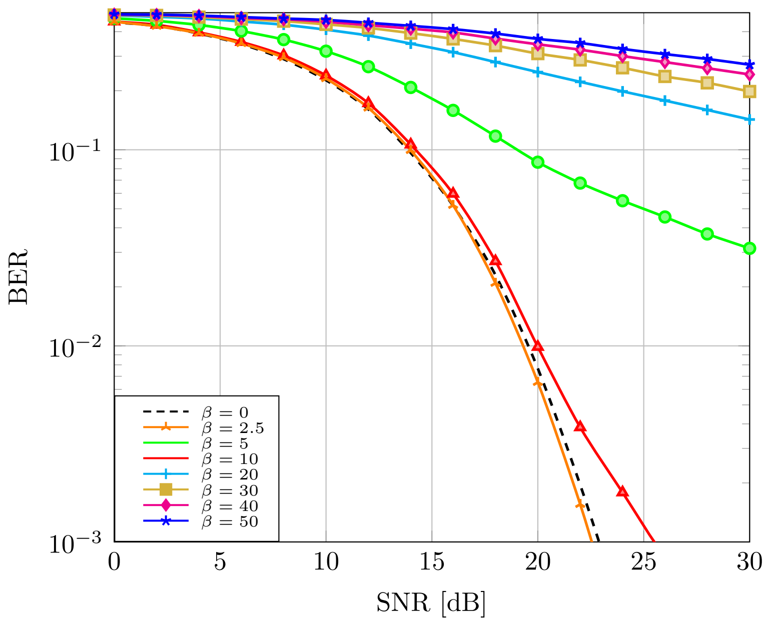

Figure 6.4: BER vs. SNR with $M_{\text{Rx}} = M_{\text{Tx}} = 2$ and $L_k = 5$ for different values of β for joint MMDDT.

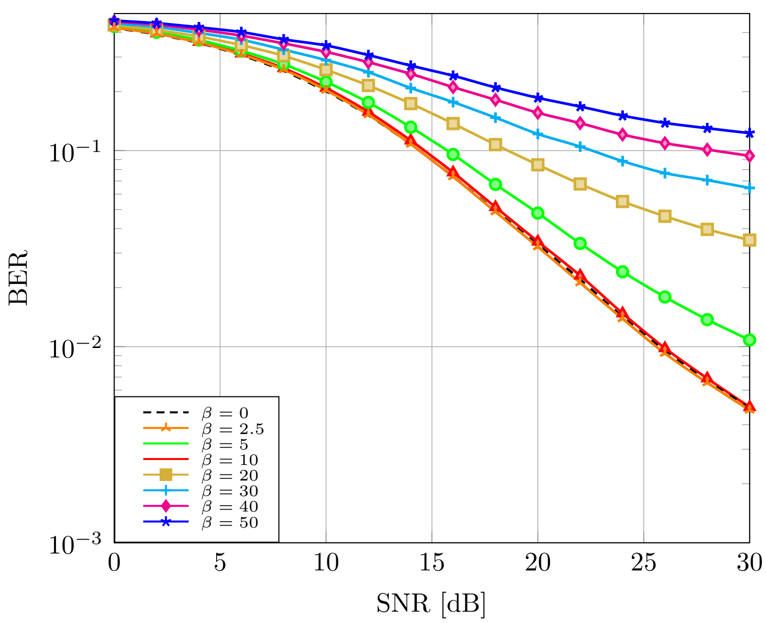

Figure 6.5: BER vs. SNR with $M_{\text{Rx}} = M_{\text{Tx}} = 2$ and $L_k = 5$ for different values of β for MMSE.

Moreover, we also considered the special case where $\tau_{l,k} = 0$, [65]. The SNR is defined as in (4-11).

Fig. 6.1 presents the BER performance in terms of β for SNR = 20dB with $L_k = 5$ paths for each user and $M_{\text{Rx}} = M_{\text{Tx}} = 2$. The results show that starting from $\beta = 5$ the BER decreases faster for both precoding techniques. Moreover, the BER for the MMSE is lower in comparison with the joint

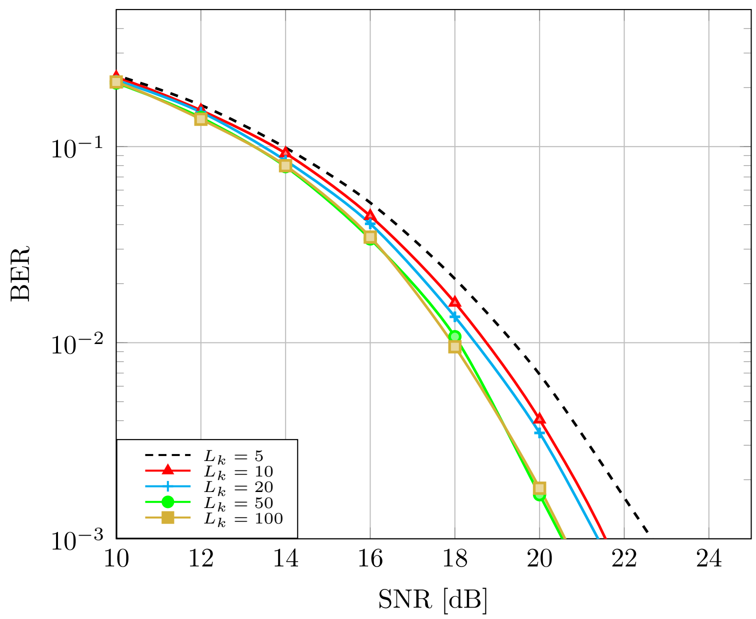

Figure 6.6: BER vs. SNR with $M_{\mathrm{Rx}} = M_{\mathrm{Tx}} = 2$ and $\beta = 1.5$ for different values of L_k for joint MMDDT.

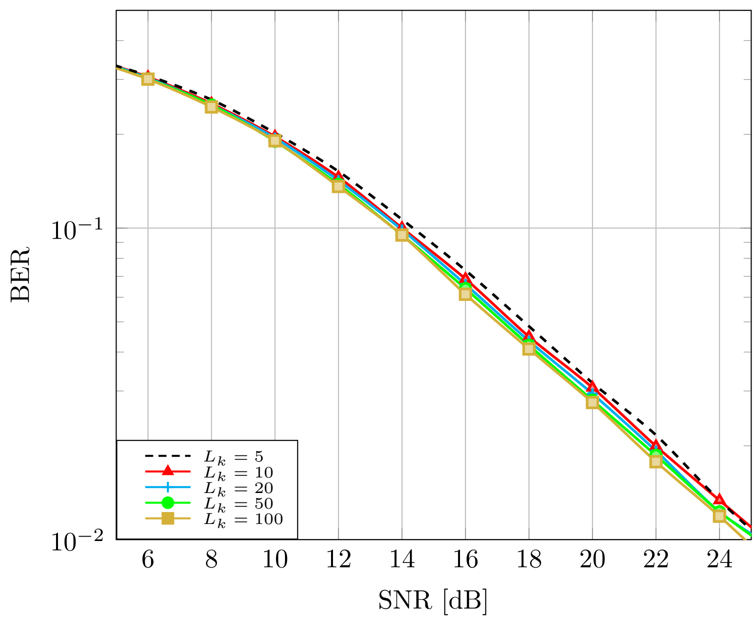

Figure 6.7: BER vs. SNR with $M_{\mathrm{Rx}} = M_{\mathrm{Tx}} = 2$ and $\beta = 1.5$ for different values of L_k for MMSE.

MMDDT precoding technique.

Fig. 6.2 shows simulation results in terms of BER where different sets of signaling rate (M_{Tx}/T) and sampling rate (M_{Rx}/T) are considered. Moreover, the same number of paths is set for all the users with $L_k = 5$ and $\beta = 1.5$. In the figure, it is possible to observe that the joint MMDDT technique reaches a better performance than the MMSE technique in the high SNR region, while

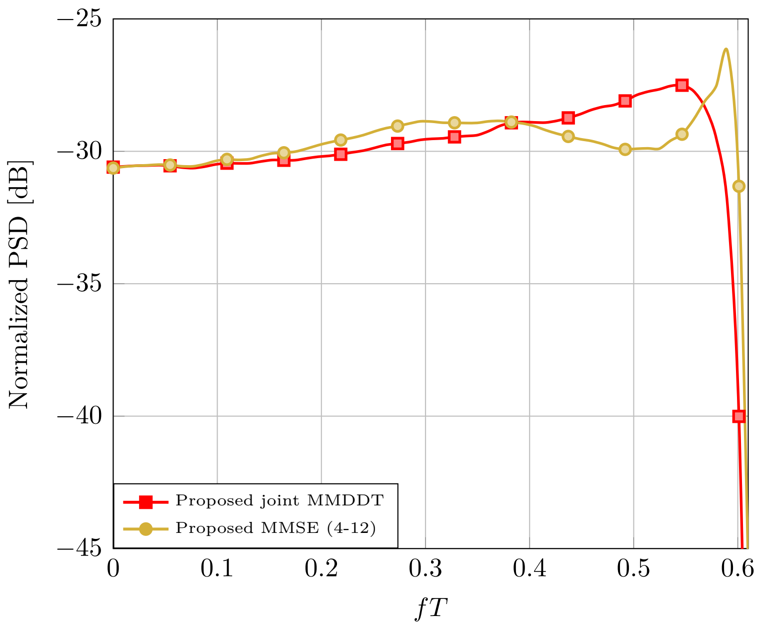

Figure 6.8: Power spectral density for $M_{\mathrm{Rx}} = M_{\mathrm{Tx}} = 2$, $L_k = 5$ and $\beta = 1.5$.

the MMSE based technique presents a better performance in the lower SNR region. Additionally, in Fig. 6.3 simulation results are presented with the same parameters as in Fig. 6.2 but considering $\beta = 0$. These results present the same trend as those presented in Section 4.3, where a channel based on a Rayleigh fading distribution is considered. Moreover Fig. 6.4 and Fig. 6.5 compare simulation results for $M_{\mathrm{Rx}} = M_{\mathrm{Tx}} = 2$ and $L_k = 5$ for different values of β, for the MMDDT precoding technique and MMSE precoding technique, respectively. From both figures, it is possible to observe that for relatively large β the BER performance decreases.

Fig. 6.6 and Fig. 6.7 show the numerical evaluation for the MMDDT precoding technique and MMSE precoding technique respectively, in terms of the number of L_k paths considering $\beta = 1.5$. The number of paths is the same for all the N_{u} users. The results indicate that when the number of paths is increased, the BER shows a slight decrease.

Finally, Simulation results in terms of normalized PSD are also presented for the joint MMDDT and MMSE precoding techniques in Fig. 6.8. The results were simulated considering $M_{\mathrm{Rx}} = M_{\mathrm{Tx}} = 2$, $L_k = 5$ and $\beta = 0.0001$ employing

$$\mathrm{PSD}_{\mathrm{dB}} = 10\log_{10}\left[\mathrm{E}\{\left|F_i(\sqrt{3N_{\mathrm{tot}}})^{(-1)}\right|^2\}\right], \tag{6-14}$$

where F_i is the discrete Fourier transform of the signal per transmit antenna given by $\boldsymbol{s}_i = \boldsymbol{G}_{\mathrm{Tx}}^{\mathrm{T}}\boldsymbol{U}\boldsymbol{p}_{\mathrm{x}_i}$.

7
Conclusions

This study proposes different precoding methods for bandlimited multiuser MIMO downlink channels with 1-bit quantization at the receivers. To compensate for the loss caused by the quantization, oversampling is considered at the receivers. For this specific channel with a given oversampling factor, a sophisticated modulation is proposed, namely TI ZX modulation. The proposed modulation conveys the information in the time-instance of the zero-crossings. Also it considers the absence of a zero-crossing during a Nyquist interval as a unique pattern, which is different from prior studies. The proposed TI ZX modulation is compared with the established method known from the literature using the existing precoding strategy [2]. Simulation results show a significant benefit of the proposed TI ZX in terms of the uncoded BER, which can be explained by the reduced number of zero-crossings in the modulated sequence. For the considered channel, in conjunction with the proposed TI ZX modulation, novel precoding techniques are developed based on the distance to the decision threshold criterion and the MMSE criterion, namely the joint MMDDT, total MMDDT ZF, MMSE, optimal MMSE ACE, iterative MMSE ACE and the iterative Gradient Descent method for MMSE.

The MMDDT based precoding techniques maximize the minimum distance to the decision threshold where the joint MMDDT maximizes the criterion jointly for space and time. An approximate solution that relies on spatial ZF precoding and quality of service constraint is developed in the proposed total MMDDT ZF method. The conventional MMSE based precoding technique minimizes the MSE between the received signal and the desired discrete output pattern. A more advanced method is proposed in terms of the optimal MMSE ACE, where the output pattern is optimized jointly. An approximate solution to the optimal MMSE ACE is devised by the iterative MMSE ACE, where the precoding vector and the output pattern are optimized with an alternating strategy.

The proposed precoding methods are evaluated in terms of the BER, MSE, and computational complexity. In general, it can be observed that the MMDDT approaches yield superior performance in the high SNR region and that the MMSE approaches are beneficial in the low SNR region. Moreover, by taking into account the ACE in the MMSE method, the BER performance significantly improves for the high SNR. Among all the considered precoding approaches, the joint MMDDT approach yields the best performance in terms of BER at high SNR regime. On the other hand, the MMSE ACE methods yield good performance for all SNR regions. The complexity analysis illustrates the benefits of the approximate solutions namely total MMDDT ZF and iterative MMSE ACE. Moreover, numerical results show that the proposed iterative gradient descent method approach has a comparable bit error rate as compared to the closed form MMSE while having significantly lower computational complexity.

In another part of the study, the TI ZX modulation and RLL sequences are compared considering the MMSE precoder, where the TI ZX offers lower complexity with only slightly lower spectral efficiency than the RLL mapping. Furthermore, numerical results showed that both mappings achieved a significantly higher SE at low SNR compared to QP method [2], while simultaneously offering a lower complexity. This demonstrates the advantage of signaling in the time-domain for systems employing 1-bit quantization and oversampling.

This study also proposes a TI ZX state machine waveform based on the TI ZX modulation. The waveform design considers the optimization of a set of coefficients that conveys the information into the time-instances of zero-crossings. The optimization is performed considering the power containment bandwidth and the maximization of the minimum distance to the decision threshold. The simulation results were compared with methods from the literature which employ techniques based on zero-crossings. The BER performance shows that the proposed method achieves a comparable BER result as the TI ZX MMDDT method but with significantly lower computational complexity.

Finally, in this work, it was also developed a precoding framework with TI ZX modulation for a mmWave channel model. The proposed framework allows the application of the previously developed precoding strategies. Two precoding techniques were considered to optimize the transmit vector, the joint MMDDT and the MMSE. Both precoding techniques jointly optimize transmitted vectors in time and space. Simulation results regarding BER show that some small delay spread can yield a performance improvement. Besides, both bandlimited precoding techniques respond well to the frequency selectivity of the mmWave channel. Moreover, comparing both precoding techniques, it can be observed that the joint MMDDT presents better performance in high SNR than the MMSE, which follows what was presented in Chapter 4.

8
Future Work

As future work we propose the investigation of advanced zero-crossing precoding methods for the multi user MIMO downlink which take into account imperfect channel state information.

Existing studies on zero-crossing precoding show promising results in terms of bit error rate which achieve high spectral efficiency simultaneously. However, the existing studies rely on perfect channel state information, which is difficult to achieve in practical downlink systems due to channel estimation errors. To evaluate the TI ZX precoding technique with imperfect CSI one aspect is to study channel estimation algorithms from the state of the art which are suitable for 1-bit quantization channels. One strategy could be the consideration of channel estimation at the user terminals by adopting the channel estimation approach for systems with 1-bit quantization and temporal oversampling. For this case, the channel estimation error statistics can be calculated in terms of the error correlation matrix. This information can be exploited in a robust precoding design for TI ZX modulation. Alternatively, the channel estimation can be done at the BS for time division duplex (TDD) with the reciprocal channel. Therefore, we propose to develop robust TI ZX precoding techniques that take into account imperfect channel state information.

In this context, one can consider that the channel can be defined by a part that is known and a part that is random $\boldsymbol{H} = \tilde{\boldsymbol{H}} + \epsilon$. For the random part ϵ some statistical information might be available in terms of $\mathrm{E}\left\{\epsilon\epsilon^H\right\}$, which can be exploited for the precoding algorithm.

Bibliography

[1] SINGH, J.; DABEER, O. ; MADHOW, U., **On the limits of communication with low-precision analog-to-digital conversion at the receiver**, IEEE Trans. Commun., vol. 57, no. 12, pp. 3629–3639, Dec. 2009.

[2] GOKCEOGLU, A.; BJÖRNSON, E.; LARSSON, E. G. ; VALKAMA, M., **Spatio-temporal waveform design for multiuser massive MIMO downlink with 1-bit receivers**, IEEE J. Sel. Topics Signal Process., vol. 11, no. 2, pp. 347–362, March 2017.

[3] CHEN, J.; ZHANG, L.; LIANG, Y.; KANG, X. ; ZHANG, R., **Resource allocation for wireless-powered IoT networks with short packet communication**, IEEE Trans. Wireless Commun., vol. 18, no. 2, pp. 1447–1461, Feb 2019.

[4] GUPTA, A.; JHA, R. K., **A survey of 5G network: Architecture and emerging technologies**, IEEE Access, vol. 3, pp. 1206–1232, 2015.

[5] RAPPAPORT, T. S.; XING, Y.; KANHERE, O.; JU, S.; MADANAYAKE, A.; MANDAL, S.; ALKHATEEB, A. ; TRICHOPOULOS, G. C., **Wireless communications and applications above 100 GHz: Opportunities and challenges for 6G and beyond**, IEEE Access, vol. 7, pp. 78729–78757, 2019.

[6] G. K. MARENGO, E. S. LIMA, G. E. S. L. A. C. S. J.; MENDES, L. L., **Propagation models for 5G signals in the 60 GHz band**, Journal of Communication and Information Systems, 2020.

[7] WALDEN, R. H., **Analog-to-digital converter survey and analysis**, vol. 17, no. 4, pp. 539–550, Apr. 1999.

[8] SHAMAI (SHITZ), S., **Information rates by oversampling the sign of a bandlimited process**, IEEE Trans. Inf. Theory, vol. 40, no. 4, pp. 1230–1236, July 1994.

[9] KOCH, T.; LAPIDOTH, A., **Increased capacity per unit-cost by oversampling**, In: PROC. OF THE IEEE CONVENTION OF ELECTRICAL AND ELECTRONICS ENGINEERS IN ISRAEL, Eilat, Israel, Nov. 2010.

[10] LANDAU, L.; DÖRPINGHAUS, M. ; FETTWEIS, G. P., **1-bit quantization and oversampling at the receiver: Communication over bandlimited channels with noise**, IEEE Commun. Lett., vol. 21, no. 5, pp. 1007–1010, May 2017.

[11] HÄLSIG, T.; LANDAU, L. ; FETTWEIS, G. P., **Spectral efficient communications employing 1-bit quantization and oversampling at the receiver**, In: PROC. OF THE IEEE VEHICULAR TECHNOLOGY CONFERENCE (FALL), Vancouver, BC, Canada, September 2014.

[12] SINGH, G.; LANDAU, L. ; FETTWEIS, G., **Finite length reconstructible ASK-sequences received with 1-bit quantization and oversampling**, In: PROC. OF THE INT. ITG CONF. ON SYSTEMS, COMMUNICATIONS AND CODING, Hamburg, Germany, Feb. 2015.

[13] SON, H.; HAN, H.; KIM, N. ; PARK, H., **An efficient detection algorithm for PAM with 1-bit quantization and time-oversampling at the receiver**, In: IEEE VEH. TECHNOL. CONF. (VTC2019-FALL), Honolulu, HI, USA, Sep 2019.

[14] LANDAU, L.; DÖRPINGHAUS, M. ; FETTWEIS, G. P., **1-bit quantization and oversampling at the receiver: Sequence-based communication**, EURASIP Journal on Wireless Communications and Networking, April 2018.

[15] NEUHAUS, P.; DÖRPINGHAUS, M.; HALBAUER, H.; WESEMANN, S.; SCHLÜTER, M.; GAST, F. ; FETTWEIS, G., **Sub-THz wideband system employing 1-bit quantization and temporal oversampling**, In: ICC 2020 - 2020 IEEE INTERNATIONAL CONFERENCE ON COMMUNICATIONS (ICC), Dublin, Ireland, June 2020.

[16] BENDER, S.; LANDAU, L.; DÖRPINGHAUS, M. ; FETTWEIS, G. P., **Communication with 1-bit quantization and oversampling at the receiver: Spectral constrained waveform optimization**, In: PROC. OF THE IEEE INT. WORKSHOP ON SIGNAL PROCESSING ADVANCES IN WIRELESS COMMUNICATIONS, Edinburgh, UK, July 2016.

[17] FETTWEIS, G.; DÖRPINGHAUS, M.; BENDER, S.; LANDAU, L.; NEUHAUS, P. ; SCHLÜTER, M., **Zero crossing modulation for communication with temporally oversampled 1-bit quantization**, In: 2019 53RD ASILOMAR CONFERENCE ON SIGNALS, SYSTEMS, AND COMPUTERS, pp. 207–214, 2019.

[18] NEUHAUS, P.; DÖRPINGHAUS, M. ; FETTWEIS, G., **Zero-crossing modulation for wideband systems employing 1-bit quantization and temporal oversampling: Transceiver design and performance evaluation**, IEEE Open Journal of the Communications Society, vol. 2, pp. 1915–1934, 2021.

[19] BENDER, S.; DÖRPINGHAUS, M. ; FETTWEIS, G., **On the spectral efficiency of bandlimited 1-bit quantized AWGN channels with runlength-coding**, IEEE Communications Letters, vol. 24, no. 10, pp. 2147–2151, 2020.

[20] BENDER, S.; DÖRPINGHAUS, M. ; FETTWEIS, G., **On the achievable rate of bandlimited continuous-time AWGN channels with 1-bit output quantization**, J Wireless Com Network, 2021.

[21] LANDAU, L.; DÖRPINGHAUS, M. ; FETTWEIS, G. P., **Communications employing 1-bit quantization and oversampling at the receiver: Faster-than-Nyquist signaling and sequence design**, In: PROC. OF THE IEEE INT. CONF. ON UBIQUITOUS WIRELESS BROADBAND, Montreal, Canada, Oct. 2015.

[22] MAZO, J. E., **Faster-than-Nyquist signaling**, Bell System Technical Journal, vol. 54, no. 1, pp. 1451–1462, Oct. 1975.

[23] HÄLSIG, T.; LANDAU, L. ; FETTWEIS, G. P., **Information rates for faster-than-Nyquist signaling with 1-bit quantization and oversampling at the receiver**, In: PROC. OF THE IEEE VEHICULAR TECHNOLOGY CONFERENCE (SPRING), 2014.

[24] NAAMAN, H.; MULLETI, S. ; ELDAR, Y. C., **Fri-tem: Time encoding sampling of finite-rate-of-innovation signals**, IEEE Transactions on Signal Processing, vol. 70, pp. 2267–2279, 2022.

[25] LANDAU, L.; KRONE, S. ; FETTWEIS, G. P., **Intersymbol-interference design for maximum information rates with 1-bit quantization and oversampling at the receiver**, In: PROC. OF THE INT. ITG CONF. ON SYSTEMS, COMMUNICATIONS AND CODING, Munich, Germany, Jan. 2013.

[26] DENG, R.; ZHOU, J. ; ZHANG, W., **Bandlimited communication with one-bit quantization and oversampling: Transceiver design and performance evaluation**, IEEE Trans. Commun., vol. 69, no. 2, pp. 845–862, Feb. 2021.

[27] KRONE, S.; FETTWEIS, G., **Communications with 1-bit quantization and oversampling at the receiver: Benefiting from intersymbol-interference**, In: 2012 IEEE 23RD INTERNATIONAL SYMPOSIUM ON PERSONAL, INDOOR AND MOBILE RADIO COMMUNICATIONS - (PIMRC), pp. 2408–2413, Sydney, NSW, Australia, Sept. 2012.

[28] BENDER, S.; DÖRPINGHAUS, M. ; FETTWEIS, G., **On the achievable rate of bandlimited continuous-time 1-bit quantized AWGN channels**, In: 2017 IEEE INT. SYMP. INF. THEORY (ISIT), pp. 2083–2087, Aachen, Germany, June 2017.

[29] LANDAU, L. T. N.; DÖRPINGHAUS, M.; DE LAMARE, R. C. ; FETTWEIS, G. P., **Achievable rate with 1-bit quantization and oversampling using continuous phase modulation-based sequences**, IEEE Trans. Wireless Commun., vol. 17, no. 10, pp. 7080–7095, August 2018.

[30] ÜÇÜNCÜ ALI BULUT; ÖZGÜR, Y. A., **Oversampling in one-bit quantized massive MIMO systems and performance analysis**, IEEE Trans. Wireless Commun., vol. 17, no. 12, pp. 7952–7964, October 2018.

[31] ÜÇÜNCÜ ALI BULUT; BJÖRNSON, E.; JOHANSSON, H.; ÖZGÜR, Y. A. ; LARSSON, E. G., **Performance analysis of quantized uplink massive MIMO-OFDM with oversampling under adjacent channel interference**, IEEE Trans. Commun., vol. 68, no. 2, pp. 871–886, November 2020.

[32] SHAO, Z.; LANDAU, L. T. N. ; DE LAMARE, R. C., **Dynamic oversampling for 1-bit ADCs in large-scale multiple-antenna systems**, IEEE Trans. Commun., vol. 69, no. 5, pp. 3423–3435, February 2021.

[33] SHAO, Z.; LANDAU, L. T. N. ; DE LAMARE, R. C., **Channel estimation for large-scale multiple-antenna systems using 1-bit ADCs and oversampling**, IEEE Access, vol. 8, pp. 85243–85256, May 2020.

[34] NEUHAUS, P.; DÖRPINGHAUS, M. ; FETTWEIS, G., **Oversampled 1-bit quantized wideband systems: Is it better to spend samples in time or in space?**, In: PROC. IEEE INT. WORKSHOP ON SIGNAL PROCESS. ADVANCES IN WIRELESS COMMUN. (SPAWC), pp. 1–5, Cannes, France, Jul. 2019.

[35] GOKCEOGLU, A.; BJÖRNSON, E.; LARSSON, E. G. ; VALKAMA, M., **Waveform design for massive MISO downlink with energy-**

efficient receivers adopting 1-bit ADCs, In: PROC. IEEE INT. CONF. COMMUN. (ICC), Kuala Lumpur, Malaysia, May 2016.

[36] LANDAU, L. T. N.; DE LAMARE, R. C., **Branch-and-bound precoding for multiuser MIMO systems with 1-bit quantization**, IEEE Wireless Commun. Lett., vol. 6, no. 6, pp. 770–773, Dec 2017.

[37] JEDDA, H.; MEZGHANI, A.; SWINDLEHURST, A. L. ; NOSSEK, J. A., **Quantized constant envelope precoding with PSK and QAM signaling**, IEEE Trans. Wireless Commun., vol. 17, no. 12, pp. 8022–8034, Dec 2018.

[38] MO, J.; HEATH, R. W., **Capacity analysis of one-bit quantized mimo systems with transmitter channel state information**, IEEE Transactions on Signal Processing, vol. 63, no. 20, pp. 5498–5512, 2015.

[39] LIU, R.; LI, M.; LIU, Q. ; SWINDLEHURST, A. L., **Joint symbol-level precoding and reflecting designs for irs-enhanced mu-miso systems**, IEEE Transactions on Wireless Communications, vol. 20, no. 2, pp. 798–811, 2021.

[40] BENDER, S.; DÖRPINGHAUS, M. ; FETTWEIS, G., **On the achievable rate of multi-antenna receivers with oversampled 1-bit quantization**, In: IEEE 7TH INT. WORKSHOP ON COMPUTATIONAL ADVANCES IN MULTI-SENSOR ADAPTIVE PROCESSING (CAMSAP), Curacao, Dutch Antilles, Dec. 2017.

[41] RAPPAPORT, T. S.; HEATH JR, R. W.; DANIELS, R. C. ; MURDOCK, J. N., *Millimeter Wave Wireless Communications*, Pearson Education, 2014.

[42] JEON, Y.-S.; DO, H.; HONG, S.-N. ; LEE, N., **Soft-output detection methods for sparse millimeter-wave MIMO systems with low-precision ADCs**, IEEE Transactions on Communications, vol. 67, no. 4, pp. 2822–2836, 2019.

[43] KIM, I.; CHOI, J., **Channel estimation via gradient pursuit for mmwave massive MIMO systems with one-bit ADCs**, Wireless Communications Network, 2019.

[44] MO, J.; SCHNITER, P.; PRELCIC, N. G. ; HEATH, R. W., **Channel estimation in millimeter wave MIMO systems with one-bit quantization**, In: 2014 48TH ASILOMAR CONFERENCE ON SIGNALS, SYSTEMS AND COMPUTERS, pp. 957–961, 2014.

[45] NEUHAUS, P.; DÖRPINGHAUS, M. ; FETTWEIS, G., **Zero-crossing modulation for wideband systems employing 1-bit quantization and temporal oversampling: Transceiver design and performance evaluation**, IEEE Open J. Commun. Soc., vol. 2, pp. 1915–1934, 2021.

[46] MELO, D. M. V., *Advanced transmit processing for MIMO downlink channels with 1-bit quantization and oversampling at the receivers*, master's degree in electrical engineering. PUC-RIO, 2020.

[47] MELO, D. M. V.; LANDAU, L. T. N. ; DE LAMARE, R. C., **Zero-crossing precoding with maximum distance to the decision threshold for channels with 1-bit quantization and oversampling**, In: ICASSP 2020 - 2020 IEEE INTERNATIONAL CONFERENCE ON ACOUSTICS, SPEECH AND SIGNAL PROCESSING (ICASSP), pp. 5120–5124, Barcelona, Spain, May 2020.

[48] MELO, D. M. V.; LANDAU, L. T. N. ; DE LAMARE, R. C., **Zero-crossing precoding with MMSE criterion for channels with 1-bit quantization and oversampling**, In: PROC. OF THE INT. ITG WORKSHOP ON SMART ANTENNAS, Hamburg, Germany, Feb. 2020.

[49] MEZGHANI, A.; HEATH, R. W., **Massive MIMO precoding and spectral shaping with low resolution phase-only DACs and active constellation extension**, IEEE Trans. Wireless Commun., vol. 21, no. 7, pp. 5265–5278, 2022.

[50] MELO, D. M. V.; LANDAU, L. T. N.; RIBEIRO, L. N. ; HAARDT, M., **Iterative MMSE space-time zero-crossing precoding for channels with 1-bit quantization and oversampling**, In: 54TH ASILOMAR CONFERENCE ON SIGNALS, SYSTEMS, AND COMPUTERS, pp. 496–500, Pacific Grove, CA, USA, Nov. 2020.

[51] NEUHAUS, P.; MELO, D. M. V.; LANDAU, L. T. N.; DE LAMARE, R. C. ; FETTWEIS, G. P., **Zero-crossing modulations for a multi-user MIMO downlink with 1-bit temporal oversampling ADCs**, In: PROC. EUROPEAN SIGN. PROC. CONF. (EUSIPCO), Dublin, Ireland, August 2021.

[52] LEE, A. J., **Characterization of bandlimited functions and processes**, Inform. Control, vol. 31, no. 3, pp. 258–271, 1976.

[53] EZIO BIGLIERI ; ANTHONY CONSTANTINIDES; ANDREA GOLDSMITH; AROGYASWAMI PAULRAJ; H. VINCENT POOR, *MIMO Wireless Communications*, Cambridge University Press, 21st edition, 2009.

[54] BOYD, S.; VANDENBERGHE, L., *Convex Optimization*, Cambridge University Press, New York, NY, USA, 2004.

[55] MICHAEL JOHAM, *MIMO Systems*, Associate Institute for Signal Processing, Munich, 2010.

[56] SPENCER, Q. H.; SWINDLEHURST, A. L. ; HAARDT, M., **Zero-forcing methods for downlink spatial multiplexing in multiuser MIMO channels**, IEEE Trans. Signal Process., vol. 52, no. 2, pp. 461–471, Feb. 2004.

[57] MELO, D. M. V.; LANDAU, L. T. N.; RIBEIRO, L. N. ; HAARDT, M., **Time-instance zero-crossing precoding with quality-of-service constraints**, In: IEEE STATISTICAL SIGNAL PROCESSING WORKSHOP, SSP 2021, Rio de Janeiro, Brazil, July 2021.

[58] JOHAM, M.; UTSCHICK, W. ; NOSSEK, J. A., **Linear transmit processing in MIMO communications systems**, IEEE Trans. Signal Process., pp. 2700–2712, Aug. 2005.

[59] JOHAM, M.; UTSCHICK, W. ; NOSSEK, J. A., **Linear transmit processing in MIMO communications systems**, IEEE Trans. Signal Process., vol. 53, no. 8, pp. 2700–2712, Aug 2005.

[60] NEUHAUS, P.; DÖRPINGHAUS, M.; HALBAUER, H.; WESEMANN, S.; SCHLÜTER, M.; GAST, F. ; FETTWEIS, G., **Sub-THz wideband system employing 1-bit quantization and temporal oversampling**, In: PROC. IEEE INT. CONF. COMMUN. (ICC), pp. 1–7, Dublin, Ireland, Jun. 2020.

[61] COVER, T. M.; THOMAS, J. A., *Elements of Information Theory*, John Wiley & Sons, New York, NY, USA, 2006.

[62] LANDAU, L. T. N.; DÖRPINGHAUS, M. ; FETTWEIS, G. P., **1-bit quantization and oversampling at the receiver: Sequence-based communication**, EURASIP J. Wireless Commun. Netw., vol. 2018, no. 1, pp. 83, Apr. 2018.

[63] NEUHAUS, P.; DÖRPINGHAUS, M.; HALBAUER, H.; BRAUN, V. ; FETTWEIS, G., **On the spectral efficiency of oversampled 1-bit**

quantized systems for wideband LOS channels, In: PROC. IEEE INT. SYMP. ON PERSONAL, INDOOR AND MOBILE RADIO COMMUN. (PIMRC), pp. 1–6, London, UK, Aug. 2020.

[64] IMMINK, K. A. S., *Codes for Mass Data Storage Systems*, Eindhoven, The Netherlands: Shannon Foundation, 2004.

[65] CHAYOT, R.; BOUCHERET, M.; POULLIAT, C.; THOMAS, N.; WAMBEKE, N. ; LESTHIEVENT, G., **Joint channel and carrier frequency estimation for M-ary CPM over frequency-selective channel using pam decomposition**, In: 2017 IEEE INTERNATIONAL CONFERENCE ON ACOUSTICS, SPEECH AND SIGNAL PROCESSING (ICASSP), pp. 3789–3793, 2017.

[66] IMMINK, K. A. S., *Codes for Mass Data Storage Systems*, Eindhoven, Netherlands: Shannon Foundation Publishers, 2004.

[67] LANDAU, L.; DÖRPINGHAUS, M. ; FETTWEIS, G., **Communications employing 1-bit quantization and oversampling at the receiver: Faster-than-Nyquist signaling and sequence design**, In: PROC. IEEE INT. CONF. ON UBIQUITOUS WIRELESS BROADBAND (ICUWB), pp. 1–5, Montreal, Canada, Oct. 2015.

[68] VITERBI, A., **Error bounds for convolutional codes and an asymptotically optimum decoding algorithm**, IEEE Trans. Inf. Theory, vol. 13, no. 2, pp. 260–269, Apr. 1967.

[69] FORNEY, G. D., **The Viterbi algorithm**, Proc. IEEE, vol. 61, no. 3, pp. 268–278, Mar. 1973.

A
Appendix

A.1
Derivation of The Space-Time MMSE Precoding

The derivation of the space-time MMSE precoder can be done with a strategy similar to what is suggested in [58]. The MSE objective function considers scaling with factor f of the received signal that could model an automatic gain control. Given the received signal (2-8) and the complex desired output pattern $\boldsymbol{c}_{\text{out}}$, the MMSE precoding problem can be cast as (4-12). With an equivalent cost function, the Lagrangian function reads as

$$\begin{aligned} L(\boldsymbol{p}_{\text{x}}, f, \lambda) =& f^2 \left(\|\boldsymbol{H}_{\text{eff}} \boldsymbol{p}_{\text{x}}\|_2^2 + \text{trace}\{\boldsymbol{G}_{\text{Rx,eff}} \boldsymbol{C}_n \boldsymbol{G}_{\text{Rx,eff}}^H\} \right) \\ & - 2f \text{Re}\{\boldsymbol{c}_{\text{out}}^H \boldsymbol{H}_{\text{eff}} \boldsymbol{p}_{\text{x}}\} + \lambda \left(\|\boldsymbol{A}\boldsymbol{p}_{\text{x}}\|_2^2 - E_0 \right). \end{aligned}$$

Equating to zero the derivative of (A-1) w.r.t. $\boldsymbol{p}_{\text{x}}^*$ yields

$$\boldsymbol{p}_{\text{x,opt}} = f^{-1} \left(\boldsymbol{H}_{\text{eff}}^H \boldsymbol{H}_{\text{eff}} + \lambda f^{-2} \boldsymbol{A}^H \boldsymbol{A} \right)^{-1} \boldsymbol{H}_{\text{eff}}^H \boldsymbol{c}_{\text{out}}, \tag{A-1}$$

which can also be written as

$$f^{-1} \boldsymbol{p}_{\text{x}}^H \boldsymbol{H}_{\text{eff}}^H \boldsymbol{c}_{\text{out}} = \boldsymbol{p}_{\text{x}}^H \left(\boldsymbol{H}_{\text{eff}}^H \boldsymbol{H}_{\text{eff}} + \lambda f^{-2} \boldsymbol{A}^H \boldsymbol{A} \right) \boldsymbol{p}_{\text{x}}. \tag{A-2}$$

The derivative of the Lagrangian function w.r.t. f reads as

$$\frac{dL(\boldsymbol{p}_{\text{x}}, f, \lambda)}{df} = 2f \boldsymbol{p}_{\text{x}}^H \boldsymbol{H}_{\text{eff}}^H \boldsymbol{H}_{\text{eff}} \boldsymbol{p}_{\text{x}} - 2\text{Re}\{\boldsymbol{p}_{\text{x}}^H \boldsymbol{H}_{\text{eff}}^H \boldsymbol{c}_{\text{out}}\} + 2f \text{trace}\{\boldsymbol{G}_{\text{Rx,eff}} \boldsymbol{C}_n \boldsymbol{G}_{\text{Rx,eff}}^H\}, \tag{A-3}$$

where the real part operator can be skipped because its argument is always real valued when taking into account the structure of $\boldsymbol{p}_{\text{x,opt}}$ (A-1). Equating (A-3) to zero yields

$$f^{-1} \boldsymbol{p}_{\text{x}}^H \boldsymbol{H}_{\text{eff}}^H \boldsymbol{c}_{\text{out}} = \boldsymbol{p}_{\text{x}}^H \boldsymbol{H}_{\text{eff}}^H \boldsymbol{H}_{\text{eff}} \boldsymbol{p}_{\text{x}} + \text{trace}\{\boldsymbol{G}_{\text{Rx,eff}} \boldsymbol{C}_n \boldsymbol{G}_{\text{Rx,eff}}^H\}. \tag{A-4}$$

Equating the RHS of (A-2) with the RHS of (A-4) gives

$$\lambda f^{-2} = \mathrm{trace}\{\boldsymbol{G}_{\mathrm{Rx,eff}}\boldsymbol{C}_n\boldsymbol{G}_{\mathrm{Rx,eff}}^H\}\left(\boldsymbol{p}_{\mathrm{x}}^H\boldsymbol{A}^H\boldsymbol{A}\boldsymbol{p}_{\mathrm{x}}\right)^{-1}. \tag{A-5}$$

Due to the fact that any precoding vector $\boldsymbol{p}_{\mathrm{x}}$ with less than the maximum transmit energy can not be optimal in the MSE sense, equality can be considered for the transmit energy constraint. With this, (A-5) can be written as $\lambda f^{-2} = \mathrm{trace}\{\boldsymbol{G}_{\mathrm{Rx,eff}}\boldsymbol{C}_n\boldsymbol{G}_{\mathrm{Rx,eff}}^H\}E_0^{-1}$. Then the optimal precoding vector can be expressed as (4-13). Inserting (4-13) into the transmit energy constraint determines the scaling factor, which is then given by $f = \left\|\boldsymbol{c}_{\mathrm{out}}^H\boldsymbol{\Delta}\right\|_2/\sqrt{E_0}$, with

$$\boldsymbol{\Delta} = \boldsymbol{H}_{\mathrm{eff}}\left(\boldsymbol{H}_{\mathrm{eff}}^H\boldsymbol{H}_{\mathrm{eff}} + E_0^{-1}\mathrm{trace}\{\boldsymbol{G}_{\mathrm{Rx,eff}}\boldsymbol{C}_n\boldsymbol{G}_{\mathrm{Rx,eff}}^H\}\boldsymbol{A}^H\boldsymbol{A}\right)^{-1}\boldsymbol{A}^H. \tag{A-6}$$

A.2
MMSE Precoding Performance Bound

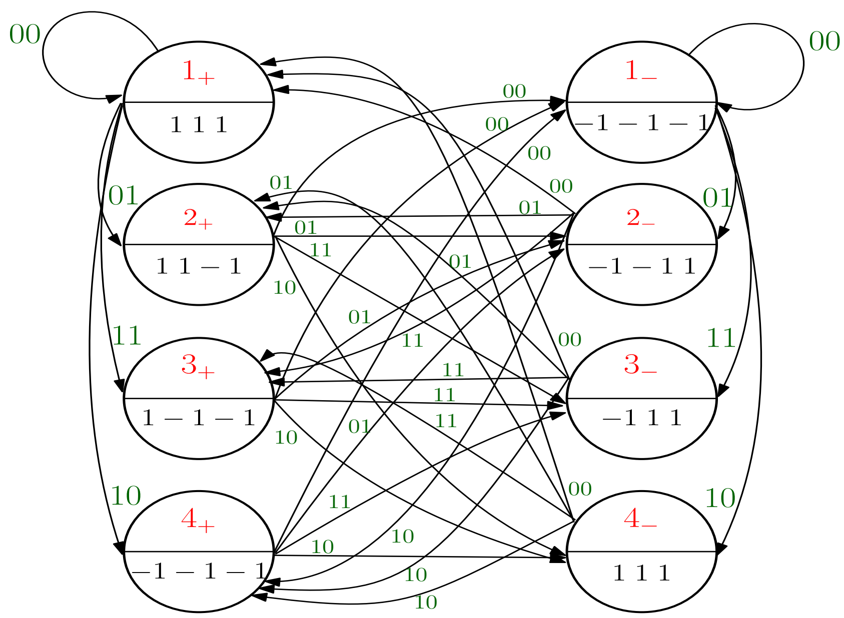

Figure A.1: Equivalent Moore machine for $M_{\mathrm{Rx}} = 3$.

Table A.1: Equivalent Moore machine for $M_{\mathrm{Rx}} = 3$.

Current state	Next state for input				Output c_{s}
	00	01	10	11	
1_+	1_+	2_+	3_+	4_+	$1 \quad 1 \quad 1$
2_+	1_-	2_-	3_-	4_-	$1 \quad 1 \ -1$
3_+	1_-	2_-	3_-	4_-	$1 \ -1 \ -1$
4_+	1_-	2_-	3_-	4_-	$-1 \ -1 \ -1$
1_-	1_-	2_-	3_-	4_-	$-1 \ -1 \ -1$
2_-	1_+	2_+	3_+	4_+	$-1 \ -1 \quad 1$
3_-	1_+	2_+	3_+	4_+	$-1 \quad 1 \quad 1$
4_-	1_+	2_+	3_+	4_+	$1 \quad 1 \quad 1$

In this section, the analytical MMSE is presented for the MMSE precoder in Section 4.2. Applying the trace operator and its properties to the MSE expression in (4-14) yields

$$\begin{aligned} J =& \mathrm{trace}\{\boldsymbol{H}_{\mathrm{eff}}\boldsymbol{X}\boldsymbol{H}_{\mathrm{eff}}^H \mathrm{E}\{\boldsymbol{c}_{\mathrm{out}}\boldsymbol{c}_{\mathrm{out}}^H\}\boldsymbol{H}_{\mathrm{eff}}\boldsymbol{X}^H\boldsymbol{H}_{\mathrm{eff}}^H\} - 2\mathrm{Re}\{\mathrm{trace}\{\boldsymbol{H}_{\mathrm{eff}}\boldsymbol{X}\boldsymbol{H}_{\mathrm{eff}}^H \mathrm{E}\{\boldsymbol{c}_{\mathrm{out}}\boldsymbol{c}_{\mathrm{out}}^H\}\}\} \\ &+ 2N_{\mathrm{tot}} + \boldsymbol{E}\{f^2 \mathrm{trace}\{\boldsymbol{G}_{\mathrm{Rx,eff}}\boldsymbol{C}_n\boldsymbol{G}_{\mathrm{Rx,eff}}^H\}\}, \end{aligned} \tag{A-7}$$

where $\boldsymbol{c}_{\mathrm{out}}^H\boldsymbol{c}_{\mathrm{out}} = 2N_{\mathrm{tot}}$ is considered. With the scaling factor $f = \left\|\boldsymbol{c}_{\mathrm{out}}^H\boldsymbol{\Delta}\right\|_2 / \sqrt{E_0}$ and $\boldsymbol{\Delta}$ from (A-6), (A-7) can be rewritten as

$$\begin{aligned} J =& \mathrm{trace}\{\boldsymbol{H}_{\mathrm{eff}}\boldsymbol{X}\boldsymbol{H}_{\mathrm{eff}}^H \mathrm{E}\{\boldsymbol{c}_{\mathrm{out}}\boldsymbol{c}_{\mathrm{out}}^H\}\boldsymbol{H}_{\mathrm{eff}}\boldsymbol{X}^H\boldsymbol{H}_{\mathrm{eff}}^H\} - 2\mathrm{Re}\{\mathrm{trace}\{\boldsymbol{H}_{\mathrm{eff}}\boldsymbol{X}\boldsymbol{H}_{\mathrm{eff}}^H \mathrm{E}\{\boldsymbol{c}_{\mathrm{out}}\boldsymbol{c}_{\mathrm{out}}^H\}\}\} \\ &+ 2N_{\mathrm{tot}} + (1/E_0)\mathrm{trace}\{\boldsymbol{\Delta}^H \mathrm{E}\{\boldsymbol{c}_{\mathrm{out}}\boldsymbol{c}_{\mathrm{out}}^H\}\boldsymbol{\Delta}\}\mathrm{trace}\{\boldsymbol{G}_{\mathrm{Rx,eff}}\boldsymbol{C}_n\boldsymbol{G}_{\mathrm{Rx,eff}}^H\}. \end{aligned} \tag{A-8}$$

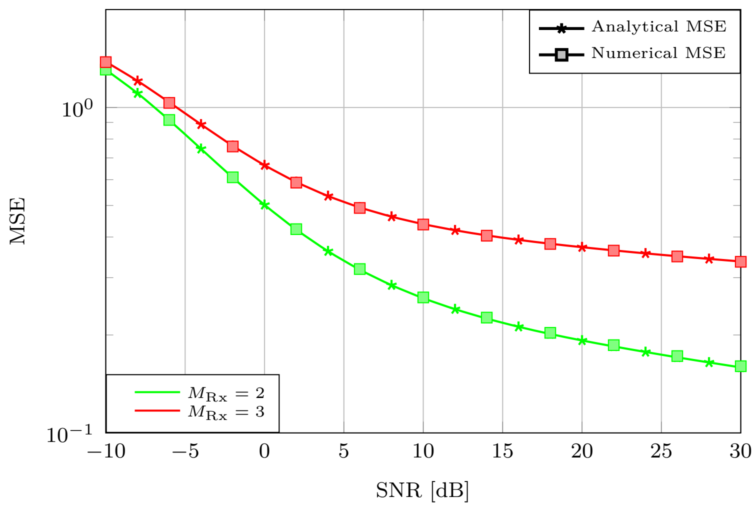

Figure A.2: Analytical and numerical MSE comparison for $M_{\mathrm{Rx}} = 2$ and $M_{\mathrm{Rx}} = 3$.

The matrix $\boldsymbol{R}_{\boldsymbol{c}_{\mathrm{out}}} = \mathrm{E}\{\boldsymbol{c}_{\mathrm{out}}\boldsymbol{c}_{\mathrm{out}}^H\}$ can be computed by following similar steps as in [64, Sec. 3.5]. First, the modulation systems are converted to the equivalent Moore machines. Table A.1 and Fig. A.1 show the Moore machine for $M_{\mathrm{Rx}} = 3$ with $\varrho = 8$ states. The states $1_+, 2_+, 3_+, 4_+$ represent sequences for $\rho = 1$ and states $1_-, 2_-, 3_-, 4_-$ for $\rho = -1$. The state transition probability matrix $\boldsymbol{Q}$ of the equivalent Moore machine, with dimensions $\varrho \times \varrho$ is defined for i.i.d. input bits. All valid state transitions have a probability $p = 1/4$ for $M_{\mathrm{Rx}} = 3$ and $p = 1/8$ for $M_{\mathrm{Rx}} = 2$ according to the Gray coding for TI ZX. Furthermore, the vector $\boldsymbol{\pi}$ of length ϱ which corresponds to the stationary distribution of the equivalent Moore machine with $\boldsymbol{\pi}^T\boldsymbol{Q} = \boldsymbol{\pi}^T$, is given by $\boldsymbol{\pi} = (1/\varrho)\mathbf{1}$. Then, the matrix $\boldsymbol{\Gamma}$ with dimensions $\varrho \times M_{\mathrm{Rx}}$ defines the Moore machine's output, in terms of the codewords c_{s}. The block-wise correlation matrix of the TI ZX mapping output is given by $\boldsymbol{R}_{\boldsymbol{c}_{\mathrm{s}}}^{\kappa} = \mathrm{E}\{\boldsymbol{c}_{\mathrm{s}_{\kappa'}}\boldsymbol{c}_{\mathrm{s}_{\kappa'+\kappa}}^T\} = \boldsymbol{\Gamma}^T\boldsymbol{\Pi}\boldsymbol{Q}^{|\kappa|}\boldsymbol{\Gamma}$ [64, eq. 3.46], where $\boldsymbol{\Pi} = \mathrm{diag}(\boldsymbol{\pi})$ and $\boldsymbol{c}_{\mathrm{s}_{\kappa'}}$ denotes the κ'th codeword of $\boldsymbol{c}_{\mathrm{out}}$. Finally, the autocorrelation matrix $\boldsymbol{R}_{\boldsymbol{c}_{\mathrm{out}}}$ is obtained by considering the concatenation of the matrices $\boldsymbol{R}_{\boldsymbol{c}_{\mathrm{s}}}^{\kappa}$ with $\kappa = 0, 1, \cdots, N$ as

$$\boldsymbol{R}_{\boldsymbol{c}_{\mathrm{out}}} = 2\mathrm{E}\{\boldsymbol{c}_{\mathrm{out}}\boldsymbol{c}_{\mathrm{out}}^T\} = 2\begin{bmatrix} \rho_0^2 & \mathrm{E}\{\rho_0{\boldsymbol{c}_{\mathrm{s}}}^{1^T}\} & \mathrm{E}\{\rho_0{\boldsymbol{c}_{\mathrm{s}}}^{2^T}\} & \cdots & \mathrm{E}\{\rho_0{\boldsymbol{c}_{\mathrm{s}}}^{N^T}\} \\ \mathrm{E}\{{\boldsymbol{c}_{\mathrm{s}}}^1\rho_0\} & \boldsymbol{R}_{\boldsymbol{c}_{\mathrm{s}}}^0 & \boldsymbol{R}_{\boldsymbol{c}_{\mathrm{s}}}^1 & \cdots & \boldsymbol{R}_{\boldsymbol{c}_{\mathrm{s}}}^{N-1} \\ \mathrm{E}\{{\boldsymbol{c}_{\mathrm{s}}}^2\rho_0\} & \boldsymbol{R}_{\boldsymbol{c}_{\mathrm{s}}}^{1^T} & \boldsymbol{R}_{\boldsymbol{c}_{\mathrm{s}}}^0 & \cdots & \boldsymbol{R}_{\boldsymbol{c}_{\mathrm{s}}}^{N-2} \\ \vdots & \vdots & \vdots & \cdots & \vdots \\ \mathrm{E}\{{\boldsymbol{c}_{\mathrm{s}}}^N\rho_0\} & \boldsymbol{R}_{\boldsymbol{c}_{\mathrm{s}}}^{N-1^T} & \boldsymbol{R}_{\boldsymbol{c}_{\mathrm{s}}}^{N-2^T} & \cdots & \boldsymbol{R}_{\boldsymbol{c}_{\mathrm{s}}}^0 \end{bmatrix}, \tag{A-9}$$

where $\mathrm{E}\{\rho_0 \boldsymbol{c}_\mathrm{s}{}^{kT}\} = \mathbf{1}^T_{\varrho\times 1}\mathrm{diag}([1, \mathbf{0}_{\varrho-1\times 1}])\boldsymbol{Q}^{|\kappa|}\boldsymbol{\Gamma}$ for the Moore machine with $M_{\mathrm{R}_x} = 3$ and $\rho_0^2 = 1$. Note that sequences with independent real and imaginary parts are considered which is supported by factor 2 in (A-9). Fig. A.3 compares the MSE obtained with (A-8) and (A-9), and the numerical MSE for $M_\mathrm{Rx} = 2$ and $M_\mathrm{Rx} = 3$. Note that, for $M_{\mathrm{R}_x} = 2$ Table 3.4 is considered.

A.3 MMDDT Precoding Performance Bound

This section presents the semi-analytical symbol error rate (SER) upper bound for the MMDDT precoder with quality of service constraint regarding the minimum distance to the decision threshold γ. Considering $M_\mathrm{Rx} = 3$, 4 different symbols b_1, b_2, b_3, b_4 can be transmitted. The SER is defined as

$$\mathrm{SER} = \mathrm{P}_\mathrm{error}. \tag{A-10}$$

Considering the probability of correct detection as P_cd, the $\mathrm{P}_\mathrm{error}$ probability is defined as $\mathrm{P}_\mathrm{error} = (1 - \mathrm{P}_\mathrm{cd})$,

$$\begin{aligned} \mathrm{SER} &= 1 - \mathrm{P}_\mathrm{cd} && \text{(A-11)} \\ &= 1 - \mathrm{P}\left(b\right)\left(\sum_{i=1}^{4}\mathrm{P}\left(\hat{x}_i = b_i | x_i = b_i\right)\right), && \text{(A-12)} \end{aligned}$$

where $\mathrm{P}(b) = 1/4$, since all input symbols have equal probability. Considering the worse case, that all N_tot samples of the temporal precoding vector $\boldsymbol{p}_x$ are equal to a value γ, where γ corresponds to the minimum distance to the decision threshold, the probability of correct detection P, can be lower bounded with

$$\mathrm{P}'\left(\hat{x}_i = b_i | x_i = b_i\right) \leq \mathrm{P}\left(\hat{x}_i = b_i | x_i = b_i\right). \tag{A-13}$$

With this, the SER upper bound is defined as

$$\mathrm{SER}_\mathrm{ub} = 1 - \mathrm{P}\left(b\right)\left(\sum_{i=1}^{4}\mathrm{P}'\left(\hat{x}_i = b_i | x_i = b_i\right)\right), \tag{A-14}$$

The probability density function of the 4-dimensional multivariate normal distribution is

$$f\left(\boldsymbol{y}, \boldsymbol{\mu}, \boldsymbol{\Sigma}\right) = \frac{1}{\sqrt{|\Sigma|\left(2\pi\right)^4}}\exp\left(-\frac{1}{2}(\boldsymbol{y}-\boldsymbol{\mu})\boldsymbol{\Sigma}^{-1}(\boldsymbol{y}-\boldsymbol{\mu})^T\right), \tag{A-15}$$

where $\boldsymbol{\mu}$ corresponds to the mean vector and $\boldsymbol{\Sigma}$ to the covariance matrix defined as $\boldsymbol{\Sigma} = \mathrm{E}\left\{(\boldsymbol{G}_\mathrm{Rx}\boldsymbol{n})(\boldsymbol{G}_\mathrm{Rx}\boldsymbol{n})^T\right\}$. Considering the received vector $\boldsymbol{y}_i$ of length $M_\mathrm{Rx} + 1$ before quantization associated with the input vector $\boldsymbol{x}_i$, the correct detection probability is defined as:

$$\mathrm{P}'\left(\hat{x}_i = b_i | x_i = b_i\right) = \iiiint_{\mathcal{R}} f\left(\boldsymbol{y}, \boldsymbol{\mu}, \boldsymbol{\Sigma}\right) dy_1 dy_2 dy_3 dy_4 \tag{A-16}$$

The integration regions $\mathcal{R}$ and $\boldsymbol{\mu}$ for each symbol b_j are presented in Table A.2.

Table A.2: Integration regions $\mathcal{R}$ for each symbol b_j.

Symbol	$\boldsymbol{\mu}$	Received sequence $\boldsymbol{z}_i$ detected as b_i	$\mathcal{R}$	
			x_l	x_u
b_1	$[\gamma,\ \gamma,\ \gamma,\ \gamma]$	$[\ 1,\ 1,\ 1,\ 1]$	$[\ 0,\ 0,\ 0,\ 0]$	$[\infty, \infty, \infty, \infty]$
		$[\ 1,\ 1, -1,\ 1]$	$[\ 0,\ 0, -\infty,\ 0]$	$[\infty, \infty,\ 0, \infty]$
		$[\ 1, -1,\ 1,\ 1]$	$[\ 0, -\infty,\ 0,\ 0]$	$[\infty,\ 0, \infty, \infty]$
b_2	$[\gamma,\ \gamma,\ \gamma, -\gamma]$	$[\ 1,\ 1,\ 1, -1]$	$[\ 0,\ 0,\ 0, -\infty]$	$[\infty, \infty, \infty,\ 0]$
		$[\ 1, -1,\ 1, -1]$	$[\ 0, -\infty,\ 0, -\infty]$	$[\infty,\ 0, \infty,\ 0]$
b_3	$[\gamma,\ \gamma, -\gamma, -\gamma]$	$[\ 1,\ 1, -1, -1]$	$[\ 0,\ 0, -\infty, -\infty]$	$[\infty, \infty,\ 0,\ 0]$
b_4	$[\gamma, -\gamma, -\gamma, -\gamma]$	$[\ 1, -1, -1, -1]$	$[\ 0, -\infty, -\infty, -\infty]$	$[\infty,\ 0\ \ 0,\ 0]$
		$[\ 1, -1, -1,\ 1]$	$[\ 0, -\infty, -\infty,\ 0]$	$[\infty,\ 0\ \ 0, \infty]$

Note that, invalid codewords are also detected as the received symbol b_j, therefore, also invalid codewords are included in Table A.2. Moreover, due to symmetry, only the codewords for positive ρ are considered. Fig. A.3 compares the numerical SER for the MMDDT precoding with (4-5) and the semi-analytical SER upper bound with noise variance $\sigma^2 = 1$. For numerical evaluation, sequences of 1 symbol only were considered.

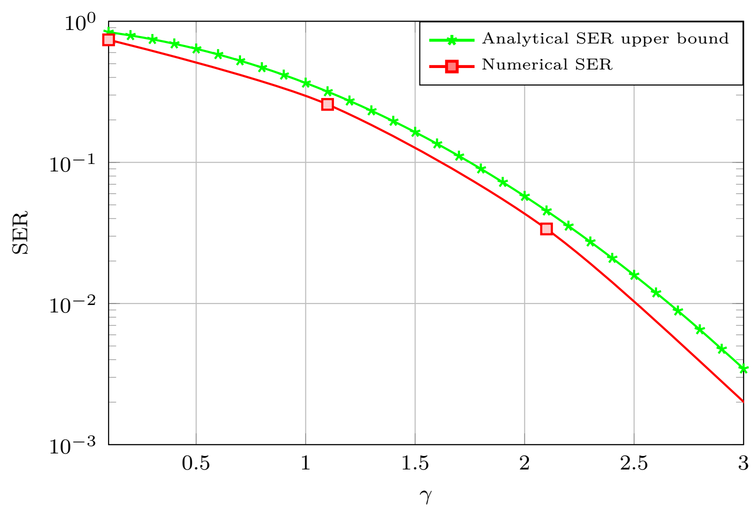

Figure A.3: Semi-analytical and numerical SER comparison for the MMDDT precoding method with $M_{\mathrm{Rx}} = M_{\mathrm{Tx}} = 3$, $N = 1$ and $\sigma^2 = 1$.

A.4 Runlength-Limited Zero-Crossing Precoding

Using RLL sequences [66] for systems employing 1-bit quantization and temporal oversampling has been proposed in [62,67]. They are a natural choice for such systems because the information is conveyed in the temporal distance between ZXs, which can be recovered after 1-bit quantization.

RLL sequences are discrete bipolar sequences, typically with amplitude ± 1, which are constraint such that the minimum and maximum distance between two amplitude transitions is given by $d+1$ and $k+1$, respectively [66]. An example for an RLL sequence with constraint $(d = 1, k = \infty)$ is given below:

$$\boldsymbol{c}_{\mathrm{out}_k} = [\ldots, +1, +1, +1, -1, -1, +1, +1, +1, -1, -1, \ldots]^T \,.$$

The minimum runlength constraint, also denoted as d-constraint, is introduced to reduce ISI, whereas the maximum runlength constraint, also denoted as k-constraint, is introduced to ensure proper synchronization. The k-constraint is omitted here, i. e., $k = \infty$, so synchronization is not considered. The reader is referred to [66] for more details on RLL sequences. This work employed the FSM RLL codes derived in [60].

The encoder is initialized to a pre-defined state $s_0 \in \mathcal{S}_{\mathrm{RLL}}$, where $\mathcal{S}_{\mathrm{RLL}}$ denotes the set of all encoder states. Then, depending on the current state s_0 and the current input block of p bits, the encoder produces an output RLL sequence block of length q and translates it into a new state s_1. The procedure is repeated for each input block. The code rate is consequently given by $R_{\mathrm{RLL}} = p/q$. The encoders are specified in Table A.3 and Table A.4 [60].

Table A.3: Finite-state machine encoder for $(1, \infty)$ RLL constraint with code rate $R_{\mathrm{RLL}} = 2/3$.

Current state	Input	Output	Next State
1	00	001	1
	01	010	2
	10	000	3
	11	010	3
2	00	100	2
	01	000	3
	10	100	3
	11	000	2
3	00	010	2
	01	010	3
	10	101	1
	11	001	1

Table A.4: Finite-state machine encoder for $(2, \infty)$ RLL constraint with code rate $R_{\mathrm{RLL}} = 1/2$.

Current state	Input	Output	Next State
1	0	00	3
	1	00	4
2	0	01	1
	1	00	3
3	0	01	1
	1	10	2
4	0	00	3
	1	00	4

A.4.1 Runlength-Limited Sequence Detection

For RLL sequence detection, we present a low-complexity minimum Hamming distance Viterbi algorithm [68]. The algorithm is implemented on the time-invariant trellis, which is defined by the FSM RLL encoders given in [60, Table I-II]. Trellis states and transitions are denoted by $s_k \in \mathcal{S}_{\mathrm{RLL}}$

Algorithm 5 Viterbi RLL Sequence Detection

Inputs: K, s_0
Initialization: $\Gamma(s = s_0) = 0, \quad \Gamma(s \neq s_0) = \infty$
for $k = 0$ to $K - 1$ **do**
for $s_{k+1} \in \mathcal{S}_{\mathrm{RLL}}$ **do**
Update path metric:
$\Gamma(s_{k+1}) = \min_{s_k \in \mathcal{S}_{\mathrm{RLL}}} \Gamma(s_k) + \lambda_k(s_k, s_{k+1})$
Store survivor sequence:
$\hat{\boldsymbol{x}}(s_{k+1}) = [\hat{\boldsymbol{x}}^T(s_k), \overleftarrow{\sigma}^T(s_k, s_{k+1})]^T$
end
end
return $\hat{\boldsymbol{x}}(s_K)$ where $s_K = \arg\min_{s_K \in \mathcal{S}_{\mathrm{RLL}}} \Gamma(s_K)$

and $(s_k = m, s_{k+1} = m') \in \mathcal{T}_{\mathrm{RLL}}$, respectively. The forward mapping $\sigma(m, m') \in \{+1, -1\}^q$ denotes the output for a transition $(m, m') \in \mathcal{T}_{\mathrm{RLL}}$. Furthermore, $\overleftarrow{\sigma}(m, m') \in \{0, 1\}^p$ denotes the inverse mapping for a transition $(m, m') \in \mathcal{T}_{\mathrm{RLL}}$, i. e. it specifies the input bits corresponding to this transition. Then, we define the Hamming distance branch metric as

$$\lambda_k(m, m') = \sum_{n=1}^{q} \frac{1}{2} \left| [\boldsymbol{z}]_{(\mathrm{k}-1)\mathrm{q}+(\mathrm{n}-1)} - [\sigma(m, m')]_n \right|, \tag{A-17}$$

where $[\boldsymbol{z}]_n$ and $[\sigma(m, m')]_n$ denote the nth element of $\boldsymbol{z}$ and $\sigma(m, m')$, respectively. Finally, the minimum Hamming distance Viterbi algorithm is given by Algorithm 5(cf. [69]), where $K = \frac{NM_{\mathrm{Rx}}}{q}$ and $s_0 \in \mathcal{S}_{\mathrm{RLL}}$ denote the number of decoder iterations and the start state, respectively.

A.5 Published Papers

- **Publications in Journals:**

  – D. M. V. Melo, L. T. N. Landau, R. C. de Lamare, P. F. Neuhaus and G. P. Fettweis, "**Zero-Crossing Precoding Techniques for Channels With 1-Bit Temporal Oversampling ADCs**," in IEEE Transactions on Wireless Communications, vol. 22, no. 8, pp. 5321-5336, Aug. 2023, doi: 10.1109/TWC.2022.3233320.

  – D. M. V. Melo, L. T. N. Landau, R. C. de Lamare, "**State Machine-based Waveforms for Channels With 1-Bit Quantization and Oversampling With Time-Instance Zero-Crossing Modulation**," in IEEE ACCESS, 2024.

- **Papers published in International Events:**

  – D. M. V. Melo, L. T. N. Landau and R. C. de Lamare, "**Zero-Crossing Precoding with MMSE Criterion for Channels with 1-BIT Quantization and Oversampling**," WSA 2020; 24th International ITG Workshop on Smart Antennas, Hamburg, Germany, 2020, pp. 1-6. (Master Thesis)

  – D. M. V. Melo, L. T. N. Landau and R. C. de Lamare, "**Zero-Crossing Precoding with Maximum Distance to the Decision Threshold for Channels with 1-Bit Quantization and Oversampling**," ICASSP 2020 - 2020 IEEE International Conference on Acoustics, Speech and Signal Processing (ICASSP), Barcelona, Spain, 2020, pp. 5120-5124, doi: 10.1109/ICASSP40776.2020.9053632. (Master Thesis)

  – D. M. V. Melo, L. T. N. Landau, L. N. Ribeiro and M. Haardt, "**Iterative MMSE Space-Time Zero-Crossing Precoding for Channels With 1-Bit Quantization and Oversampling**," 2020 54th Asilomar Conference on Signals, Systems, and Computers, Pacific Grove, CA, USA, 2020, pp. 496-500, doi: 10.1109/IEEECONF51394.2020.9443574.

  – D. M. V. Melo, L. T. N. Landau, L. N. Ribeiro and M. Haardt, "**Time-Instance Zero-Crossing Precoding with Quality-of-Service Constraints**," 2021 IEEE Statistical Signal Processing

Workshop (SSP), Rio de Janeiro, Brazil, 2021, pp. 121-125, doi: 10.1109/SSP49050.2021.9513848.

- P. Neuhaus, D. M. V. Melo, L. T. N. Landau, R. C. de Lamare and G. Fettweis, "**Zero-Crossing Modulations for a Multi-User MIMO Downlink with 1-Bit Temporal Oversampling ADCs**," 2021 29th European Signal Processing Conference (EUSIPCO), Dublin, Ireland, 2021, pp. 816-820, doi: 10.23919/EUSIPCO54536.2021.9616302.

- D. M. V. Melo, L. T. N. Landau, R. C. de Lamare, "**Time Instance Zero-Crossing Precoding for mmWave channels employing 1-bit quantization and oversampling**," submitted to WSA 2024; Presented at 27th International ITG Workshop on Smart Antennas, Dresden, Germany, 2024.